ADDIS ABABA UNIVERSITY

ADDIS ABABA INSTITUTE OF TECHNOLOGY

SCHOOL OF GRADUATE STUDIES

SCHOOL OF MECHANICAL AND INDUSTRIAL ENGINEERING

Analytical and Numerical Modelling of Failure in Aluminum Matrix Composite for Connecting Rod Application

A Thesis Submitted to the School of Graduate Studies of Addis Ababa University in Partial Fulfillment of the Requirement for the Degree of Master of Science (MSc.) in Mechanical Engineering (Manufacturing Engineering)

By: **Ephrem Yemane**

Advisor: **Dr. Desalegn Wogaso**

Addis Ababa, Ethiopia

June, 2022

Declaration

Addis Ababa University

School of Graduate Studies

I hereby declare that this thesis entitled "**Analytical and Numerical Modelling of Failure in Aluminum Matrix Composite for Connecting Rod Application**'' is my original work, done with the guidance of my advisor, and has not been submitted in whole or in part for a degree in any university/institution/.The resources of materials used for this thesis have been duly acknowledged and a list of references are given.

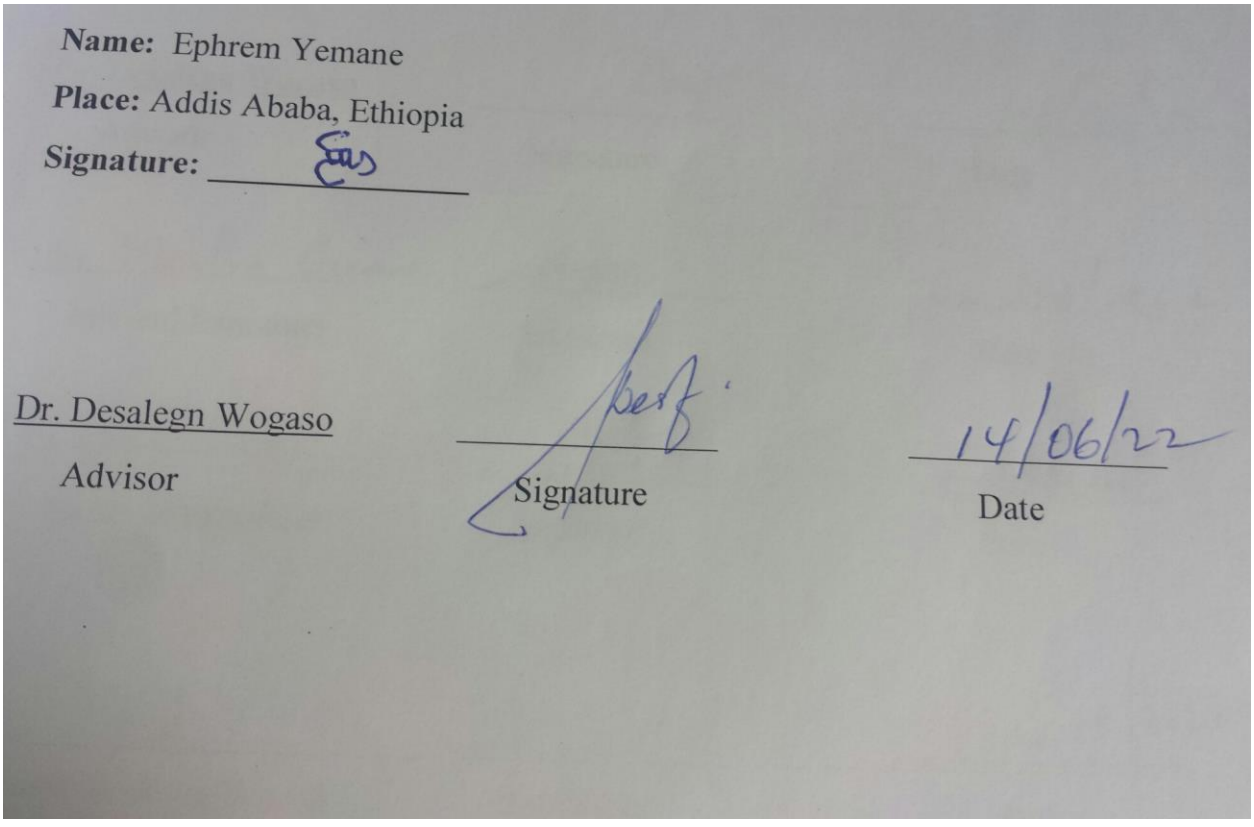

Approval Page

Addis Ababa University

Addis Ababa Institute of Technology

This is to certify that the thesis prepared by **Ephrem Yemane**, entitled:

"Analytical and Numerical Modelling of Failure in Aluminum Matrix Composite for Connecting Rod Application" submitted as partial fulfillment for the award of MSc. degree in Mechanical Engineering (Manufacturing Engineering) complies with the regulations of the university and meets the accepted standards concerning originality, content, and quality.

Approved by Board of Examiners:

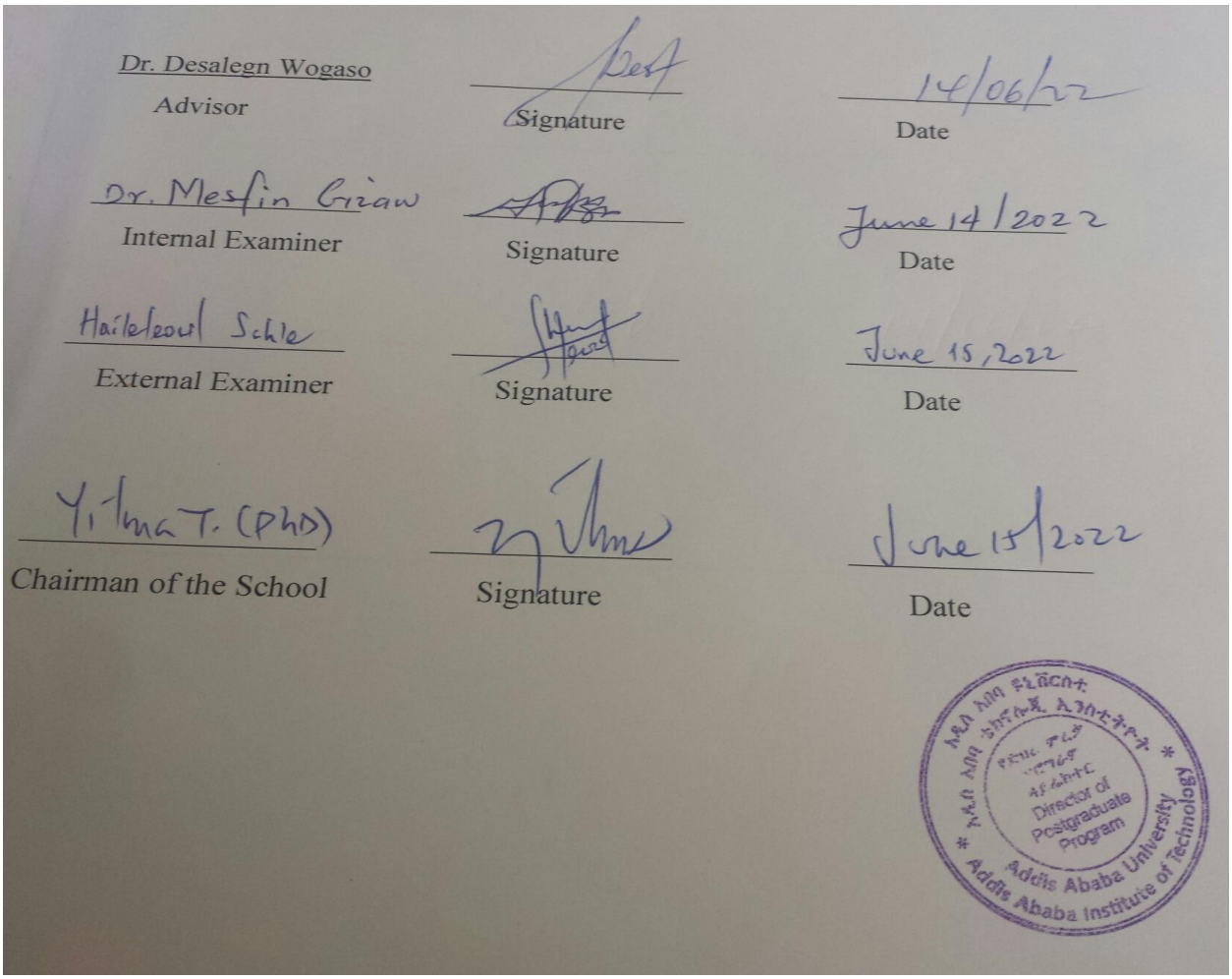

Acknowledgment

The completion of this thesis becomes a reality with the kind support and help of many individuals. I would like to extend my sincere thanks to all of them

Foremost I would like to thank and gratify Jesus Christ and St. Mary who are the bases for all the success of my life as a whole and this research in particular. Next, I would like to thank my advisor Dr.Desalegn Wogaso for his support, guidance and valuable criticism during this thesis work.

I also owe thanks to my family for their unconditional love, support and understanding. I thank you so much and love you more for all the things you did to support and motivate me.

Last but not least I would like to acknowledge my fellow classmates for having my back and supporting me whenever I needed help.

Thank you all!!

Abstract

The failures in composites are due to failure in their matrix, re-enforcement parts, or both. Failure in the composite structure could cause pin failure, stress failure, fatigue failure, hydro lock as well as overheating of the connecting rod. Thus, the implementation of analysis and predicting tools is preferred to prevent failures. The objective of this thesis work is to predict and analyze the failure possibilities in automobile connecting rods. The connecting rods are made of an aluminum matrix with silicon carbide reinforcements which were modeled by varying the volume fraction of re-enforcements in the form of laminates and particulates. The laminate reinforced aluminum matrix composites were modeled by varying laminate orientation while the particulate reinforced ones were modeled by varying the composite aspect ratio. The connecting rod models passed through available failure criteria like Tsai-Hill or Tsai-Wu and Von-Mises stress values. Both models were analyzed using ABAQUS software. Additionally, the particulate reinforced composites were analyzed using representative volume element /RVE/ on DIGIMAT software. The results showed that the material properties of AA6061-SiC composites increased with an increasing reinforcement volume fraction by the reduction in thickness of the bulky connecting rod. Failure in the connecting rod was predicted to occur in stress-concentrated areas located at corners where the SiC reinforcements are found, as well as, areas of load application and the middle cross-section of the connecting rod. The particulate reinforced models were preferred than the laminate reinforced ones because they sustained higher load gradients prone to less failure. The aluminum MMC'S with a five percent SiC reinforcement volume fraction in particulate form, as well as, twenty percent volume fraction SiC in laminate form with 0^o or 90^o orientation were found suitable for automobile connecting rod application based on the parameters provided by the author.

Keywords: *Connecting Rod, Failure Prediction, Laminate, Particulate, Simulation, Criterions, Laminate Orientation, Aspect Ratio, Volume Fraction*

Contents

List of Figures

List of Tables

List of Abbreviations

ABAQUS	Architecture-based analysis communication and understanding of system
AMMC	Aluminum metal matrix composites
FEA	Finite element analysis
FEM	Finite element modelling
MMF	Micro mechanics failure
PRMMC	Particulate Reinforced metal matrix composites
RVE	Representative Volume element
SiC	Silicon Carbide
MMC	Metal matrix composite

Nomenclature

$\bar{\Sigma}$	Composite flow Stress
V	Volume of particle
V_o	Reference Volume
Σ	Stress value
S_{23}	Strength Normal direction
S_1	Strength parallel direction
P_c	Density of Composite
P_m	Density of the matrix material
P_f	Density of the Reinforcement material
V_m	Matrix Volume Fraction
V_f	Reinforcement Volume Fraction
V_{12_m}	Poisson's Ratio of matrix
V_{12_F}	Poisson's Ratio of fiber
G_{12_m}	Shear Modulus of matrix
G_{12_F}	Shear Modulus of fiber
$(T_{12})_m$	In plane Shear Strength of matrix
$(T_{12})_F$	In plane Shear Strength of fiber
Σ_m	Tensile Strength of matrix material
Σ_f	Tensile strength of Reinforcement material
A_m	Co-efficient of Thermal expansion of matrix material
A_f	Co-efficient of Thermal expansion of Reinforcement material

E_m	Young's Modulus of Matrix material
E_f	Young's Modulus of Reinforcement material
B	Width of the Section
H	Depth of the Section
A	Area of the Section
s	Aspect Ratio
I_{xx} and I_{yy}	Moment of Inertia along x-axis and y-axis respectively
K_{xx} and K_{yy}	Radius of Gyration along x-axis and y-axis respectively
W_B	Buckling Load
ϵ_x and σ_y	Global Strain and Global Stress respectively
ϵ_1 and σ_1	Local Strain and local Stress respectively
σ_c	Tensile Strength of Composite
A_c	Cross Sectional Area
l	Thickness
K_{xx}	Radius of Gyration of Cross Section
α	Rankine Constant
σ_c	Tensile Strength of Composite
E	Elastic Modulus

Chapter One

1. Introduction

1.1. Background of the Study

Failure of composites is a complex multi-stage process that may get triggered in a certain "mode" but its propagation and final failure modes may be significantly different. In most cases composite failure gets initiated internally so, changes in the composite behavior are mostly observed after the failure has propagated beyond a certain extent [1][2].

The internal failure of a composite can be breaking of fibers, development of micro-cracks in the matrix, de-bonding between fibers and matrix, Delamination for the laminate reinforcement. While particle fracture, interface de-cohesion and particle clustering are the failures for the particulate reinforcements. Thus there is a need of finding ways of prediction and analysis of failure before it occurs [3].

The possibilities for the manipulation of properties (property combinations) to suit specific requirements of material and component properties enhanced performance. This lead to increased utilization of aluminum metal matrix composites (AMMC's) in current and future industrial applications. The main challenges faced when using these aluminum matrix composites are failures due to longitudinal compression, transverse tension, biaxial loading, progressive damage, micro-damage, and fatigue damage in the aluminum metal matrix structure. However, there are promising signs of technological breakthroughs by various research efforts dedicated to finding solutions to those challenges [4].

Automobile connecting rods made of aluminum 6061 alloy matrix reinforced with silicon-carbide (SiC) as laminate and particulate forms were assumed to have better mechanical properties than the general material used for connecting rods like C70 steel [5][6]. Because, as the need for comfort, lightness, and fuel efficiency increases, the use of lightweight materials like titanium and aluminum alloys with composites has now become common. In addition to desired mechanical

properties, it is assumed to work in operative conditions, subjected to pressure and inertial forces [7].

The Aluminum-matrix composites used in connecting rods are materials whose mechanical properties can be modified. The matrix alloy, the reinforcement material, the form, volume, the situation of the reinforcement, and fabrication method can all be varied to realize the required properties[7][8].In addition to providing less cost over most other metal matrix composites(MMC's), they have higher mechanical properties. Aluminum metal matrix composites (AMMC) are produced by casting, powder metallurgy, foil, and fiber processing techniques [8].

During operation, the connecting rods may fail because of the stress involved when the connecting rod is stretched and pressed at each stroke including other factors related to temperature and environment[9].

1.2. Problem Statement

The potential aluminum matrix offer in the development of composites with desired properties is quite good. Particularly use of aluminum matrix with silicon carbide reinforcements has become commonly used for applications in automotive components like connecting rods and pistons, which work on various complicated conditions. But despite the promising applications of AMC's certain conditions were not considered because there is a tendency of focusing on the mechanical characterization of these materials. The conditions needed to be considered were variation of volume fraction with laminate orientation as well as particulate aspect ratio. They would help to understand what the variation contributes in changing the performance of these connecting rods for failure prediction and analysis. In addition, a comparative study between laminate reinforced and particulate reinforced models is also a concern due to the focus on individual characterization.

The Reliance on experiments for conducting research by costly and destructive tests is also a concern. This is because of the loss researchers face financially and morally if their experiments fail after allocating a huge sum of money for procuring the aluminum alloy and silicon carbide raw materials, manufacturing them and also the time wasted. Thus determining the operative status of the materials in normal conditions through simulations gives guidance on which model is preferable for further processing or even experimentation. This would give reassurance before

undergoing manufacturing easing the work of metalworking industries in their selection of the models prone to lesser failure, which encourages creativity for further researches.

1.3. Objective of the Study

1.3.1. General Objectives

The general objective of this thesis is to analyze and predict failure in Al-matrix composite connecting-rod models reinforced with SiC in laminate and particulate form by using analytical and simulative modelling.

1.3.2. Specific Objectives

- ➔ To model the aluminum-silicon carbide composite connecting rod with (5, 10, 15, 20, 25, 30) percent volume fraction of reinforcements in laminate and particulate form.
- ➔ To analyze and predict the damage of laminate composite connecting rod models with (0, 30, 45, 90) degree orientation using Tsai-Hill and Tsai-Wu failure criterion.
- ➔ To compare the analytical failure prediction results of the laminate reinforced composite modeling with the FE modeling simulation results using error percentage.
- ➔ To simulate the Von-Mises damage values for the PRC connecting rod models with 0.6 and 1.8 composite aspect ratio by using both the RVE from DIGMAT software and the actual connecting rod model.
- ➔ To simulate the modeling and predictive analysis of aluminum metal matrix composite /AMMC/ connecting rods using ABAQUS.
- ➔ To select a suitable aluminum-based composite for connecting rod application.

1.4. Scope of the Study

The research predicted and analyzed failures in aluminum-silicon carbide composite for connecting rod application. It modeled the composite with varying ranges of volume fraction (5,10,15,20,25,30) percent with (0,30,45,90) degree laminate orientation as well as (0.6 and 1.8) composite aspect ratio of particulate. The composite was modelled to check the failure by subjecting the material to static loading using failure criteria for laminates and Von-Misses for particulates. In addition, the particulate reinforced MMC's was analyzed with a representative volume element /RVE/ using DIGIMAT software. Finally, numerical data, as well as other

necessary parameters, were fed into ABAQUS software that works on simulating the failure of the material through the suggested criteria.

1.5. Significance of the Study

The research modeled an automobile connecting rod by substituting the most commonly used iron material with an aluminum-silicon carbide composite. The connecting rods were modeled by varying the volume fraction of reinforcement in laminate as well as particulate form. These models passed through suitable failure prediction criterion to determine the possible areas that failure could occur when the connecting rod is under static loading during operation. The prediction was done by undergoing analytical and FE simulation procedures using ABAQUS software. Furthermore, the RVE of the particulate reinforced composites was done using DIGIMAT to determine the corresponding effective properties of the macroscopic model.

The results obtained from simulations and analytics help not only for the prediction of possible failure. But also, in suggesting a good connecting rod model that could be used in automotive industries with relevant data for future researches.

1.6. Limitations of the Study

These thesis is limited to the prediction of failure in an automobile /Toyota Vitz/ engine component which is the connecting rod, limited to static loading. In addition the vast scope of the research it fails to consider other variables which could cause failure of the connecting rod in the long run such as temperature, fatigue failure, hydrolock and over revving [9][10].

1.7. Motivation Statement

The motivation behind this research is the simulation proven replacement of iron connecting rods with better performance aluminum ones by undergoing certain modifications. These is accomplished by using various forms of silicon carbide reinforcements, with laminate orientations and particulate aspect ratio. The results obtained from simulations using ABAQUS software would serve as a guideline for manufacturers for future applications.

1.8. Methodology

The methods used for the fulfillment of the research objectives are:-

First the material properties data were obtained from literature reviews on journals, articles and books about aluminum and silicon-carbide. Next the property logs of automobile connecting rods were acquired from Retail Company catalogues. Then, after the needed material properties were obtained all required steps for numerical analysis and modeling were extracted from relevant works of literature. This is followed by FEM analysis and modeling techniques for simulations performed on ABAQUS and DIGIMAT softwares with an additional guidance from the original software manuals. Finally after the results were obtained comparison of numerical results with FEM results was done followed by conclusion, recommendation and suggestions for future works.

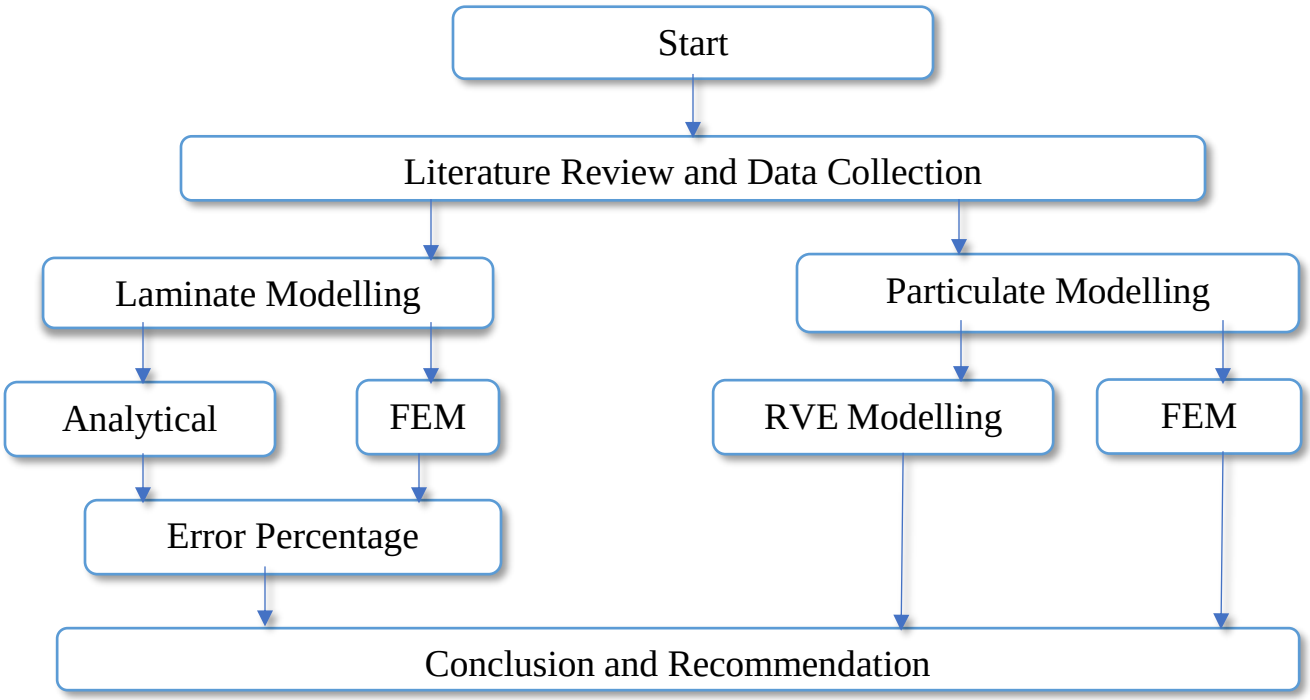

Figure 1.1 Methodology

1.9. Research Questions

- ➔ What is the effect of varying the volume fraction of SiC reinforcement on the performance of the aluminum-silicon carbide connecting rod models?
- ➔ What is the effect of varying laminate orientation as well as particulate aspect ratio on the connecting rod models performance?
- ➔ Which failure prediction criterion gives the optimum results?
- ➔ What is the preferred reinforcement (particulate or laminate) for the AA6061-SiC composite connecting rod model application?
- ➔ Can the representative volume element (RVE) analysis of the particulate reinforced composite be addressed using DIGIMAT software platform?
- ➔ Does the ABAQUS simulation address all the needed scenarios of failure analysis and prediction?
- ➔ Which connecting rod model is suitable for application for the selected automobile?

1.10. Organization of the Thesis

The thesis document includes five chapters.

Chapter One: Contains the Introduction, Background, Objectives, Scope, Significance, Limitations, motivation, and organization of the thesis.

Chapter Two: Designated to an extensive literature review on aluminum matrix composites, failure prediction, analysis and FE simulation

Chapter Three: Reports on the materials, methods, including procedures for numerical and FEM software analysis.

Chapter Four: Presents the obtained analytical and FEM simulation results which address the specific objectives with relevant discussion.

Chapter Five: Gives conclusions, recommendations and suggestion of future study areas.

Chapter Two

2. Literature Review

2.1. Introduction

After more than half a century of active research composites based on metals are now beginning to make a significant contribution to industrial and engineering practice. Which is partly a consequence of developments in processing methods [11].Modern technological demands for systems and machines that are more energy efficient, stronger, light-weight, cost-effective, etc., dictate that the search for new and advanced materials will remain a subject of interest all the time. The trouble in designing materials for such demanding specifications cannot be overstated, owing to the conflicting nature of these specifications. In addition to material design in the developing modern world. It's extremely important to predict the properties of the strength charactestics of the materials and those parts made from them. The failure of composites has been investigated extensively based on point of view [3]. But failure analysis and predictions based on the macro mechanical point of view are preferred than the micromechanical ones with regards to accuracy of predicting global failure of a lamina and also due to the wide variation of the failure mechanisms and processes with the type of loading.

Aluminum matrix composites (AlMC's) are a class of materials that have proven successful in meeting most of the rigorous specifications in applications where light-weight, high stiffness and moderate strength are the requisite properties [7].They are widely used for high performance applications such as automotive, industrial, military, aerospace and electricity industries. Various kinds of ceramic materials like Al203, SiC, MgO and B_4C are extensively used to reinforce aluminum matrices. Essential properties of these materials such as, high hardness, high compressive strength, wear resistance, refractoriness etc. Make them suitable for use as reinforcements in the matrix of composites.

2.2. Silicon Carbide Reinforcements in AMC's

Divecha et al. [12] presented the mechanical properties of silicon carbide reinforcement volume fraction and aluminum matrix in a variety of shapes. From these studies it was observed that the transverse properties of these materials are nearly as high as the longitudinal properties. So, there is much more design flexibility than most other composites.

Li et al. [13] stated that a widely used particle for reinforcing aluminum matrix is silicon carbide (SiC). This reinforcement promotes an increase in the elastic modulus and tensile strength of the aluminum matrix composites, and another improvement of composites regarding aluminum matrix is the behavior at high temperature.

2.3. Effects of Varying Reinforcement Volume Fraction on Properties of AMC's

Rashed et al. [14] studied the microstructures, mechanical properties, and wear at cast of silicon carbide (SiC) reinforced aluminum matrix composites by varying the silicon content using (0, 5, 10 and 20)% volume fraction. It was observed that introducing SiC reinforcements in aluminum matrix increased hardness and tensile strength. In addition, the aluminum matrix reinforced with 20 % volume fraction of silicon carbide (SiC) showed maximum hardness and tensile strength.

Mahendra et al. [15] carried a study which considered the mechanical properties of the AMMC to the percentage of the SiC re-enforcing material that shows that it decreases with the increase in SiC content because of the silicon carbide particles lower density. In addition, other mechanical properties, such as tensile strength, yield strength, hardness, impact strength and wear resistance, all of which increase (improve) with an increase in silicon carbide content. This has showed that the reasons for this increase in these properties allotted to the number of SiC particles directly proportional to the stress needed to initiate and then propagate the cracks in the composite.

However, the elongation percentage reduces as the silicon carbide content grows. The work of Singla et al. [16] shows that when SiC increases to above twenty-five percent, properties such as hardness and impact strength reduce. The authors stated this was due to the increasing quantities of silicon carbide particles that react with each other (clustering) and settle down, thereby contributing to a local lower hardness and reduction in density (of silicon carbide particles).

Neelima et al. [17] compared the percentage of SiC content with tensile strength and elongation. It was observed that the tensile strength increases with the SiC content up to 15% after which it drops. The percentage of elongation, unlike Mahendra et al. [15] seen to be proportional to the SiC percentage. The study regarded that tensile strength drops when the SiC content crosses fifteen percent probably due to the increased total area of the interface or number of interfaces which, could result in void nucleation and coalescence leading to failure at lower stresses to elongation. Both Mahendra et al. [15] and Neelima et al. [17] showed contradicting results. They advocated that there are some anomalies in the latter study's data since there is always a tradeoff between ductility and strength and, both cannot rise/fall simultaneously as described in the studies or where both tensile strength and elongation percentage are proportional to each other till fifteen percent SiC content.

Table 2.1 Properties at different silicon carbide content [18]

Property	SiC-5%	SiC-10%	SiC-15%	SiC-20%
Density (g/cm^3)	2.4660	2.3125	N/A	N/A
Yield strength (N/mm^2)	236	257	N/A	N/A
Hardness (BHN)	85.3	87.2	N/A	N/A
Tensile strength (N/mm^2)	248	265	N/A	N/A
Elongation (%)	19.0	18.2	N/A	N/A
Tensile strength (N/mm^2)	80.84	88.11	94.21	83.00
Elongation (%)	5.42	5.92	5.57	6.87
Hardness (BHN)	40.2	41.1	43.7	44.4
Impact strength (N-M)	22	24	N/C	30

2.4. Damage Models of Aluminum Metal Matrix Composite Laminates

Hu et al. [19] presented a material constitutive model suitable for the failure analysis of composite laminates under biaxial loads. In the material model, both the fiber and matrix were thought to behave as elastic-plastic, the in-plane shear is assumed to behave non-linearly with a variable shear parameter. Failure in lamina was detected by a mixed failure criterion composed of maximum stress and Tsai-Wu criterion. Finally, they tested their models against experimental data and discovered a good agreement.

Falcon et al. [20] presented a three-dimensional mechanics-based continuum damage material model implemented in an impact finite element code to simulate the progressive intra-laminar

degradation of fiber-reinforced laminates. It considered the full non-linear stress-strain relations for lamina in shear and under compressive and transverse loads. The application of these damage models on structural examples showed it could capture damage initiation and propagation to predict the final failure accurately.

2.5. Numerical Failure Analysis of Laminate AMMC's

Nali et al. [21] wrote a paper devoted to failure criteria which are most popular employed in the analysis and design of anisotropic materials/layered/ plates. The failure criteria are grouped into Failure criteria that neglect interactions between stress components and failure criteria that consider interactions between stress components that include Maximum stress and maximum strain criteria. Another group is failure criteria that propose one single inequality to define the failure envelope and failure criteria that proposes a combination of interactive and non-interactive components that include Hoffman, Tsai-Wu, Liu-Tsai, Tsai-Hill, Hashin & Rotem, puck and Schuerman, and larco3 criterions.

Tsai et al. [22] stated that failures in composites are complicated further by a multitude of independent and interacting mechanisms, including micro-buckling and filament breaks, de-wetting, delamination, matrix cavitation, and crack propagation. But noted that an operationally simple strength criterion can't possibly explain the actual failures mechanisms. Serving as a tool to characterize materials for determining how many independent strength components exist and how they are measured and for design requires a relatively simple method of estimating the load caring capacity of a structure. Thus, the stress-space for the failure surface from their assumed strength criterion given as

$$f(\sigma_k) = f_i\sigma_i + f_{ij}\sigma_i\sigma_j \quad (1)$$

Further expanded as:-

$$f_1\sigma_1 + f_2\sigma_2 + f_3\sigma_3 + f_4\sigma_4 + f_5\sigma_5 + f_6\sigma_6$$

$$f_{11}\sigma_1^2 + 2f_{12}\sigma_1\sigma_2 + 2f_{13}\sigma_1\sigma_3 + 2f_{14}\sigma_1\sigma_4 + 2f_{15}\sigma_1\sigma_5 + 2f_{16}\sigma_1\sigma_6$$

$$f_{22}\sigma_2^2 + 2f_{23}\sigma_2\sigma_3 + 2f_{24}\sigma_2\sigma_4 + 2f_{25}\sigma_2\sigma_5 + 2f_{26}\sigma_2\sigma_6$$

$$f_{33}\sigma_3^2 + 2f_{34}\sigma_3\sigma_4 + 2f_{35}\sigma_3\sigma_5 + 2f_{36}\sigma_3\sigma_6$$

$$f_{44}\sigma_4^2 + 2f_{45}\sigma_4\sigma_5 + 2f_{46}\sigma_4\sigma_6$$

$$f_{55}\sigma_5^2 + 2f_{56}\sigma_5\sigma_6$$

$$f_{66}\sigma_6^2 = 1$$

Assuming symmetry the symmetry properties of strength tensors are given in the following matrix

$$f_i = \begin{Bmatrix} f_1 \\ f_2 \\ f_3 \\ f_4 \\ f_5 \\ f_6 \end{Bmatrix} \qquad f_{ij} = \begin{bmatrix} f_{11} & f_{12} & f_{13} & f_{14} & f_{15} & f_{16} \\ & f_{22} & f_{23} & f_{24} & f_{25} & f_{26} \\ & & f_{33} & f_{34} & f_{35} & f_{36} \\ & & & f_{44} & f_{45} & f_{46} \\ & & & & f_{55} & f_{56} \\ & & & & & f_{66} \end{bmatrix}$$

Basically, to reach to isotropic materials the following cases need to be addressed.

- Assuming orthotropic properties $f_4, f_5, \& f_6$ were assumed to be zero and also that shear strengths are uncoupled that is

$$f_{45} = f_{56} = f_{64} = 0$$

- For transversely isotropic material the following conditions are met.

$$f_2 = f_3\ ,\ \ f_{12} = f_{13}\ , f_{22} = f_{33}\ , f_{55} = f_{66}\ , f_{44} = 2(f_{22} - f_{23})$$

- Internal stresses or Bauschinger's effect is ignored and only f_i components will be assumed to be zero from f_i and f_{ij} in isotropic materials

- For isotropic materials 1,2 & 3 indices are identical $f_{12} = {}^{-f_{11}}/_{2}$

- The three shear components are identical $f_{44} = f_{55} = f_{66} = 2(f_{11} - f_{12}) = 3f_{11}$

- For zero internal stresses as well plastically incompressible strength tensors are $f_i = \{0\}$

Then the matrix becomes:-

$$f_{ij} = f_{11}\begin{bmatrix} 1 & -1/2 & -1/2 & 0 & 0 & 0 \\ & 1 & -1/2 & 0 & 0 & 0 \\ & & 1 & 0 & 0 & 0 \\ & & & 3 & 0 & 0 \\ & & & & 3 & 0 \\ & & & & & 3 \end{bmatrix}$$

Equivalent /von misses/ stress is given by

$$\sigma_e = \sqrt{3J_2} = \sqrt{\frac{1}{2}[(\sigma_1 - \sigma_2)^2 + (\sigma_2 - \sigma_3)^2 + (\sigma_3 - \sigma_1)^2]} \quad (2)$$

$$\tau_{oct} = \sqrt{\frac{2}{3}J_2} = \frac{1}{3}\sqrt{(\sigma_1 - \sigma_2)^2 + (\sigma_2 - \sigma_3)^2 + (\sigma_3 - \sigma_1)^2}$$

The criterion proposed by Hill which is a generalization of the von-misses criterion to account for the effect of orthotropy. This criterion is useful in modelling the effects of hydrostatic pressure and have different behaviors in tensions and compression. Failures (deficiency) in this criterion is given by: -

$$H(\sigma_{11} - \sigma_{22})^2 + F(\sigma_{22} - \sigma_{33})^2 + G(\sigma_{33} - \sigma_{22}) + 2L\sigma_{23}^2 + 2M\sigma_{31}^2 + 2N\sigma_{12}^2 = 1$$

$\sigma_1 T, \sigma_2 T$ and $\sigma_3 T$ are yield strengths in the principal directions of anisotropy.

$$f = \frac{1}{2}\left\{\frac{1}{\delta_{2T}^2} + \frac{1}{\sigma_{3T}^2} - \frac{1}{\sigma_{1T}^2}\right\} \quad (3)$$

$$G = \frac{1}{2}\left\{\frac{1}{\delta_{3T}^2} + \frac{1}{\sigma_{1T}^2} - \frac{1}{\sigma_{2T}^2}\right\} \quad (4)$$

$$H = \frac{1}{2}\left\{\frac{1}{\delta_{1T}^2} + \frac{1}{\sigma_2^2} - \frac{1}{\sigma_3^2}\right\} \qquad L = \frac{1}{2(\tau_{23}^s)^2} \quad M = \frac{1}{2(\tau_{31}^s)^2} \qquad N = \frac{1}{2(\tau_{12}^s)^2}$$

Inspired by von-misses criterion the stress-strain relations are expressed as:-

$$\begin{Bmatrix}\varepsilon_{11}\\ \varepsilon_{22}\\ \varepsilon_{33}\\ \varepsilon_{23}\\ \varepsilon_{13}\\ \varepsilon_{12}\end{Bmatrix}=\begin{bmatrix} 1/E_1 & -v_{21}/E_2 & -v_{31}/E_3 & 0 & 0 & 0\\ -v_{12}/E_1 & 1/E_2 & -v_{32}/E_3 & 0 & 0 & 0\\ -V_{13}/E_1 & -v_{23}/E_2 & 1/E_3 & 0 & 0 & 0\\ 0 & 0 & 0 & 1/2G_{23} & 0 & 0\\ 0 & 0 & 0 & 0 & 1/2G_{13} & 0\\ 0 & 0 & 0 & 0 & 0 & 1/2G_{12}\end{bmatrix}\begin{Bmatrix}\sigma_{11}\\ \sigma_{22}\\ \sigma_{33}\\ \sigma_{23}\\ \sigma_{13}\\ \sigma_{12}\end{Bmatrix}$$

Stating that the Tsai-Hill criterion fails to differentiate between tensile stretching and compression failures. Beklemysheva et al. [23] described the Tsai-Wu criterion which is more complete than Tsai-hill criterion and is able to differentiate between the limits of elongation and compression.it also includes the total deformation energy. Thus the criterion is given as:-

$$F_{11}\sigma_{xx}+F_2\sigma_{yy}+F_3\sigma_{zz}+F_{11}\sigma_{xx}^2+F_{22}\sigma_{yy}^2+F_{33}\sigma_{zz}^2+F_{44}\sigma_{yz}^2+F_{55}\sigma_{xz}^2+F_{66}\sigma_{xy}^2 + 2F_{12}\sigma_{xx}\sigma_{yy}+2F_{13}\sigma_{xx}\sigma_{zz}+2F_{23}\sigma_{yy}\sigma_{zz}=1$$

Where:

$$F_{11}=\left(\frac{1}{x_1^T}-\frac{1}{x_1^c}\right),\quad F_2=F_3=\left(\frac{1}{x_2^T}-\frac{1}{x_2^C}\right),$$

$$F_{11}=\frac{1}{x_1^T x_1^c},F_{22}=F_{33}=\frac{1}{x_2^T x_2^C},$$

$$F_{44}=\frac{1}{(S_{23})^2},F_{55}=\frac{1}{(s_1)^2}=F_{66},$$

$$F_{23}=\frac{-1}{2}\frac{1}{x_2^T x_2^C},$$

$$F_{12}=F_{13}=-\frac{1}{2}\sqrt{\frac{1}{x_1^T x_1^C}\frac{1}{x_2^T x_2^C}}$$

Also according to Wang et al. [24] the general yield criterion of materials can be expressed in a general form as follows.

$$f(\sigma)=\sigma^T P\sigma 6+\sigma^T Q-1=0 \qquad (5)$$

Where $f(\sigma)$- yield function interms of strength parameters P and Q given as for isotropic materials:-

$$p = \begin{bmatrix} 1/\sigma_s^2 & -1/2\sigma_s^2 & -1/2\sigma_s^2 & 0 & 0 & 0 \\ -1/2\sigma_s^2 & 1/\sigma_s^2 & -1/2\sigma_s^2 & 0 & 0 & 0 \\ -1/2\sigma_s^2 & -1/2\sigma_s^2 & 1/\sigma_s^2 & 0 & 0 & 0 \\ 0 & 0 & 0 & 3/\sigma_s^2 & 0 & 0 \\ 0 & 0 & 0 & 0 & 3/\sigma_s^2 & 0 \\ 0 & 0 & 0 & 0 & 0 & 3/\sigma_s^2 \end{bmatrix} \qquad Q = [0\ 0\ 0\ 0\ 0\ 0]^T$$

Table 2.2 Summary of relevant works on failure analysis on laminates

Author name	Title of the journal	Main findings
Nali et al. [21]	A numerical assessment on 2D failure criteria for composite layered structures	Larco3 criterion gives a good result but was the most conservative. The middle Tsai-Hill and Tsai-Wu criteria were preferred.
Beklemysheva et al.[23]	Numerical simulation of the failure of composite materials by using grid-characteristics method	Calculation of model problems show that the failure areas obtained in the calculations by the use of various criteria are considerably different both in shape and in size. The Drucker prager, Hashin and Tsai-wu criterion yield similar evaluation of the size of the failure area. The Tsai-Hill criterion yields a considerably smaller size The puck's criterion yields a considerably larger size of the failure area.

* From the summary of relevant works on failure analysis on laminates we can observe that there are many criterions to assess and simulate failures in laminate composites. This has a significant contribution to our study of the prediction of failure in AMC laminate composite connecting rods. The Tsai-Hill and Tsai-Wu criterions were selected from the summaries. This is because they give a considerably smaller size that could be obtained from calculation that could be compared to the simulation values. Additionally, the consideration of tensile/compressive values in their analysis agrees to the loading condition used in our analysis.

2.6. Analysis Models of Particulate Reinforced (AMMC) Composites

Chu et al. [25] proposed a bond-based peri-dynamic model that considers strength-softening and rate dependence of ceramic materials. The rate-dependent model was used to simulate the complete damage and fracture process under impact loading for ceramic materials. The simulations show that the model can capture the entire damage process, the dynamic response during ballistic impact and the damage and fracture process of ceramic materials under slam from low to high velocity.

Lloyd et al. [26] investigated the tensile deformation and fracture behavior of the aluminum alloy AA6061 reinforced with silicon carbide (SiC) particulates. The investigations indicated that

* The elastic modulus decreases with increasing particle allowing a damage parameter to be identified,

* The macroscopic fracture is initiated by the SiC plastic clusters present in the composites,

* The matrix within the clusters is subjected to high levels of tri-axial stress due to the constraints exerted on the matrix by the surrounding particles and

* Elastic misfits and final fracture is produced by crack propagation through the matrix between the clusters.

Gad et al. [27] proposed an integrated numerical model to investigate the effects of volume fraction and particulate size on the deformation and failure behaviors of PRMMC's. These numerical models were studied in the framework of random microstructure-finite element analysis. It extended damage models, and Johnson cook plasticity to simulate the elastoplastic behavior and cracking of the A359 matrix material respectively. Surface-based CZM was employed to model the A359-SiC interphase decohesion. Lastly, the proposed model was implemented into ABAQUS/explicit/ software in parallel with DIGIMAT software. This predicted that failure was with a good argument with experimental data in the forms of true stress-strain curves and failure shape. The result shows that the probability of fracture of silicon carbide particles increases by rising its volume fraction, whereas the damage mechanism starts with matrix cracking at low volume fraction.

Gad et al. [28] stated that the mechanical properties of materials are greatly affected by the occurrence of the first damage during the loading process. Thus based on the random microstructure-based model, a computational FE model is proposed to explore the deformation behavior and the damage analysis of PRMMC's. The models worked under tensile loading accounting for all positive failure modes. These are Johnson-cook constitutive relation and ductile fracture model used to model the matrix plastic deformation and cracking respectively. The cohesive zone method was adopted to simulate the particle-interfacial de-bonding and an elastic-brittle cracking model was used to simulate the particle fracture. In addition, an extensive parametric study explored the effects of a single particle shape and combinations of different particle shapes on the damage of A359/SiC particulate composites. The results show that:-

* The predominant failure mechanism in the composite reinforced with

    - Low corner angle was the brittle cracking of the particles /triangular and square/ -Whereas high corner angle particles (circular and hexagonal) were the ductile cracking in the matrix.

* Increase in corner angle of SiC particle shows an increase in the ultimate tensile strength and elongation of the composites.

* Whereas triangular shaped SiC particle causes an early stage particle fracture phenomenon.

2.7. Analysis Models of Particulate Reinforced MMC's

Budarpu et al. [29] studied the micro-structure modeling, deformation, and damage analysis of aluminum-based metal matrix reinforced by titanium carbide particles using peridynamic theory and experiment. They extracted the geometry of the TiC particles using the image processing method with four representative volume elements (RVE's).The results were analyzed using overall stress-strain curve, destination of equivalent stress and plastic strain distribution of damage parameter, the number of damaged interactions, and total plastic stretch of all interactions. They observed that the stress concentration happened at the sharp corners of the particles whereas the main plastic deformation happened in the matrix. In the loading process, several damage mechanisms were initiated and propagated, and finally, a principal crack was created that led to the final fracture. By comparison of the microscopic images of the fractured surface with

experimental results they noted that the developed model predicts the progressive damage behavior of composite particulates.

Zhang et al. [30] developed a FEM of PRMMC that considers grain refinement, load transfer, plastic strain gradient, thermal residual stress(strain), and damage of the matrix together. The results showed that the main reason causing the size effect is grain refinement. The strain gradient causes a higher work hardening rate for PRMMC with smaller particles. In addition, a dominant role is played by load transfer while residual strain/stress is steady.

Weng et al. [31] discussed the influence of interphase damage on the uniaxial tensile elastic-plastic behavior of MMC's reinforced by spherical or cubic particles having identical dimension and volume fraction using 3D cubic particles. The results showed that a better reinforcement effect than spherical ones were achieved. The stress which was concentrated at the edges makes them higher and reinforced composite suffers more reduction on the strength of composites than others. The spherical particle model that shows a large uniform strain when interphase damage occurs.

Wu et al. [32] developed a microstructure based model to describe the particle shape and distribution as well as the material deformation and failure behavior PRMMC's using A359/SiC as a material example. They stated that the most important factors that influence the material behavior such as particle shape, particle distribution, the particle is integrated into the modeling to gain results such as stress concentration occurs at the clustered particles, especially at the sharp corners, particle-matrix interphases, and the edges along the loading direction also particle fracture happens near its sharp corners, while matrix failure initiates around the particle crack tips and propagates to connect the micro-cracks caused by particle fracture or through the area with high stress/strain concentration/ leading to whole work piece fracture.

Castellanos et al. [33] studied the applicability of the anisotropic criterion of von misses characterizing initial yielding of (PRMMC's) with a computational micromechanics approach. The cells used in the numerical experiments consist of a representative volume element (RVE) of the material including several reinforcing particles, randomly distributed inside the RVE. The scheme developed allowed to qualitatively describe the relationship between anisotropy of the mechanical behavior and the anisotropy of the microstructure. The results show that the anisotropic criterion of von misses is a good candidate to characterize the initial yield of particulate composites.

Table 2.3 Summary of relevant works on failure analysis on particulate reinforced composites

Author name	Title of the journal	Main findings
Paknia et al. [34]	Effect of size, content and shape of reinforcements in the behavior of MMC's under tension	MMC's with rectangular particles showed highest stiffness compared to others. Principal stresses acting along the direction of applied displacement remained unchanged for all cases except MMC'S with triangular particles. The rectangular particles experienced the highest first principal stress among all other shapes. The stiffness of the MMC's depended not only on the length of the interphases but also on the state of the matrix material which is influenced by the shape, size and reinforcement content.
Gao et al. [35]	Plastic deformation and fracture behaviors in particle-reinforced aluminum composites: a numerical approach using an enhanced FEM	The stress concentration at the sharp corners of the particles resulted in the early stage of interfacial de-cohesion and particle fracture. Interfacial de-cohesion was caused by crack propagation from the particle to the interphase.
Shaima et al. [27]	Predictive computational model for damage behavior of metal matrix composites emphasizing the effect of particle size and volume fraction	The probability of fracture of SiC particles increases by rising the VF whereas the matrix cracking happens at low VF. As volume fraction of SiC increases the true strains needed for the onset of matrix cracking, particle fracture, and complete failure and reaching the UTS decrease
Yuan et al. [36]	Numerical analysis of the stress-strain distributions in the PRMMC SiC-6064 Al	Peak stress and plastic formation occurs at the interphase at some angle from the tensile axis The flow stress decreases with increasing of interfacial fracture toughness. The smaller the reinforcement aspect ratio the lower the stress in the composite
Suo et al.[37]	Numerical analysis of mechanical properties and particle cracking probability of MMC's	Under uniaxial quasi-static tensile loading, the tensile strength and failure strain of the composite gradually decrease as the aspect ratio of particles increases with unchanged volume fraction. Under a certain applied strain the probability of particle cracking shoes an increasing trend

		with an increasing of aspect ratio (AR) with unchanged volume fraction Probability of particle cracking tends to increase by increasing particle volume fraction when aspect ratio remained unchanged.

* From the summary of relevant works on failure analysis on particulates we can observe certain conditions. The particle shape, size, volume fraction and aspect ratio have a significant effect on the failure analysis of PRMMC's, which is part of our research. The stress created in the composites due to loading was studied using RVE. The RVE/representative volume element/ cells use von-misses stress values to characterize the initial yield of the particulate composite.

2.8. Failure Analysis using FE Simulation on Composite Models

Debski et al. [38] conducted a research to examine the process of composite failure using the FEM. The phenomenon of composite failure was described by the Tsai-Wu failure criterion using the commercial software suite abacus. Concluding that the total loss of columns stability in composite was preceded by failure of successive plies until the failure criterion was met in all plies of the composite failure.

Ayimerich et al. [39] studied energy-based failure models accounting for matrix and fiber intra-laminar damage and interphase cohesive elements simulation delamination at the interphase between layers to model the low-velocity impact response of multi-directional laminated plates over a wide range of impact energies. The consecutive models for both intralaminar and interlaminar damage modes were implemented into the ABACUS/explicit/ FE code through special user-written UMAT sub-routines.

Anthony et al. [40] stating the use of connecting rods in internal combustion engines by connecting the piston to the crank or crankshaft. Their objective was to optimize the existing connecting rods design by changing some design variables. Thus they modeled the connecting rod, designed and analyzed it using CATIA and ABAQUS/CAE/. The optimization was done with the same static and dynamic loading conditions for the variation of a few fatigue and stress parameters.

Ogierman et al. [41] wrote a paper which focused on the particle shape influence prediction on yield stress, effective elastic properties and stress distribution on PRMMC's by using RVE/representative volume element/ to create RVE geometry on DIGMAT FE software. The

considered shapes are shown in the figure below.in his study he investigated the elastic plastic effective properties of composites considering spherical, prismatic and cylindrical particle shapes. It was observed that cylindrical particles provide the highest stiffness and yield stress while spherical particles that gives the lowest values.

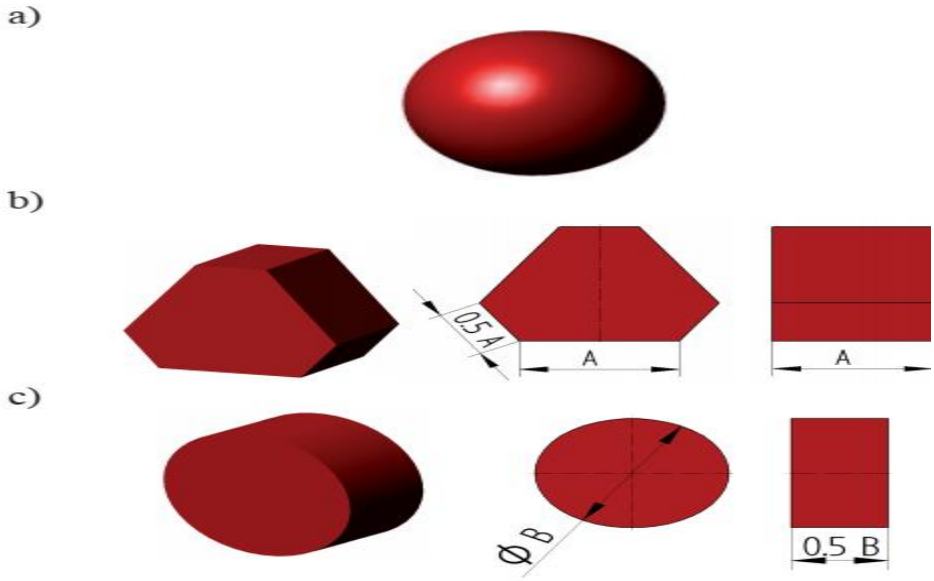

Figure 2.1 Shapes of the inclusions: a) spherical; b) prismatic; c) cylindrical [41]

Amirmelaki et al. [42] defined RVE to be a small volume of microstructure that has the general characteristics of the whole microstructure such as morphology, randomness and volume fraction of the phases. The RVE should be sufficiently large to include the essential microstructure characteristics and small as possible so that the state of stress and strain can be approximately considered as homogenous in the whole RVE.

Sahu et al. [43] developed an experimental approach on nanoparticles/GRNPS/ reinforced Al-alloy composites using the stir casting process. Furthermore, a 3D microstructure RVE model of the Al nanocomposite was generated using DIGIMAT-FE software to realize the microstructural deformation behavior under uniaxial tensile load to reveal that the experimental values are in agreement with the predicted tensile properties of the aluminum nanocomposites.

Jagadeesh et al. [44] stated that computational micromechanics starts with modeling of RVE.The RVE represents a small volume of the microstructure which has characteristics features of the entire composite such as, size, shape, and volume fraction. The most commonly used software

program for the generation of RVE'S are ABAQUS, ANSYS, DIGIMAT, and dream 3D which use mori-Tanaka's approach or modified random sequential adsorption algorithm approach or real microstructure approach for generating RVE's of composite material.

Ansar et al. [45] wrote a paper that systematically reviews the modeling techniques along with their limitations and capabilities for characterization of the micro-geometry, mechanical/thermo-mechanical/ behavior, and impact behavior of 3D woven composites. In this paper, the mechanical behavior of 3D woven composites was characterized through analytical and numerical /variational, and finite element analysis/ methods at the unit cell level or representative volume element levels.

Calarnyte et al. [46] stated that the experimental determination of stiffness and strength of textile composites is expensive and time-consuming. Thus, they proposed a FE multiscale analysis to predict the material behavior of textile composites via virtual tests. These virtual tests compared with experimental results where data were available. Finally, they simulated to prove the algorithm performance, material models, failure criteria, and softening formulations. To conclude that multiscale analysis can complement and replace experimental tests because it works reliably and offers wider possibilities.

* From the relevant work on FE simulation of composite models that aid in our research. We can observe that CATIA was appropriate in the modelling of the connecting rod that could be integrated to the FE analysis modules. The analysis of laminate composites to check failures using Tsai-Hill and Tsai-Wu criterions was done using the commercial software ABAQUS. The ABAQUS software runs using either the normal run or using special user written UMAT sub-routines. The analysis of the particulate reinforced composites was done using DIGIMAT FE software which is integrated to the ABAQUS FE .The particulate shape used in the FE analysis of PRMMC'S was the cylindrical one due to its provision of the highest stiffness and yield stress.

2.9. AMMC Connecting Rods

Connecting rods are essential components of an automobile IC engine used to convert the linear motion of the piston stroke into a rotational motion of the crankshaft and vise-versa by being an intermediate link. In addition, transfers lubricating oil between the two structures [47].

These connecting rods consist of a long shank, a big end, and a small end. The cross-section of the shank could be circular, tabular, I-section, and rectangular section, where I-section used for high-speed engines used in all automobiles while a circular one is being used for low-speed [48].

Naik et al. [49] stated that the automobile engine connecting rod is a high-volume production and critical component. Thus most researches were being done to redesign a connecting rod to have lightweight properties that bear all the stress applied to it. The lightness of the rod helps in keeping the inertial forces as small as possible. In addition, they acknowledged that numerous compressive and tensile loads are acting on the connecting rod due to fuel consumption so that failures can occur. These developed loads are due to engine operation influenced by the weight of the connecting rod.

Andoko et al. [50] explored connecting rods with metal matrix composites by selecting aluminum as a matrix and silicon carbide as a reinforcement to replace the steel connecting rod. This connecting rod was modeled using CATIA software using dimensions obtained to design the connecting rod as per properties of the aluminum matrix and various percentage combinations of reinforcements. Finally, they analyzed the connecting rod for stress and total deformation in the Ansys workbench.

Lastly Babu et al. [51] stated that connecting rods used in internal combustion engines are subjected to millions of stresses impacted. Even though these composite connecting rods are lighter and may offer better mechanical properties than conventional ones, their design still presents crucial technical challenges. Thus, they modeled and analyzed the composite connecting rods using CATIA V5 and ABACUS software to predict the structural and thermal behavior of connecting rods using 3D FEM. It was confirmed that even though the performance is the same as the standard connecting rods, the stress and thermal analysis of the AMC's connecting rods are better than the connecting rods.

2.10. Gaps in the Literatures

- ➔ Although researchers suggest the applicability of aluminum-silicon carbide composites in connecting rods due to the needed properties of the matrix and reinforcements. Distinctive simulation and models for further studies were insufficient.
- ➔ Comparative research between laminate reinforcements with particulate reinforcements were rarely found but rather focused on individual characterization.
- ➔ The effect of the connecting rod models as well as fem analysis methods /tools used/ were low as such various connecting rod models could be found.
- ➔ Most studies which show what varying the volume fraction for the laminates with different orientations, as well as, particulates bring about in changing the performance of the composite were insufficient for failure prediction and analysis. But, rather for mechanical characterization.

Chapter Three

3. Materials and Methods

3.1. Materials

3.1.1. Selected Materials and their Properties

Since the early 19's the preferred material for production of automobile and airplane parts had been aluminum, especially the AA6xxx aluminum alloy series in which magnesium and silicon are the principal alloying elements. Thus this material has gained particular interest [52]. The AA6061 is chosen because it is the most versatile alloy among the 6xxx series in addition its ease in extrusion, good mechanical properties, formability and machinability that is generally suitable for medium to high strength requirements and good toughness. The reinforcement silicon carbide (SiC) which is also known as carborundum has good thermal and mechanical properties [5]. The comparable density of SiC to that of aluminum in addition to their exceptional tribological and mechanical properties makes them the typical choice of materials for various functionalities in structural, aviation, automobile, manufacturing and defense industries.

Basic material properties of the matrix and reinforcements are given in the Table 3.1 as:-

Table 3.1 Mechanical properties of AA6061-SiC [53][54]

Property	Symbol	Units	AA6061	SiC
Density	ρ_c	g/cc	2.7	3.21
Longitudinal Elastic Modulus	E_c	GPA	70	137
Poisson's Ratio	v_{12}	-	0.33	0.37
Shear Modulus	G_{12}	GPA	26	51
Ultimate Tensile Strength	$(\sigma^T)_{ult}$	MPA	310	1625
Ultimate Compressive Strength	$(\sigma^C)_{ult}$	MPA	142	1395
Coefficient Of Thermal Expansion	$\propto$	$10^{-6}/_{c^o}$	23.2	11
Ultimate In-Plane Shear Strength	$(\tau_{12})_{ult}$	MPA	26.0	1300
Tensile strength	σ	MPA	115	345

* Information provided by The Aluminum Association, Inc. from Aluminum Standards and Data 2000 and/or International Alloy Designations and Chemical Composition Limits for Wrought Aluminum and Wrought Aluminum Alloys (Revised 2001).

3.1.2. Automobile Connecting Rod Datasheet

The material is selected to be a connecting rod made of aluminum (AA6061) reinforced with silicon carbide (SiC). Thus, to model the connecting rod a suitable Toyota vitz automobile was selected which is well known for their reliability, durability, exceptional fuel consumption and less cost along with great engine performance. They are popular in Ethiopia due to the stated features and small body side suitable in city environment [55].

Car type: -1999 Toyota Vitz I 1.5 VVT-I 16V (109HP) Automatic

Bore * stroke = 75 * 84.7 mm

Compression ratio = 10.5

Maximum power = 109 HP at 6000rpm

Maximum torque = 143 Nm at 4200rpm

Density of petrol = 740 kg/m^3 [56]

Molecular weight of petrol = 114.228g/mol

Mass of petrol= density * volume = 740 * 0.001496 = 1.10704 kg

Ideal gas constant R=8.3143 J/mol.k

3.2. Numerical Modelling and Analysis Methods for the Laminate Reinforced Composite

Step 1- The aluminum AA6061 matrix reinforced with silicon carbide (SiC) laminates are modelled using rule of mixtures to determine the density, young's modulus, tensile and compressive strength [57].

Density of the composite was calculated using equation (6) as:-

$$\rho_c = \rho_m V_m + \rho_f V_f \quad (6)$$

Young's modulus of the composite was calculated using equation (7) as:-

$$E_c = E_m V_m + E_f V_f \quad (7)$$

Tensile and compressive strength of the composite was calculated using equation (8) as:-

$$\sigma_{C,T} = \sigma_m V_m + \sigma_f V_f \quad (8)$$

Shear modulus of the composite was calculated using equation (9) as:-

$$G_{12_C} = G_{12_m} V_m + G_{12_f} V_f \quad (9)$$

Poisson's ratio of the composite was calculated using equation (10) as:-

$$v_{12_C} = v_{12_m} V_m + v_{12_f} V_f \quad (10)$$

Ultimate in-plane shear strength was calculated using equation (11) as:-

$$(\tau_{12})_C = (\tau_{12})_m V_m + (\tau_{12})_f V_f \quad (11)$$

Co-efficient of thermal expansion was calculated using equation (12) as:-

$$\alpha_c = \left(\alpha_m E_m v_m + \alpha_f E_f v_f\right) \Big/ \left(E_m v_m + E_f v_f\right) \quad (12)$$

The equations above use (5,10,15,20,25,30) percent volume fraction of SiC reinforcement to determine the density, young's modulus and other important mechanical properties.

➔ An example of this analysis for 5 % reinforcements are shown as:-

$$\rho_c = (2.7 * 0.95) + (3.21 * 0.05) = 2.7255 \ {}^{g}/_{cc}$$

$$E_c = (70000 * 0.95) + (137000 * 0.05) = 73{,}350\text{Mpa}$$

$$(\sigma^T)_C = 310(0.95) + 1625(0.05) = 375.75\text{Mpa}$$

$$(\sigma^C)_C = 142(0.95) + 1395(0.05) = 204.65\text{Mpa}$$

$$\alpha_c = \left(23.2 * 70000 * 0.95 + 11 * 137000 * 0.05\right) \Big/ \left(70000 * 0.95 + 137000 * 0.05\right)$$

$$= 22.0606\text{Mpa}$$

$$v_{12_C} = 0.33(0.95) + 0.37(0.05) = 0.332$$

$$(\tau_{12})_C = 26000(0.95) + 1300(0.05) = 24{,}765\text{Mpa}$$

$$G_{12_C} = 207(0.95) + 51000(0.05) = 2746.65\text{Mpa}$$

The results for the other reinforcement volume fraction are shown in chapter 4

Step 2- The thickness of the connecting rod is calculated by the Rankine formula. But first, it is important to note that the connecting rod has generally three parts: pin end, crank end and long shank. The shank can be tabular, circular. H-section, I-section [58]. The selected is an I-section which is used for high-speed engine as well as easier to analyze.

The thickness of the I-section of the connecting rod could be calculated by using either Rankine or Euler formula. But, since the Euler formula is valid for long columns and does not give a reliable result for short column and length of column intermediate between very long to short, the Rankine formula is selected [59]. The Rankine formula is shown in equation 13 as:-

$$w_B = \frac{(\sigma_c * A_c)}{(1 + \alpha(\frac{l}{k_{xx}})^2} \quad (13)$$

It is also known Buckling load w_B = maximum gas force $*$ factor of safety FOS = 4

The Rankine constant was calculated by equation (14):-

$$\text{Rankine constant } (\alpha) = \frac{(\sigma_c)}{(\pi^2 * E)} \quad (14)$$

From gas equation [60] Design strength (P) is taken to be gas pressure obtained from the following equation 15:-

$$pv = m * R_{specific} * T \quad (15)$$

$$R_{specific} = \frac{8.3143}{0.114228} = 72.78688$$

Temperature (T) in the combustion chamber is calculated in equation 16 as [61] page 3:-

$$r = (T_{Burn}/T_{Normal})^{\frac{1}{2}*(\gamma-1)} \quad (16)$$

Where:- r = Compression Ratio (10.5) T_{Burn}=Temperature at Combustion (variable)

T_{Normal}=Room Temperature (300^{o}k) Then T_{Burn} is calculated to be 1968.21k

But, metal parts of the engine cannot be allowed to get this hot as steel melts at 1644 k, and aluminum alloys melt at about 922 k. Therefore, modern automotive engines have intricate cooling systems designed to keep the metal surfaces in and around the combustion chamber at much lower temperatures [62]. The following examples detail the typical temperatures of various combustion-related engine parts during normal operation:-

Intake valve: 519 k Exhaust valve: 922 k Spark plug: 866 k Piston face: 574 k

Cylinder wall: 463 k [62]

Thus we take the temperature at the piston face for our calculation of design strength 574k

Then design strength (P) is calculated as:-

$$p = \frac{1.10704 * 72.78688 * 574}{0.001496} = \frac{46{,}251.764}{0.001496} = 31\text{Mpa}$$

$$\text{Maximum Gas Force } (F_c) = \frac{\pi(D_{bore})^2 p}{4} \quad (17)$$

$$= \frac{\pi(75)^2 * 31}{4} = \frac{547{,}815.2}{4} = 136{,}953\text{N}$$

$$w_B = 136953 * 4 = 547{,}812\text{N}$$

Step 3- Determination of dimension of the connecting rod including thickness

The standard dimension of the I-section is given in figure 3.2 as [63]: -

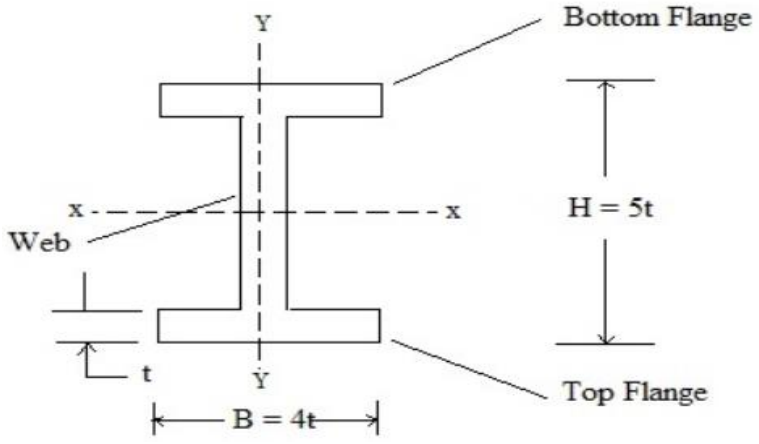

Figure 3.1 Geometric dimensions of the I-section

Width of the section was calculated by equation (18) as:-

$$B = 4t \tag{18}$$

Depth of the section was calculated by equation (19) as:-

$$H = 5t \tag{19}$$

Area of the section was calculated by equation (20) as:-

$$A = 2(4t * t) + (5t - 2t) * t = 8t^2 + 3t^2 = 11t^2 \tag{20}$$

Height of the big end=$H_2(\text{crank end})$ was calculated by equation (21) as :-

$$1.1H \text{ to } 1.25H \tag{21}$$

Height of the small end= $H_1(\text{piston end})$ was calculated by equation (22) as :-

$$0.9H \text{ to } 0.75H \tag{22}$$

Moment of inertia about X-axis was calculated by equation (23) as :-

$$I_{xx} = \frac{1}{12}(4t)(5t)^3 - \frac{1}{12}(4t - t)(5t - 2t)^3 = \frac{1}{12}(500t^4 - 81t^2)$$

$$I_{xx} = \left(\frac{419}{12}\right)t^4 = 34.91t^4 \tag{23}$$

Radius of gyration of cross section xx was calculated by equation (24) as :-

$$k_{xx} = \sqrt{\frac{I_{xx}}{A}} = \frac{34.91t^4}{11t^2}$$

$$\sqrt{3.17t^2} = 1.781t \tag{24}$$

➔ An example of thickness determination for 5% VF of reinforcement is shown as:-

$$547{,}812N = {(\sigma_c * A_c)} \Big/ {(1 + a(\frac{l}{k_{xx}})^2}$$

$$(\alpha_1) = \frac{375.75}{\pi^2(73350)} = 0.000519$$

$$547{,}812\text{N} = \frac{(375.75 * 11\text{t}^2)}{1 + 0.000519(\frac{169.4}{1.781\text{t}})^2} \qquad \text{t} = 11.708\text{mm}$$

Width of the section $\text{B} = 4\text{t} = 4 * 11.708 = 46.832\text{m}$

Height of the section $\text{H} = 5\text{t} = 5 * 11.708 = 58.54\text{mm}$

Area of the section $\text{A} = 11\text{t}^2 = 11 * 11.708^2 = 1507.84\text{mm}^2$

Height of the big end=H_2(crank end) 1.1H to 1.25H $= 1.1 * 58.54 = 64.394\text{mm}$

Height of the small end= H_1(piston end) 0.9H to 0.75H $= 0.75 * (58.54) = 43.905\text{mm}$

The remaining dimensions for the other volume fraction of reinforcements are shown in chapter 4 section.

Step 4- Calculation of the compliance matrix as well the transformed compliance matrix of the composite is done using excel

The compliance matrix is given by equation (25): -

$$\begin{bmatrix} \epsilon_1 \\ \epsilon_2 \\ \gamma_{12} \end{bmatrix} = \begin{bmatrix} S_{11} & S_{12} & 0 \\ S_{12} & S_{22} & 0 \\ 0 & 0 & S_{66} \end{bmatrix} = \begin{bmatrix} \sigma_1 \\ \sigma_2 \\ \tau_{12} \end{bmatrix} \tag{25}$$

Where these are the only five constants. The orthotropic compliances in terms of the elastic constants were given as:-

$$S_{11} = \frac{1}{E_1}; \quad S_{22} = \frac{1}{E_2}; \quad S_{12} = S_{21} = -\frac{V_{21}}{E_2} = -\frac{V_{12}}{E_1}; \quad S_{66} = \frac{1}{G_{12}}$$

The transformed compliance matrix was given by equation (26):-

$$\overline{S_{11}} = S_{11}\cos^4{}_\theta + (2S_{12} + S_{66})\sin^2\theta\cos^2\theta + S_{22}\sin^4{}_\theta \tag{26}$$

$$\overline{S_{12}} = S_{12}(\sin^4{}_\theta + \cos^4{}_\theta) + (S_{11} + S_{22} - S_{66})\sin^2{}_\theta\cos^2{}_\theta$$

$$\overline{S_{22}} = S_{11}\sin^4{}_\theta + (2S_{12} + S_{66})\sin^2{}_\theta\cos^2{}_\theta + S_{22}\cos^4{}_\theta$$

$$\overline{S_{16}} = (2S_{11} - 2S_{12} - S_{66})\sin\theta\cos^3{}_\theta - (2S_{22} - 2S_{12} - S_{66})\sin^3{}_\theta\cos\theta$$

$$\overline{S_{26}} = (2S_{11} - 2S_{12} - S_{66})\sin^3{}_\theta\cos\theta - (2S_{22} - 2S_{12} - S_{66})\ \sin\theta\cos^3{}_\theta$$

$$\overline{S_{66}} = 2(2S_{11} + 2S_{22} - 4S_{12} - S_{66})\sin^2{}_\theta\cos^2{}_\theta + S_{66}(\sin^4{}_\theta + \cos^4{}_\theta)$$

Expressed in the form using equation 27:-

$$\begin{bmatrix} \epsilon_x \\ \epsilon_y \\ \gamma_{xy} \end{bmatrix} = \begin{bmatrix} \overline{S_{11}} & \overline{S_{12}} & \overline{S_{16}} \\ \overline{S_{12}} & \overline{S_{22}} & \overline{S_{26}} \\ \overline{S_{16}} & \overline{S_{26}} & \overline{S_{66}} \end{bmatrix} \begin{bmatrix} \sigma_x \\ \sigma_y \\ \tau_{xy} \end{bmatrix} \quad (27)$$

* The results of the analysis could be found at the Appendex-I

Step 5- The determination of local strain and local stress

The local strain is calculated in equation 28 as:-

$$\begin{bmatrix} \varepsilon_1 \\ \varepsilon_2 \\ \gamma_{12} \end{bmatrix} = \begin{bmatrix} (\cos\theta)^2 & (\sin\theta)^2 & (2\sin\theta\cos\theta) \\ (\sin\theta)^2 & (\cos\theta)^2 & -(2\sin\theta\cos\theta) \\ -(\sin\theta\cos\theta) & (\sin\theta\cos\theta) & (\cos\theta^2 - \sin\theta)^2 \end{bmatrix} \begin{bmatrix} \varepsilon_x \\ \varepsilon_y \\ \gamma_{xy} \end{bmatrix} \quad (28)$$

The local stress is given by the equation 29 below.

$$\begin{bmatrix} \sigma_1 \\ \sigma_2 \\ \tau_{12} \end{bmatrix} = \begin{bmatrix} (\cos\theta)^2 & (\sin\theta)^2 & (2\sin\theta\cos\theta) \\ (\sin\theta)^2 & (\cos\theta)^2 & -(2\sin\theta\cos\theta) \\ -(\sin\theta\cos\theta) & (\sin\theta\cos\theta) & (\cos\theta^2 - \sin\theta)^2 \end{bmatrix} \begin{bmatrix} \sigma_x \\ \sigma_y \\ \tau_{xy} \end{bmatrix} \quad (29)$$

* The results for the local strain and local stress which was analyzed using Microsoft excel are found in chapter 4

Step 6- Prediction of failure in the laminate composite using Tsai-Hill and Tsai-Wu criterions [23].

Tsai-Hill criterion was expressed in equation 30 as:-

$$\left[\frac{\sigma_1}{(\sigma_1{}^T)_{ult}}\right]^2 - \left[\frac{\sigma_1\sigma_2}{(\sigma^T{}_1)^2{}_{ult}}\right] + \left[\frac{\sigma_2}{(\sigma^T{}_2)_{ult}}\right]^2 + \left[\frac{\tau_{12}}{(\tau_{12})_{ult}}\right]^2 \leq 1 \quad (30)$$

The Tsai-Wu criterion was expressed in equation 31 as:-

$$H_1\sigma_1 + H_2\sigma_2 + H_6\tau_{12} + H_{22}{\sigma_2}^2 + H_{66}{\tau_{12}}^2 + 2H_{12}\sigma_1\sigma_2 \leq 1 \quad (31)$$

The co-efficient for the local stresses are calculated as:-

$$H_1 = \frac{1}{(\sigma_1{}^T)_{ult}} - \frac{1}{(\sigma_1{}^T)_{ult}} \qquad H_2 = \frac{1}{(\sigma_2{}^T)_{ult}} - \frac{1}{(\sigma_2{}^C)_{ult}} \qquad H_6 = 0$$

$$H_{11} = \frac{1}{(\sigma_1{}^T)_{ult}(\sigma_1{}^C)_{ult}} \qquad H_{22} = \frac{1}{(\sigma_2{}^T)_{ult}(\sigma_2{}^C)_{ult}} \qquad H_{66} = \frac{1}{(\tau_{12})_{ult}{}^2}$$

$$H_{12}A = -\frac{1}{2(\sigma_1{}^T)_{ULT}{}^2} \qquad \text{as per Tsai} - \text{Hill}$$

$$H_{12}B = -\frac{1}{2(\sigma_1{}^T)_{ULT}(\sigma_1{}^C)_{ULT}} \qquad \text{as per Hoffman}$$

Finally error percentage is calculated by comparing the numerical results with the fem simulation using equation 32 as:-

$$\%\ \text{Error} = \left(\frac{\text{Hand Calculation} - \text{FEM Simulation}}{\text{FEM Simulation}}\right) * 100\% \tag{32}$$

3.3. Numerical Modelling and Analysis Methods for the Particulate Composites

Step 1- The aluminum AA6061 matrix reinforced with silicon carbide (SiC) particulates were modelled using Halpin-Tsai equations to determine the density, young's modulus, tensile and compressive strength given in equation (33-39) [64]:-

$$E_c = \frac{E_m(1+\xi\eta V_r)}{1-\eta V_r} \tag{33}$$

$$\eta = \frac{\left(E_r/E_m\right)-1}{\left(E_r/E_m\right)+\xi} \tag{34}$$

$$\xi = 2s \tag{35}$$

$$(\sigma_{ult})_c = \frac{\sigma_m(1+\xi\eta V_r)}{1-\eta V_r} \tag{36}$$

$$\eta = \frac{(\sigma_r/\sigma_m)-1}{(\sigma_r/\sigma_m)+\xi} \tag{37}$$

$$(G_{12})_c = \frac{E_m(1+\xi\eta V_r)}{1-\eta V_r} \tag{38}$$

$$\eta = \frac{\left(G_r/G_m\right)-1}{\left(G_r/G_m\right)+\xi} \tag{39}$$

The equations above use (5,10,15,20,25,30) percent volume ration of SiC reinforcement to determine the density, young's modulus and other important parameters using 0.6 and 1.8 aspect ratio. The aspect ratios of 0.6 and 1.8 were selected because they are the minimum and maximum values in most researches [64]. Additionally the values obtained from the intermediate aspect ratios in the ranges found between yielded similar values which failed to show the effect of varying volume fraction in the analysis of PRMMC's.

➔ An example of this analysis for 5 % reinforcements with 0.6 aspect ratio is shown as:-

$$\xi = 2s = (2 * 0.6) = 1.2$$

$$\eta = \frac{\left(E_r/E_m\right) - 1}{\left(E_r/E_m\right) + \xi} = \frac{\left(137000/70000\right) - 1}{\left(137000/70000\right) + 1.2} = 0.303$$

$$E_c = \frac{70000(1 + (1.2 * 0.303 * 0.05))}{1 - (0.303 * 0.05)} = 72{,}370\text{Mpa}$$

$$\eta = \frac{\left(\sigma_r/\sigma_m\right) - 1}{\left(\sigma_r/\sigma_m\right) + \xi}$$

$$\eta = \frac{\left(1625/310\right) - 1}{\left(1625/310\right) + 1.2} = 0.658$$

$$(\sigma_{ult})_c = \frac{\sigma_m(1 - \xi\eta V_r)}{1 - \eta V_r}$$

$$(\sigma_{ult})_c = \frac{310(1 + (1.2 * 0.658 * 0.05)}{1 - (0.658 * 0.05)} = 333.2\text{MPa}$$

$$\eta = \frac{\left(G_r/G_m\right) - 1}{\left(G_r/G_m\right) + \xi}$$

$$\eta = \frac{\left(51000/207\right) - 1}{\left(51000/207\right) + 1.2} = 0.9911$$

$$(G_{12})_c = \frac{E_m(1+\xi\eta V_r)}{1-\eta V_r}$$

$$(G_{12})_c = \frac{207\left(1+(1.2*0.05*0.9911)\right)}{1-(0.9911*0.05)}$$

$$= 230.743\text{MPa}$$

* The results for the other reinforcement volume fraction are shown in chapter 4

Step 2- The thickness of the connecting rod is calculated by the Rankine formula.

$$w_B = {(\sigma_c * A_c)}\Big/{(1+\alpha(\frac{l}{k_{xx}})^2}$$

Then thickness is calculated as:-

$$547{,}812\text{N} = {333.2*11t^2}\Big/{1+0.000467(\frac{169.4}{1.781t})^2}$$

$$t = 12.392\text{mm}$$

Then:-

Width of the section $B = 4t = 49.568\text{mm}$

Height of the section $H = 5t = 61.96\text{mm}$

Area of the section $A = 11t^2 = 1689.178\text{mm}^2$

Height of the big end $H_2(\text{crank end})$ $H_2 = 1.1H = 68.156\text{mm}$

Height of the small end $H_1(\text{piston end})$ $H_1 = 0.75H = 46.47\text{mm}$

* The remaining dimensions for the other volume fraction of reinforcements are shown in chapter 4 section.

Step 3- The representative volume element./RVE/ analysis of the composite is done using Digimat software.

3.4. Geometric Model of the Connecting Rod

Being one of the integral parts of an engine, the connecting rod design must withstand higher loads and transmit a great deal of power. The connecting rods smaller end is connected to the piston while the bigger end is connected to the crankshaft using crank pin journal [40]. There are various designs of the connecting rod available, each one have their own distinctive features that differentiate them from each other. But from the design of various connecting rods observed one can see that there are similarities in the middle section of the connecting rods. The middle section of the connecting rod could be I-section, H-section, circular section etc [57]. I-section middle is considered for the connecting rod since it has a higher value of section modulus and gives a higher moment of inertia.

The Geometric model of the connecting rod used for analysis adopted the works of Sebastian et al.[40],Rinju et al.[57] and retail catalogues. The big end bore diameter(43mm) and the small end bore diameter (17.98mm) were taken as a common element in the connecting rod design while the cross section was designed considering the analysis found in chapter 3 and chapter 4.

But there are certain differences between the designed laminate reinforced and particulate reinforced models.

- ➔ The laminate reinforced connecting rod models used sharp corners and avoided fillets wherever possible. These design is chosen because it makes the failure prediction of the laminate possible using ABAQUS. The ABAQUS software which needed to be partitioned for meshing using hexagonal element shape mesh which is structured. The only type of mesh that worked for the connecting with chamfered ends as the previous works was a tetrahedron and wedge element shape. These intern failed to give outputs for failure prediction.
- ➔ The particulate reinforced connecting rod models were modelled with a ninety nine percent similarity to the previous works.
- ➔ The negligible merits of using the suggested design for connecting rod application is sustenance of lesser stress under loading. Additionally since the suggested connecting rod can be partitioned for hexagonal element size enabled certain analysis and prediction outputs which could not be computed using the tetrahedron element meshing of the works

under consideration which was done for the particulate reinforced composites. But since the failure prediction was done using Von-Mises stress for particulate reinforced metal matrix composites, these problem is resolved.

A

B

Figure 3.2 Comparison of A) Actual [57], B) Developed Connecting Rod Models

3.5. FEM Modelling and Analysis Methods (ABAQUS)

The ABAQUS software suite is used for computer aided engineering (CAE) and finite element analysis (FEA).The product suit offers powerful and complete solutions for both sophisticated and routine engineering problems covering a vast spectrum of industrial applications. For example in the automotive industry engineering work groups could consider various loading parameters using a common model data structure and integrated solver technology [65]. Thus in analysis of connecting rod failure prediction this software was used from the CATIA connecting rod model which was analyzed using Tsai-Hill and Tsai-Wu criterion platforms in its module given in the steps below.

Step 1 - The connecting rod was modelled using CATIA software with dimensions like thickness, height, width, height of the piston end, height of the crank end and total length obtained from the analysis (eqn.18 to 22).

Step 2 – The connecting rod models from CATIA were imported to ABAQUS software for FEM analysis.

Step 3 - After the model import was completed. The property module was selected to add essential material properties like density and elastic modulus. Which, were obtained using rule of mixtures for the laminates (eqn.6 to 12) and Halpin-Tsai method (eqn.33 to 39) for the particulate reinforced composite.

Step 4 - The section toolbar from the property module was selected to insert thickness and ply orientation (0^o, 30^o, 45^o, 90^o) as a continuum shell composite type

Step 5 - The section assignment toolbar was selected to assign the essential properties defined in step 3 and step 4 into the connecting rod model.

Step 6 - The step module was selected to create a static, general analysis step with a general procedure type

Step 7 - The created step was edited to select an additional Cfailure component to the default values already defined like- S, stress components and invariants-stresses

E, total strain components-strains

U, translations and rotations

RF, reaction forces and moments-forces/reactions

Cfailure, failure measure components

Step 8 - The load module was selected

Step 9 - The boundary conditions manager from the load module was selected to fix the crankshaft end and identify the load application area (piston end)

Step 10 - The pressure type load is selected for application at the piston end with a magnitude from the maximum gas force which is 136,953N.this value was determined using equation 17.

Step 11 - The mesh module was selected

Step 12 - The partition cell toolbar was selected to define a cutting plane for the connecting rod model.

Step 13 - The seed part toolbar was used to select sizing controls. The approximate global size 3 which was automatically defined by the software was used. Here it is important to note that these is the lowest possible size to fulfil the finer mesh for a better analysis scenario.

Step 14 - The element type toolbar was selected to use the standard element library with a continuum shell family on a linear geometric order.it is given a code SC8R which means an 8-node quadrilateral in-plane general purpose continuum shell, reduced integration with hourglass control finite membrane strains.

Step 15 - The hex type element shape is automatically selected for a finer mesh from the mesh controls toolbar

Step 16 - The connecting rod model is meshed

Step 17 - The job module was selected and a job with a certain name is created for the full analysis.

Step 18 - The created job was submitted for analysis which runs for the needed output variables in step 7.

Step 19 - The completed job is observed from the results in the visualization module to obtain the needed results.

Step 20 - The results are saved and the job completed.

3.6. FEM Modelling and Analysis Methods (DIGIMAT)

Today's major challenge is the shift from the metal to composite for the composite for the improved mechanical properties. Thus DIGIMAT provides tools that give the user hundred percent confidence in their composite product design thanks to an accurate description of the local composite behavior. The DIGIMAT software lets engineers perform both macro and micro-scale analysis of composites to predict their performance and calculate their thermal, electrical and mechanical properties for use in all sorts of downstream FEA analysis.in these research DIGIMAT FE was used to generate a realistic representative volume element /RVE/ for the AA6061-SiC composite microstructure in particulate reinforcement which allows to describe the microstructure of the AA6061-SiC composites [66].

The steps for the FEA modelling of the composites were given as:-

Step 1 - The DIGMAT software was opened and the FE modelling was selected

Step 2 - The analysis module was selected to define the general parameters like:-

-Name

-Material modeler--DIGMAT FE

-FE code--ABAQUS/standard

-Analysis type--mechanical

-RVE type--3D

Step 3 - The material module was selected to add the density young's modulus and poison's ratio of the matrix and the reinforcement independently.

Step 4 - The microstructure module was selected to define:-

-The phase name and phase material for the matrix

-The phase name, phase type/inclusion/, phase material for the particulate reinforcement

- Volume fraction (5, 10, 15, 20, 25, 30) %

-Inclusion/particulate shape/-cylindrical

-Aspect ratio/0.6 and 1.8/

Step 5 - The RVE module was selected to create a single layer analysis type.

Step 6 - The geometry is generated in the RVE module

Step 7 - The RVE is meshed with an automatic element size definition which is the default setting and C3D10M element type which is the automatic fine mesh settings of the DIGIMAT software

Step 8- The mechanical loading module is selected with an automatic digimat loading source

Step 9 - The solution module is selected with an automatic parasolid geometric file format

Step 10 - The export button is selected which saves the parameters from step 1 to step 9 into a python script

Step 11- The ABAQUS software is opened to run the phyton script

Step 12 - The job module is selected to create a job which is submitted for analysis

Step 13 - The results of the analysis are observed and saved for further analysis.

Chapter Four

4. Results and Discussions

4.1. Introduction

This chapter includes the results and discussions on the failure prediction of AA6061-SiC composite connecting rods for use in Toyota Vitz automobile which was modelled by varying the volume fraction at (5,10,15,20,25,30) percent. It modelled the laminate reinforced composites with (0,30,45,90) degree orientation and particulate reinforced composite with (0.6,1.8) aspect ratio. The failure prediction was done using Tsai-Hill and Tsai-Wu criterions for the laminates and Von-Mises stress simulative values for the particulates. Additionally, analysis of particulate reinforcements was done using RVE (representative volume element) using DIGIMAT. Which, was integrated into the ABAQUS software. The comparison of the analytical results with the FE simulation ones was done using error percentage.

4.2. Numerical Modeling and FEA of the AA6061-SiC Laminate Composites

4.2.1. Numerical Modeling and Analysis

The combined properties of AA6061-SiC determined using rule of mixtures from equation 6 to equation 12 is given in table 4.1 as:-

Table 4.1 Combined material properties for the AA6061-SiC laminate

	5%	10%	15%	20%	25%	30%
$\mathbf{E_c}$	73,350	76,700	80,050	83,400	86,750	90,100
$(\boldsymbol{\sigma^T})_C$	375.75	441.5	507.25	573	638.75	704.5
$(\boldsymbol{\sigma^C})_C$	204.65	267.3	329.95	392.6	455.25	517.9
$\boldsymbol{\alpha_c}$	22.06	21.02	20.06	19.19	18.383	17.634
$\mathbf{v_{12_C}}$	0.332	0.334	0.336	0.338	0.34	0.342
$(\boldsymbol{\tau_{12}})_C$	24,765	23,530	22,295	21,060	19,825	18,590
$\mathbf{G_{12_C}}$	2746.65	5286.3	7825.95	10365.6	12905.25	15444.9
$\boldsymbol{\rho_c}$	2.7255	2.751	2.7761	2.802	2.8275	2.853

The mechanical properties such as density, elastic modulus, ultimate tensile strength, ultimate compressive strength and shear modulus of the laminate reinforced AMMC increase while the ultimate in-plane shear strength and coefficient of thermal expansion decrease as the reinforcement volume fraction increase. This property is further validated by Song et al. [67] on the same materials that exhibit the increase in mechanical properties like yield strength and tensile strength that indicate the improvement of these properties as the volume fraction increase but degrade the plasticity of the composites.

The dimensions of the connecting rod with the laminate SiC reinforcement VF calculated by using equation 18 to 22 on Microsoft excel is given in table 4.2 as:-

Table 4.2 Geometric dimension of laminate reinforced AA6061-SiC composite connecting rod

Geometric Dimensions	5%	10%	15%	20%	25%	30%
Thickness (t) (mm)	11.70	10.85	10.18	9.63	9.17	8.79
Width(b)(mm)	46.83	43.42	40.72	38.53	36.70	35.16
Height(H)(mm)	58.54	54.27	50.91	48.16	45.88	43.95
Area(A) (mm^2)	1507.84	1296.14	1140.47	1020.74	926.18	850.05
Crank end(H2)(mm)	64.39	59.70	56.00	52.98	50.46	48.34
Piston end(H1)(mm)	43.90	40.70	38.18	36.12	34.41	32.96

From table 4.2 it could be observed that the thickness, width and other important dimensions of the connecting rod decrease as the reinforcement volume fraction increase due to the increase in mechanical properties of the material owing to the inclusion of carbides in the soft AA6061 matrix which increased the mechanical properties of the connecting rod but decrease the ductility [68][69].

The resulting AA6061-SiC connecting rod with 5% volume fraction of SiC laminate reinforcement which was modelled using CATIA is shown in figure 4.1 as:-

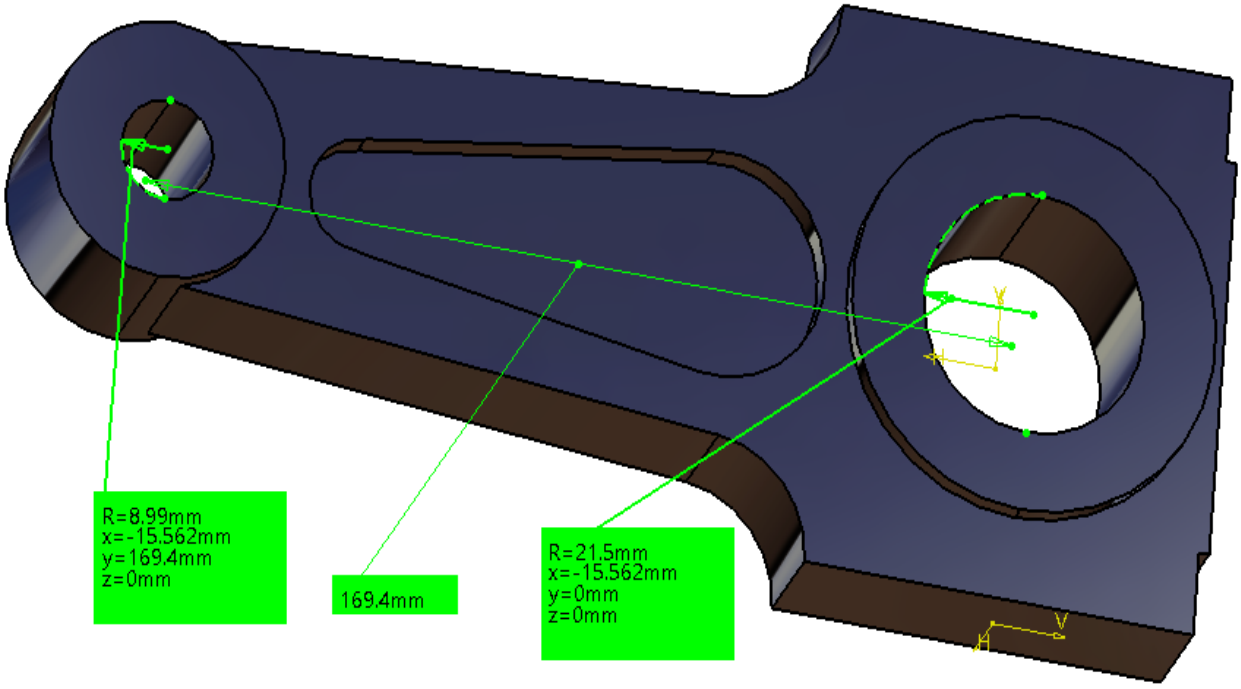

Figure 4.1 CATIA modelled AA6061-SiC laminate reinforced connecting rod

The results for local strains calculated using equation 28 on Microsoft excel are given from table 4.3 to table 4.6 as:-

Table 4.3 Local strain values for 0^o orientation

Volume Fraction	ε_1	ε_2	γ_{12}
5%	0.0004111	0	0.03255
10%	0.0004601	0	0.01966
15%	0.0005040	0	0.01508
20%	0.0005437	0	0.01230
25%	0.0005795	0	0.01124
30%	0.0006115	0	0.01023

The calculated local strain ε_1 increases as the reinforcement volume fraction increase, constant zero in ε_2 while the shear strain γ_{12} decrease as the reinforcement volume fraction increase. The stress in the e_1 increase because when the composite is loaded it strongly constrains the laminate reinforcement because of the strong bond between them and thus higher stress is needed to cause

the same deformation as the composite with less reinforcements. But when we come to table 4.4 to 4.6 we do not obtain the same results even though the concept is the same this is due to the effect of orientation on the strain of the composite.

Table 4.4 Local strain values for 30^o orientation

Volume Fraction	ε_1	ε_2	γ_{12}
5%	0.002480	-0.001325	0.001574
10%	0.002530	-0.001243	0.001131
15%	0.002672	-0.001267	0.0009950
20%	0.002688	-0.001225	0.0007910
25%	0.002964	-0.001364	0.0009107
30%	0.003096	-0.001414	0.0008987

Table 4.5 Local strain values for 45^o orientation

Volume Fraction	ε_1	ε_2	γ_{12}
5%	0.001915	-0.0009039	-0.008267
10%	0.002135	-0.001008	-0.004996
15%	0.002330	-0.001101	-0.003836
20%	0.002391	-0.001123	-0.003235
25%	0.002659	-0.001258	-0.002864
30%	0.002797	-0.001325	-0.002607

Table 4.6 Local strain values for 90^o orientation

Volume Fraction	ε_1	ε_2	γ_{12}
5%	-0.001238	0.0004111	-0.03255
10%	-0.001377	0.0004601	-0.01966
15%	-0.001500	0.0005040	-0.01508
20%	-0.001608	0.0005437	-0.01230
25%	-0.001704	0.0005795	-0.01124
30%	-0.001788	0.0006115	-0.01023

The calculated local strain ε_1 decreases as the reinforcement volume fraction increases while the local strain ε_2 and shear strain γ_{12} increases as the reinforcement volume fraction increases.

The results for local stress calculated using equation 29 on Microsoft excel are given from table 4.7 to 4.10 as:-

Table 4.7 Local stress and shear stress values for 0^o orientation

Volume Fraction	σ_1	σ_2	τ_{12}
5%	0	-90.82	89.42
10%	0	-105.66	103.96
15%	0	-120.08	118.07
20%	0	-134.17	127.49
25%	0	-147.86	145.18
30%	0	-161.10	158.13

The calculated local stress σ_1 is zero throughout, σ_2 decreases while τ_{12} increases as the reinforcement volume fraction increases. When the results on table 4.7 to 4.10 are observed in comparison to the local strain results we could say the addition of reinforcements increases the stress of the AA6061-SiC composite connecting rod except the 0 degree and 90 degree orientation that yield different results.

Table 4.8 Local stress and shear stress values for 30^o orientation

Volume Fraction	σ_1	σ_2	τ_{12}
5%	54.73	-145.56	5.38
10%	63.61	-169.27	6.22
15%	72.23	-192.31	7.04
20%	76.86	-211.03	5.65
25%	88.76	-236.62	8.56
30%	96.66	-257.77	9.30

The calculated local stress σ_1 and shear stress τ_{12} increases as the reinforcement volume fraction increases while σ_2 decreases.

Table 4.9 Local stress and shear stress values for 45^o orientation

Volume Fraction	σ_1	σ_2	τ_{12}
5%	44.01	-134.83	-45.41
10%	51.12	-156.79	-52.83
15%	58.03	-178.11	-60.04
20%	60.41	-194.58	-67.08
25%	71.24	-219.11	-73.93
30%	77.57	-238.68	-80.55

The calculated local stress σ_1 increases while σ_2 and shear stress τ_{12} decreases as the reinforcement volume fraction increases.

Table 4.10 Local stress and shear stress values for 90^o orientation

Volume Fraction	σ_1	σ_2	τ_{12}
5%	-90.82	0	-89.42
10%	-105.66	0	-103.96
15%	-120.08	0	-118.07
20%	-134.17	0	-127.49
25%	-147.86	0	-145.18
30%	-161.10	0	-158.13

The calculated local stress σ_1 and shear stress τ_{12} decreases as the reinforcement volume fraction increase. But σ_2 is zero throughout.we can also observe that the shear stress values for zero degree and ninety degree orientation are similar, while the σ_1 and σ_2 for zero degree is equal to the σ_2 and σ_1 stress values for ninety degree because the reverse properties of both angles.

The Tsai-Hill criterion values calculated using equation 30 on Microsoft excel are given in table 4.11 as:-

Table 4.11 Tsai-Hill criterion analysis values

Volume Fraction	Tsai-Hill 0^0	Tsai-Hill 30^0	Tsai-Hill 45^0	Tsai-Hill 90^0
5%	0.05844	0.7173	0.5895	0.1969
10%	0.05729	0.5725	0.4696	0.1562
15%	0.056072	0.4876	0.3994	0.1324
20%	0.05486	0.4122	0.333	0.1168
25%	0.05364	0.3908	0.3194	0.1055
30%	0.05237	0.3594	0.2935	0.0968

The results are expressed in figure 4.2 as:-

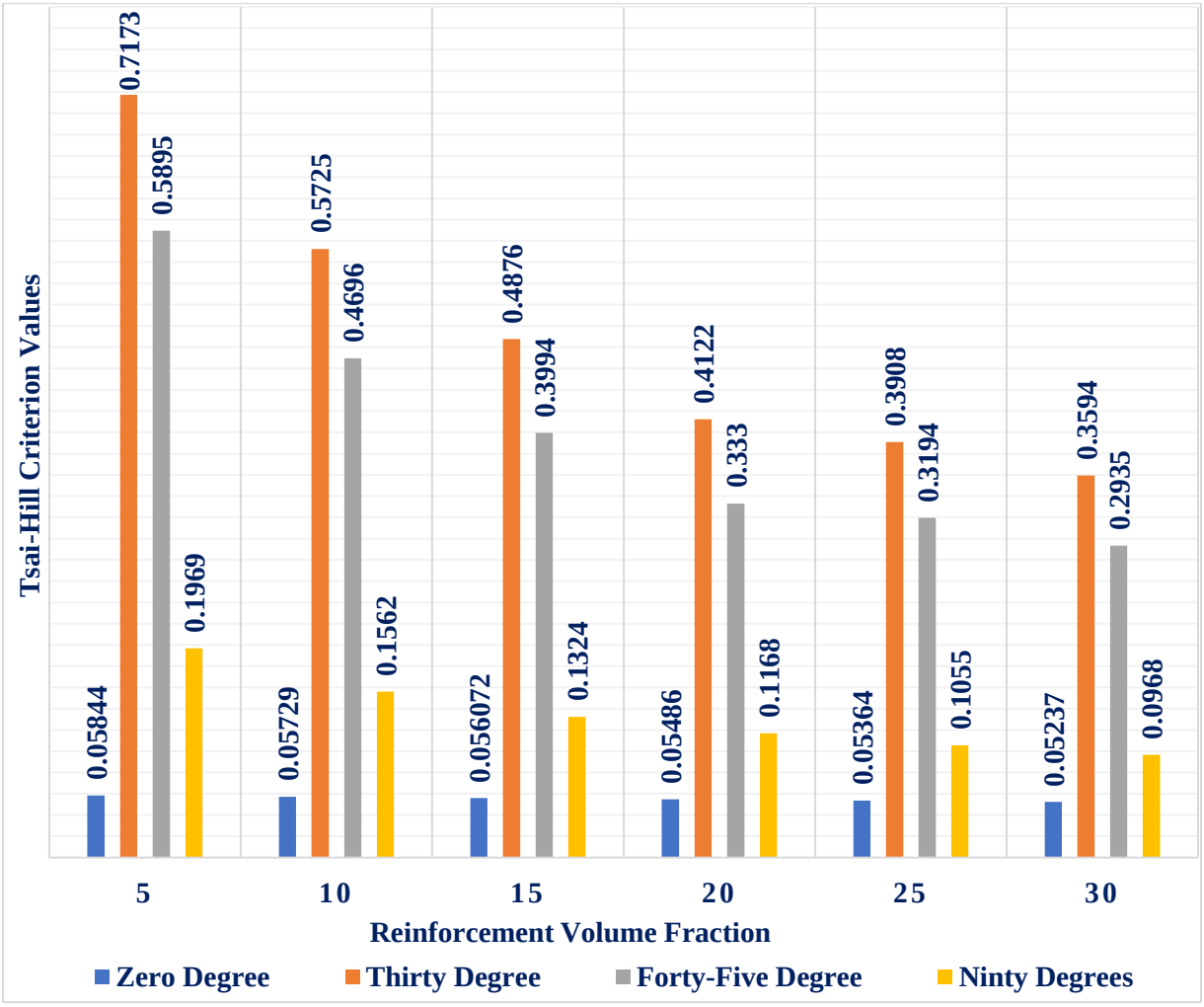

Figure 4.2 Analysis values (Tsai-Hill criterion vs Reinforcements)

From the results of numerical analysis in table 4.11 and figure 4.2 for Tsai-Hill criterion failure prediction model. It was observed that all the results have values less than one. Thus have not failed. The Tsai-Hill criterion values decreased as the volume fraction of reinforcement increased. The highest values were found at 30^{o} orientation followed by 45^{o} laminate orientation. While, the lowest values were found at 0^{o} degree orientation preceded by 90^{o} laminate orientation. Specifically the connecting rod model with 5 % volume fraction and 30^{o} laminate orientation had the highest values. While, the connecting rod models with 30% volume fraction at 0^{o} laminate orientation had the lowest values. It is important to note that the Tsai-Hill criterion considers either tensile load or compressive load but not both in its analysis depending on the values of local stress determined using equation 29 from table 4.7 to 4.10

The Tsai-Wu criterion values calculated using equation 31 on Microsoft excel considering the Tsai-Hill and Hoffman local-stress coefficient are given in table 4.12 and 4.13 as:-

Table 4.12 Tsai-Wu criterion analysis values as per Tsai-hill local-stress coefficient

Volume Fraction	Tsai-Wu 0^0	Tsai-Wu 30^0	Tsai-Wu 45^0	Tsai-Wu 90^0
5%	0.3093	0.573	0.5057	0.3093
10%	0.2505	0.48831	0.4275	0.2505
15%	0.2133	0.4333	0.37706	0.2133
20%	0.1876	0.3812	0.3279	0.1876
25%	0.1685	0.3644	0.3141	0.1685
30%	0.1536	0.3403	0.2923	0.1536

Table 4.13 Tsai-Wu criterion analysis values as per Hoffman local-stress coefficient

Volume Fraction	Tsai-Wu 0^0	Tsai-Wu 30^0	Tsai-Wu 45^0	Tsai-Wu 90^0
5%	0.3093	0.6202	0.5408	0.3093
10%	0.2505	0.5243	0.4543	0.2505
15%	0.2133	0.4623	0.3986	0.2133
20%	0.1876	0.4039	0.3443	0.1876
25%	0.1685	0.3851	0.3295	0.1685
30%	0.1536	0.3584	0.3057	0.1536

The results were expressed in figure 4.3 as:-

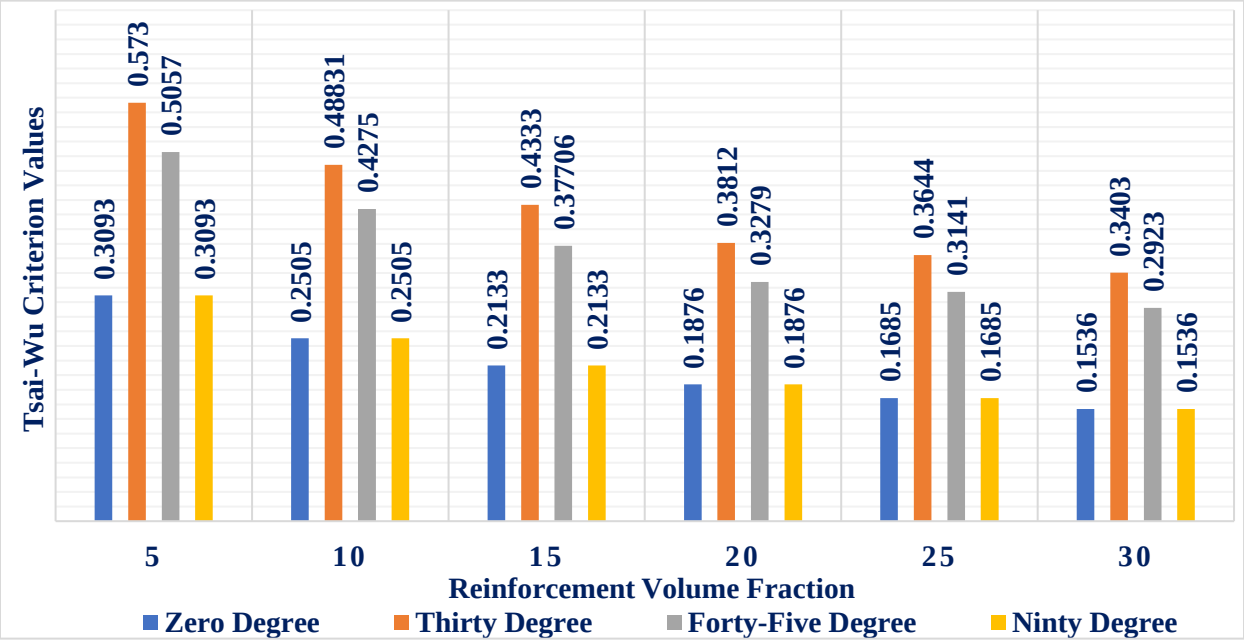

Figure 4.3 Analysis values (Tsai-Wu criterion vs Reinforcements)

Table 4.12 and Table 4.13 as well as figure 4.3 show the Tsai-Wu criterion failure prediction values for the modelled connecting rod. It is observed that the obtained results have values less than one that indicate the models have not failed. The Tsai-Wu criterion values decreased as the volume fraction of reinforcements increased. The laminate with 0^o and 90^o orientation showed similar values for both Hoffman and Tsai-Hill local stress co-efficient. Furthermore the values for 30^o and 45^o laminate orientation for the Hoffman local stress coefficient were higher than the Tsai-hill local stress co-efficient. The highest values were found 30^o orientation followed by 45^o orientation. While, the least values were found in both 0^o and 90^o orientation. Specifically the connecting rod models with 5% volume fraction at 30^o laminate orientation showed the highest values. While, the 30% volume fraction at 0^o and 90^o orientation showed the lowest values. The higher value ranges observed had been due to the consideration of both tensile and compressive forces in the analysis.

4.2.2. FEM Simulation

FEM simulation results computed using ABACUS for 5% VF AA6061-SiC connecting rod with 0^o laminate orientation is given in figure 4.4 as:-

A

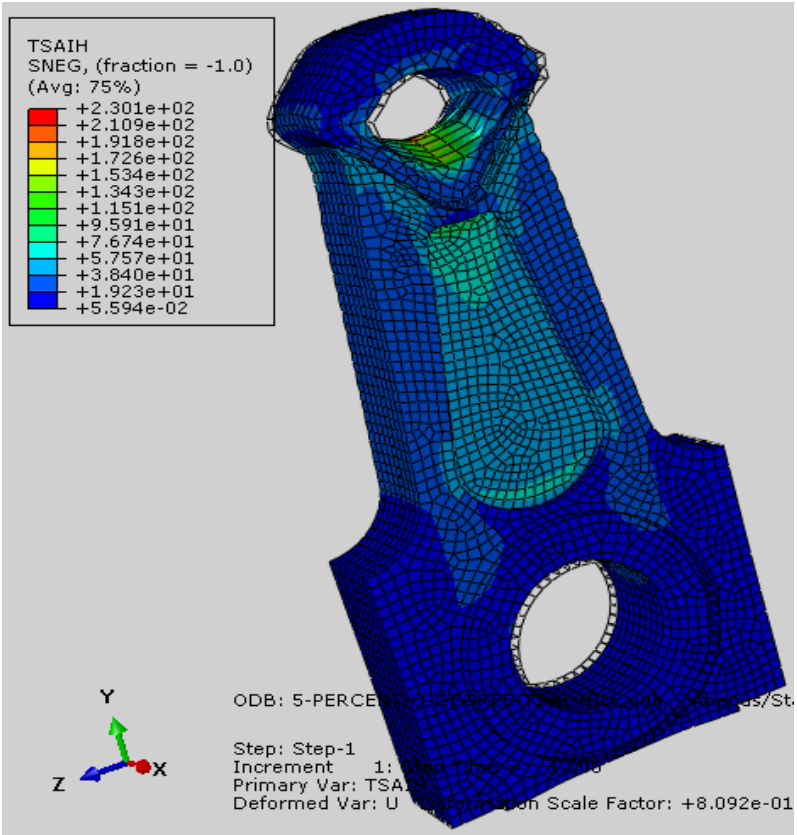

B

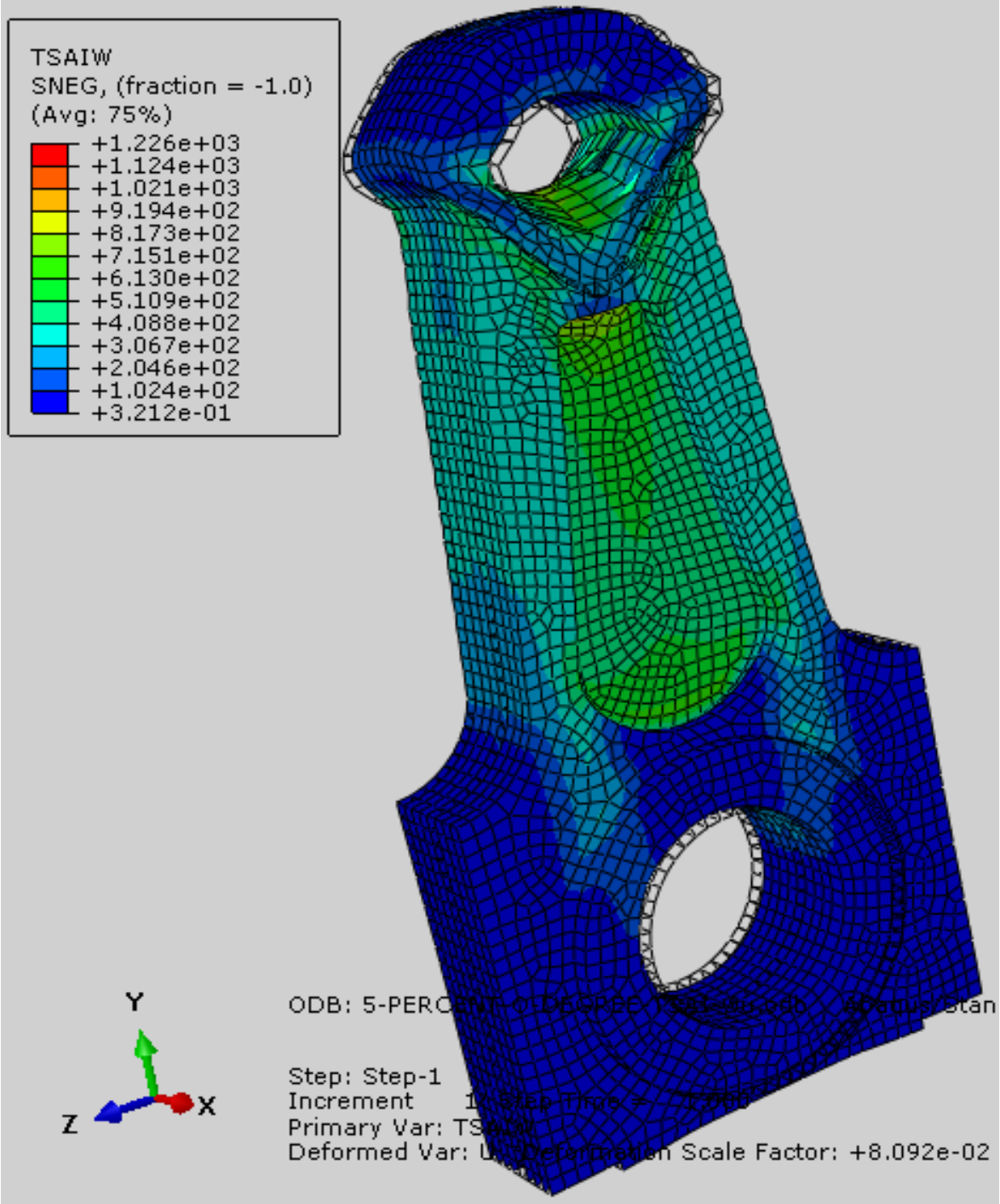

Figure 4.4 FEM simulation values of Tsai-Hill (A) and Tsai-Wu (B) criterion

The figure 4.4 shows Tsai-Hill and Tsai-Wu citerion values for connecting rod fem models with 5% volume fraction and 0^{o} laminate orientation.Additional results could be found at the appendex.An observation of the results indicated that the connecting rod models changed from bulky to thin and rigid as the volume fraction increased.Stress could be seen to be concentrated at

the corners ,the middle cross section and load application areas.The 30º laminate orientation twisted as the load was applied.While,the rest deformed normally in the direction of load application.Additionally the connecting rod models with lower volume fraction showed unwanted results of defoemation at load application areas of piston head.From figure 4.4 as well as results in the appendex failure is predicted to occur at the piston head near the cross section as well as connecting rod with 30º laminate orientation.

The minimum of the above results including of that of (30, 45 and 90) degree SiC reinforcements is expressed in table 4.14 as:-

Table 4.14 FEM simulation results for Tsai-Hill criterions

Volume Fraction	Tsai-Hill 0º	Tsai-Hill 30º	Tsai-Hill 45º	Tsai-Hill 90º
5%	0.05594	0.7348	0.5429	0.1915
10%	0.05454	0.565	0.4409	0.164
15%	0.05302	0.5022	0.4083	0.1358
20%	0.0532	0.3948	0.3163	0.1217
25%	0.05205	0.3678	0.3287	0.1085
30%	0.04981	0.3399	0.3062	0.09402

The tabular results are expressed in figure 4.5 as:-

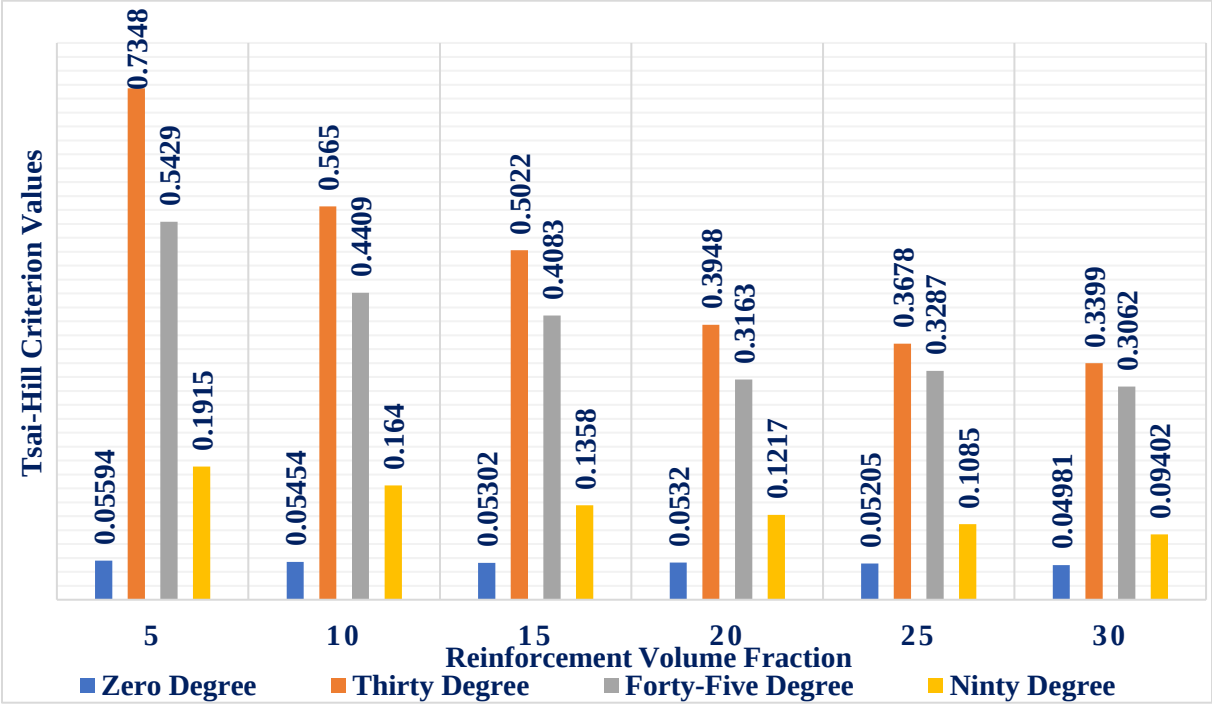

Figure 4.5 FEM values (Tsai Hill vs Reinforcements)

Table 4.14 and figure 4.5 the Tsai-Hill criterion values of the fem modelled connecting rod.it is observed that the Tsai-Hill criterion values decreased gradually with slight fluctuation at certain points. The highest range of values is found at 30^o laminate orientation followed by 45^o orientation. While, the lowest range of values is found 0^o orientation preceded by 90^o.Additionally 5% volume fraction at 30^o orientation gave the highest value while the 30% volume fraction with 90^o orientation gave the lowest values.

The FEM simulation values for the Tsai-Wu criterion was given in table 4.15 as:-

Table 4.15 FEM simulation results for Tsai-Wu criterion

Volume fraction	Tsai-Wu 0º	Tsai-Wu 30º	Tsai-Wu 45º	Tsai-Wu 90º
5 %	0.3212	0.5936	0.529	0.3212
10 %	0.2443	0.4613	0.4536	0.2443
15 %	0.2211	0.4643	0.3988	0.2025
20 %	0.1752	0.3915	0.3536	0.1755
25 %	0.1602	0.3465	0.302	0.1602
30 %	0.1517	0.3699	0.3166	0.1626

The Tabular results are expressed in figure 4.6 as:-

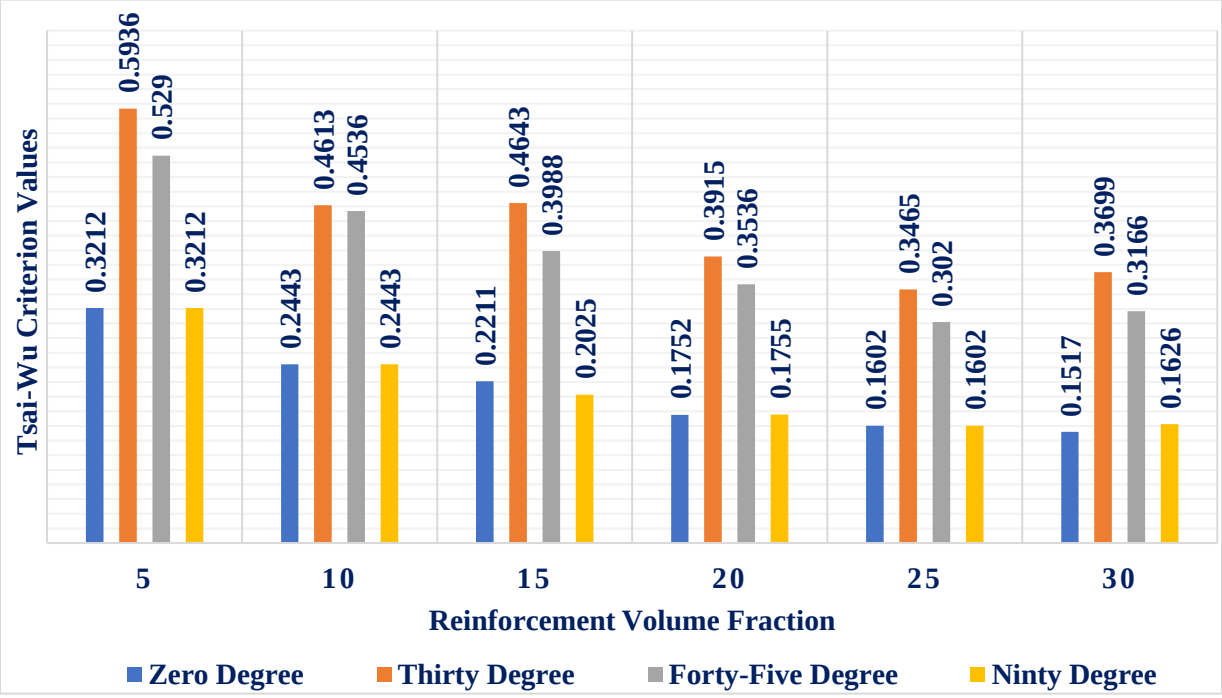

Figure 4.6 FEM values (Tsai-Wu criterion vs Reinforcements)

Table 4.15 and figure 4.6 the Tsai-Hill criterion values of the fem modelled connecting rod.it is observed that the Tsai-Hill criterion values decreased gradually with slight fluctuation at certain points. The highest range of values is found at 30^o orientation followed by 45^o laminate orientation. While, the lowest values are found in both 0^o and 90^o orientation which have approximately similar values. Additionally 5% volume fraction at 30^o orientation gave the highest values. While 30% volume fraction with at 0^o orientation gave the lowest values.

4.2.3. Error Percentage

The error percentage for the Tsai-Hill criterion calculated using equation 32 were given in table 4.16 as:-

Table 4.16 Error percentage values of Tsai-Hill criterion

Volume Fraction	0^o	30^o	45^o	90^o
5 %	4.46	2.38	8.57	2.82
10 %	5.04	1.32	6.5	4.71
15%	5.74	2.91	2.16	2.48
20%	3.12	4.4	5.27	4
25%	3.05	6.25	2.83	2.78
30%	5.13	5.72	4.13	3

The results in table 4.16 are expressed in Figure 4.7 as:-

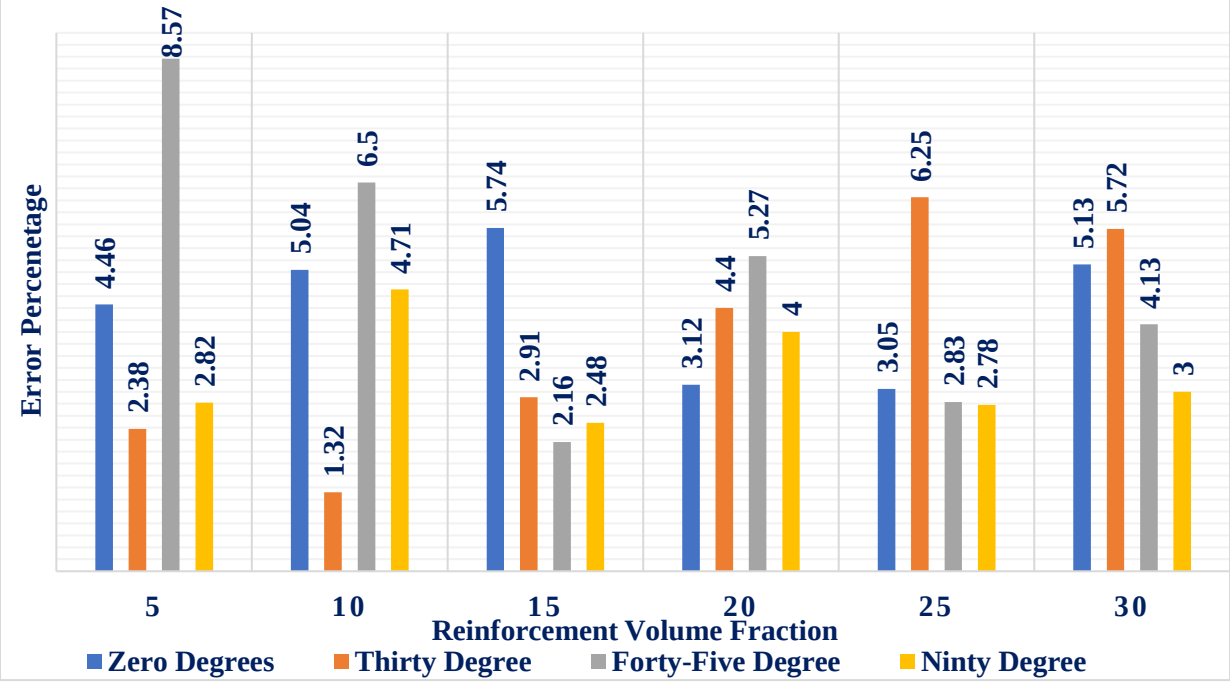

Figure 4.7 Error percentage values of Tsai-Hill criterion

From table 4.16 and figure 4.7 it could be observed that the error percentage of the Tsai-Hill criterion models is fluctuating but in the range that is less than 10%. The lowest range of error is found at 90^o laminate orientation while the highest range of errors is found at 45^o laminate orientation. The fluctuation observed in the error percentage is due to the effect of software analysis that analyzed the whole connecting rod while the numerical calculations analyzed the middle I section but still the results obtained are less than ten percent.

The Error percentage for the Tsai-Wu criterion were given in table 4.17 as:-

Table 4.17 Error percentage values of Tsai-Wu criterion

Volume Fraction	0^o	30^o	45^o	90^o
5%	3.68	3.47	4.4	3.68
10%	2.55	5.84	5.74	2.55
15%	3.5	6.67	5.45	5.34
20%	7.05	2.64	7.26	6.91
25%	5.14	5.15	4.01	5.14
30%	1.2	8	7.66	5.53

The results from table 4.17 are expressed in figure 4.8 as:-

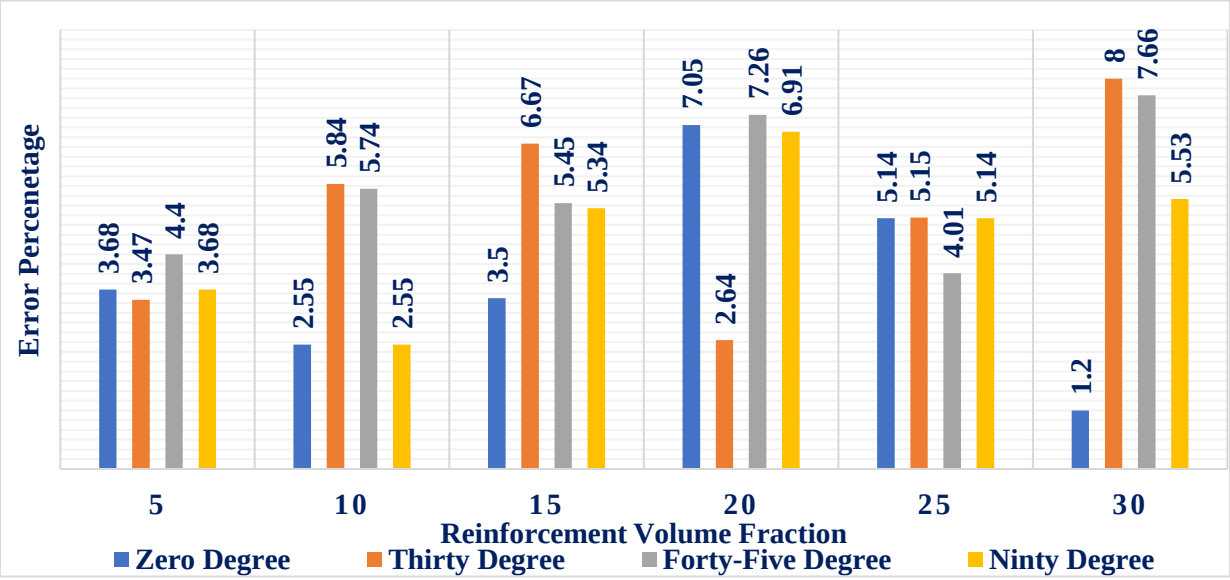

Figure 4.8 Error percentage values for Tsai-Wu criterion

From table 4.17 and figure 4.8 it can be observed that the values are fluctuating with the range less than 10 percent. The highest range of errors is found at 45^o laminate orientation while the lowest range of errors is found at 0^o laminate orientation

4.3. Numerical Modelling and FEA of the AA6061-SiC particulate composites

4.3.1. Numerical Modelling and Analysis

The combined properties of the AA6061-SiC calculated using Halpin-Tsai formula using equation 33 to 39 are given in table 4.18 and table 4.19 as:-

Table 4.18 Combined material properties for the AA6061-SiC particulate (0.6 aspect ratio)

Volume Fraction	E_C 0.6	σ_T 0.6	G_{12} 0.6	σ_C 0.6	τ_{12} 0.6	υ_{12}
5 %	72370.3	333.21	230.74	155.02	23905	0.33190
10 %	74814.7	358.07	257.10	169.18	21959	0.33381
15 %	77336.8	384.74	286.52	184.62	20146	0.33573
20 %	79940.2	413.44	319.58	201.54	18452	0.33766
25 %	82629.1	444.39	357	220.15	16867	0.33960
30 %	85407.6	477.89	399.70	240.72	15379	0.34155

Table 4.19 Combined material properties for the AA6061-SiC particulate (1.8 aspect ratio)

Volume Fraction	E_C 1.8	σ_T 1.8	G_{12} 1.8	σ_C 1.8	τ_{12} 1.8	υ_{12}
5 %	72797.1	345.04	256.14	164.19	24463	0.33195
10 %	75643.2	381.86	310.64	187.95	22966	0.33390
15 %	78539.6	420.57	371.40	213.44	21506	0.33586
20 %	81487.7	461.34	439.59	240.87	20082	0.33783
25 %	84488.9	504.34	516.65	270.45	18693	0.33980
30 %	87544.59	549.74	604.44	302.45	17337	0.34178

It can be obseved from table 4.18 and table 4.19 that the material properties of the particulate composite increases except for the shear stress that decreases as the reinforcement volume fraction increases.the justification is the same to that of the alumunium matrix reinforced by laminate silcon carbide which is an increase in volume fraction of reinforcement increases the mechanical properties of the composites.

The dimensions of the connecting rod with various percentage of reinforcement calculated using equation 18 to equation 22 is given in table 4.20 and 4.21 as:-

Table 4.20 Geometric dimensions for PR AA6061-SiC composite with 0.6 aspect ratio

Geometric Dimensions	5%	10%	15%	20%	25%	30%
Thickness (t) (mm)	12.39	11.97	11.56	11.18	10.80	10.44
Width(b)(mm)	49.56	47.88	46.27	44.72	43.22	41.78
Height(H)(mm)	61.96	59.86	57.84	55.90	54.03	52.22
Area(A) (mm2)	1689.17	1576.61	1472.25	1375.2	1284.77	1200
Crank end(H2)(mm)	68.15	65.84	63.62	61.49	59.43	57.44
Piston end(H1)(mm)	46.47	44.89	43.38	41.93	40.52	39.16

Table 4.21 Geometric dimensions for PR AA6061-SiC composite with 1.8 aspect ratio

Geometric Dimensions	5%	10%	15%	20%	25%	30%
Thickness (t) (mm)	12.18	11.61	11.09	10.62	10.19	9.79
Width(b)(mm)	48.75	46.45	44.38	42.5	40.78	39.19
Height(H)(mm)	60.94	58.07	55.48	53.12	50.98	48.99
Area(A) (mm^2)	1634.02	1483	1354.45	1241.79	1143.38	1056.22
Crank end(H2)(mm)	67.03	63.87	61.03	58.43	56.07	53.89
Piston end(H1)(mm)	45.70	43.55	41.61	39.84	38.23	36.74

From table 4.20 and 4.21 it can be observed that the thickness, width and other important dimensions decrease as the reinforcement volume fraction increases due to an increased mechanical property. Which is the same with the laminate reinforced composite.

4.3.2. FEM Simulation

For the 5% volume fraction composites with a 0.6 and 1.8 aspect ratio are given in figure 4.9 as:-

A

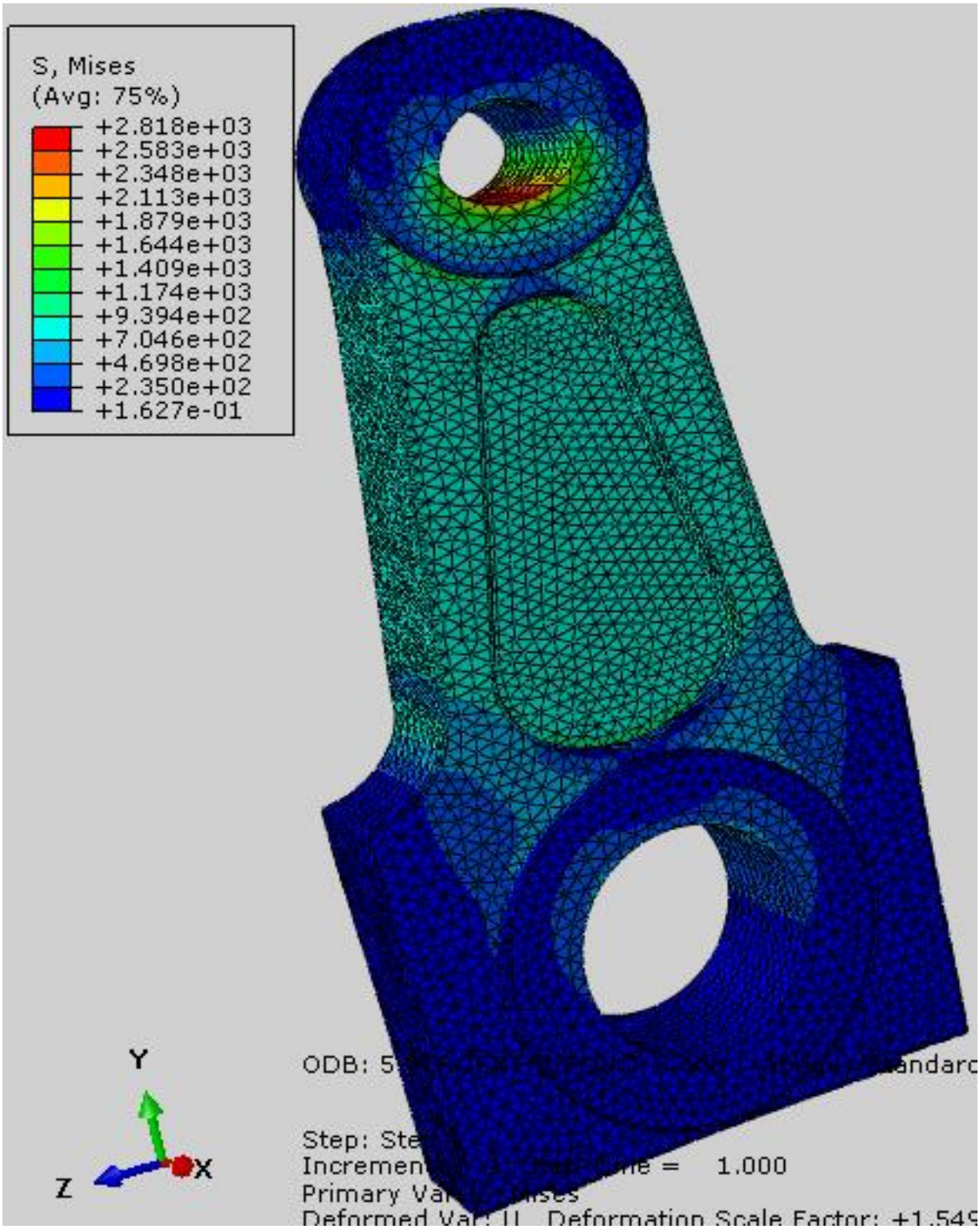

B

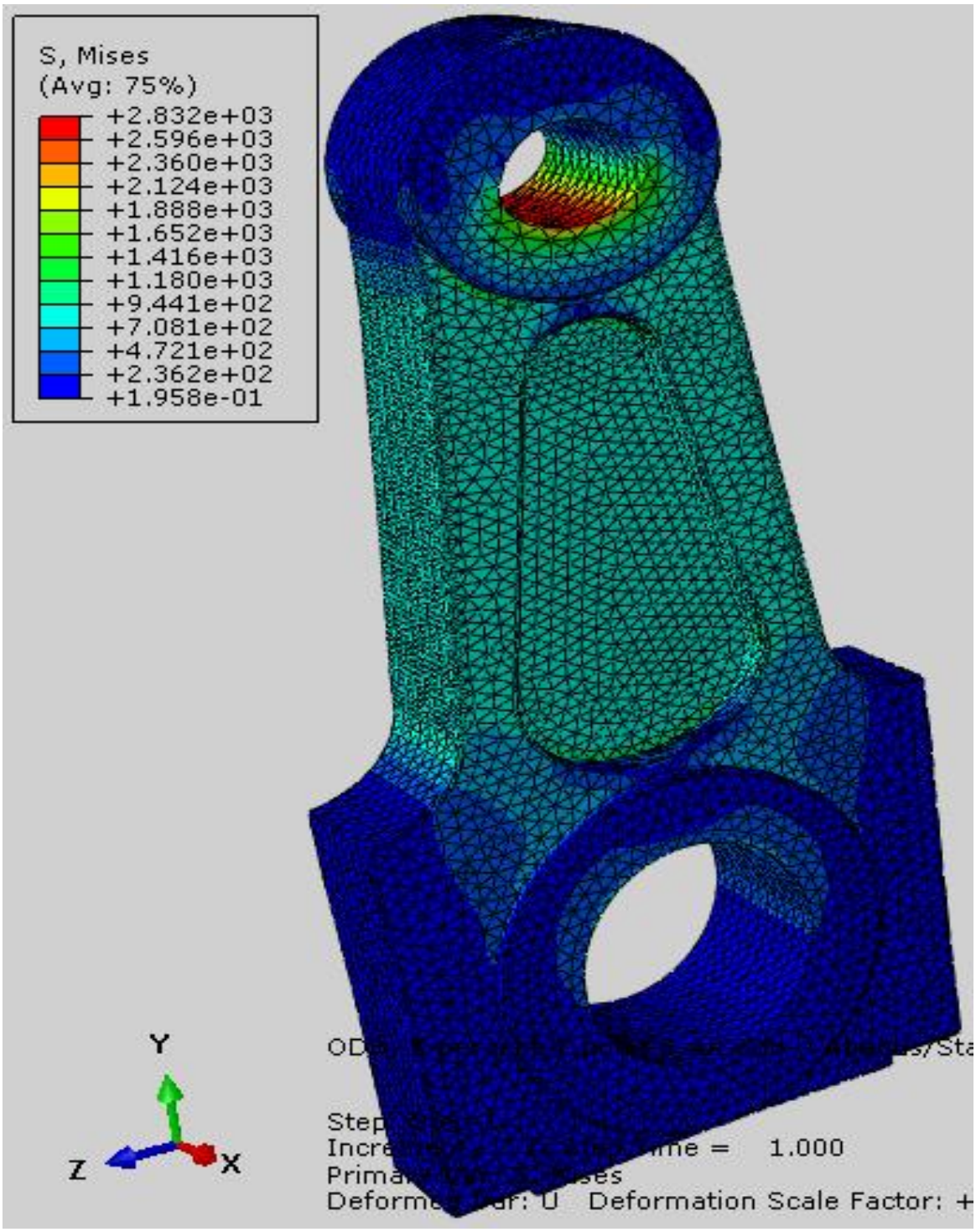

Figure 4.9 FEM values for particulate connecting rods (A) 0.6 AR (B) 1.8 AR

From figure 4.9 it could be observed that as the reinforcement volume fraction increase the middle section gets longer and rigid, Stress is seen to be concentrated at the loading area and more on the inner corners and place near to the corners.

Von-Mises stress of particulate composites from the actual modelling in ABAQUS is given table 4.22 and 4.23 as well as figure 4.10 and 4.11 as:-

Table 4.22 Von-Mises stress values for actual modelling (0.6 A.R)

	Volume Fraction	Minimum Values (MPa)	Maximum Values (MPa)
	5 %	0.1627	2817.91
	10 %	0.1399	2881.2
For 0.6 AR	15 %	0.1318	2925.88
	20 %	0.1499	2948.2
	25 %	0.1816	2999.97
	30 %	0.1354	3044

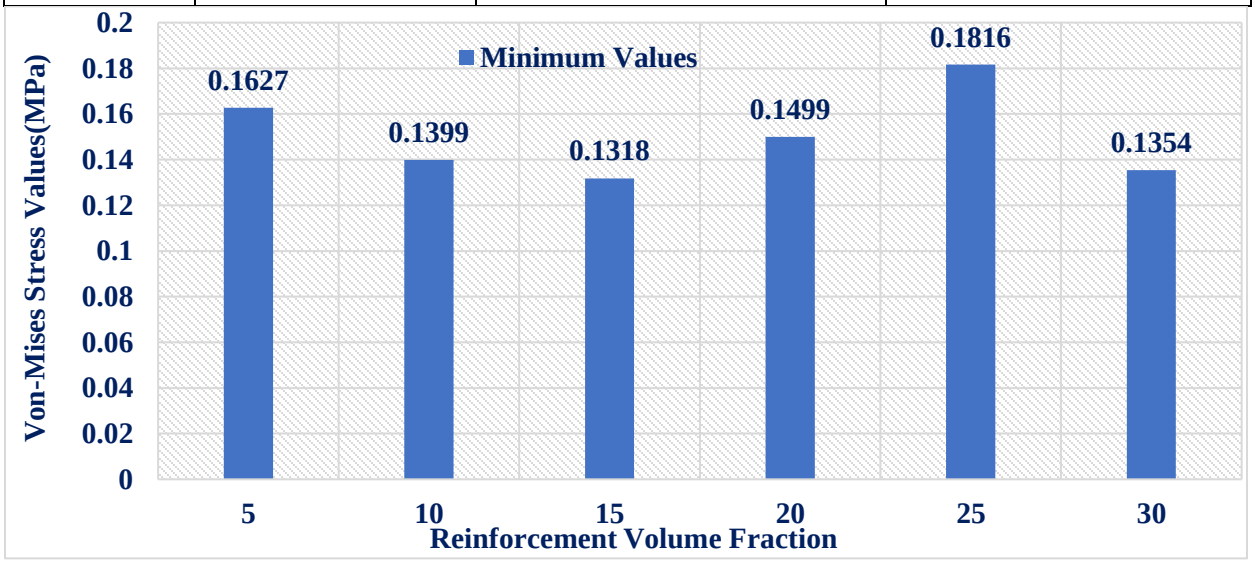

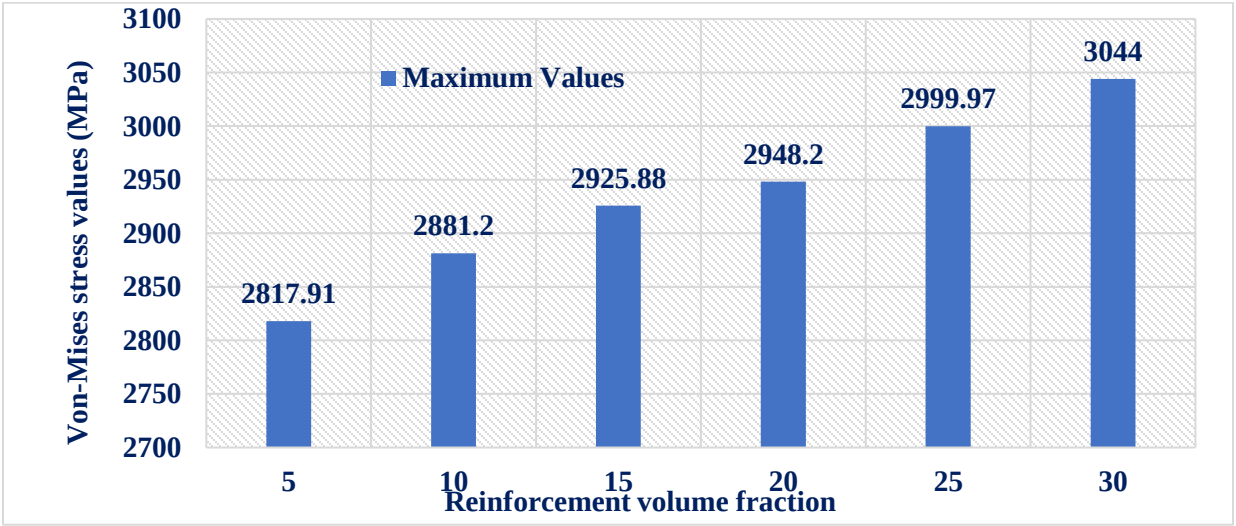

Figure 4.10 Min and Max Von-Mises stress values for (0.6 A.R)

From table 4.22 and figure 4.10 the minimum and maximum Von-Mises stress values for 0.6 AR AA6061-SiC PRMMC could be seen. The minimum Von-Mises stress values range from 0.131 to 0.181 MPa. While, the maximum values range from 2817 to 3044 MPa. A fluctuation of the results is observed the minimum values. While a steady increase could be seen in the maximum values. Additionally, the minimum Von-Mises stress values is found at the 15 percent volume fraction for the minimum and 5 percent for the maximum stress ranges. In addition,the maximum Von-Mises stress value is found at 25 percent volume fraction for the minimum stress ranges and 30 percent volume fraction for the maximum stress ranges.

Table 4.23 Von-Mises stress values for actual modelling (1.8 A.R)

	Volume Fraction	Minimum Values (MPa)	Maximum values (MPa)
	5 %	0.1958	2831.86
	10 %	0.1626	2931.61
For 1.8 AR	15 %	0.2621	2932.04
	20 %	0.1380	3045.21
	25 %	0.1893	3078.14
	30 %	0.1613	3147.84

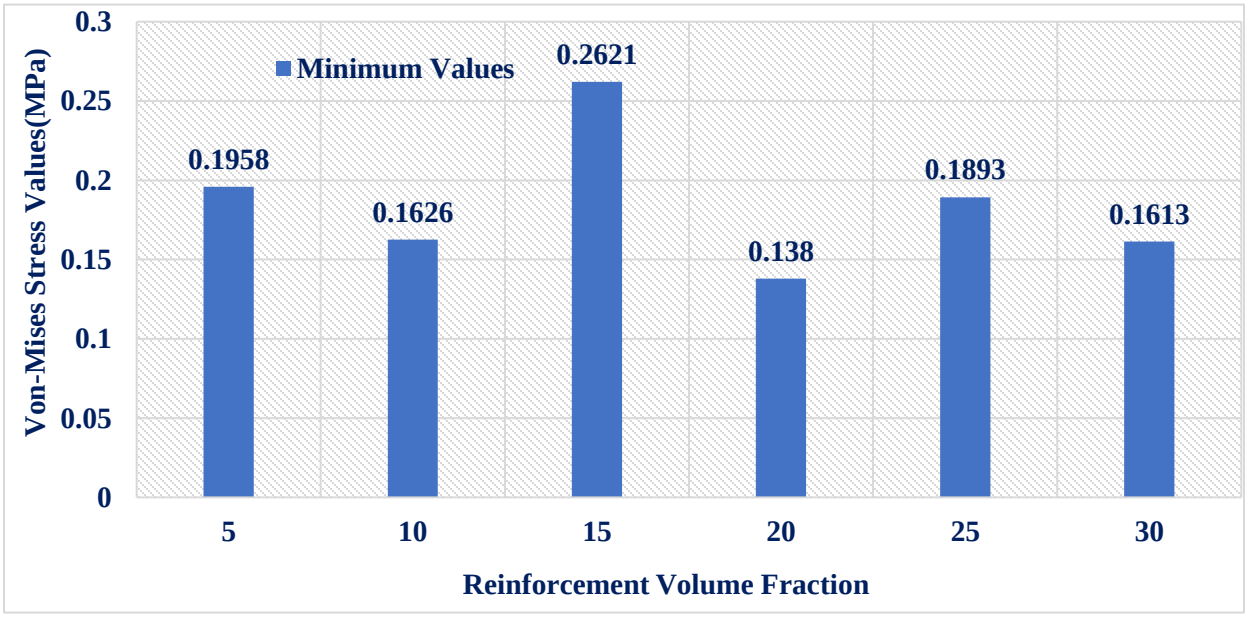

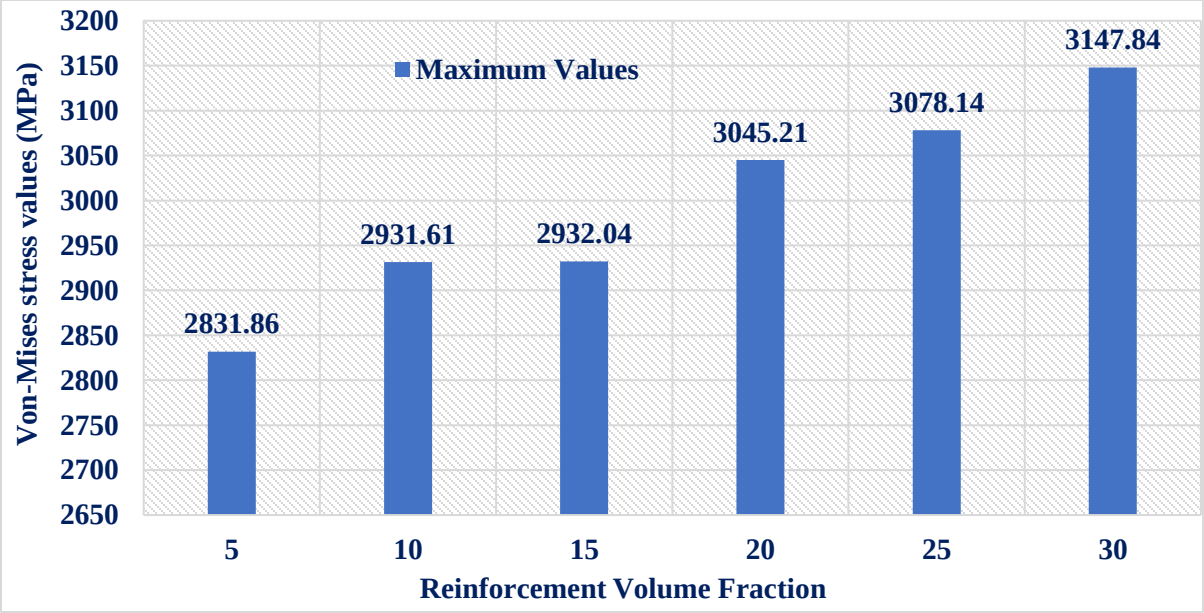

Figure 4.11 Min and Max Von-Mises stress values for (1.8 A.R)

From table 4.23 and figure 4.11 the minimum and maximum Von-Mises stress values for 1.8 AR AA6061-SiC PRMMC could be seen. The minimum Von-Mises stress values range from 0.138 to 0.262 MPa. While, the maximum Von-Mises stress values range from 2831 to 3147 MPa. The higher ranges in 1.8 Aspect ratio than 0.6 AR indicate that these could sustain more loads that makes them prone to lesser failure than the 0.6 AR. A fluctuation of the results is observed the minimum values. While an increase could be seen in the maximum values. The minimum Von-Mises stress values are observed at 20 percent volume fraction for the minimum stress ranges and 5 percent volume fraction for the maximum stress ranges. While the maximum Von-Mises stress value is found at 15 percent volume fraction for the minimum stress ranges and 30 percent volume fraction for the maximum stress ranges.

The justification to the gradual fluctuation of the maximum Von-Mises stress values as compared to the minimum ones throughout figure 4.11 and 4.12 agreed to the work by Gad et al. [27] that observed that even though a rising volume fraction increases some mechanical properties of the composite the probability of tensile cracking increase at the high volume fraction of reinforcements. Whereas, at low volume fraction matrix cracking occurs. Thus this is why the values fluctuate.

4.3.3. RVE Analysis from DIGMAT to ABAQUS

For 5% volume fraction reinforcement using 0.6 and 1.8 aspect ratio are given in figure 4.12 and 4.13 respectively as:-

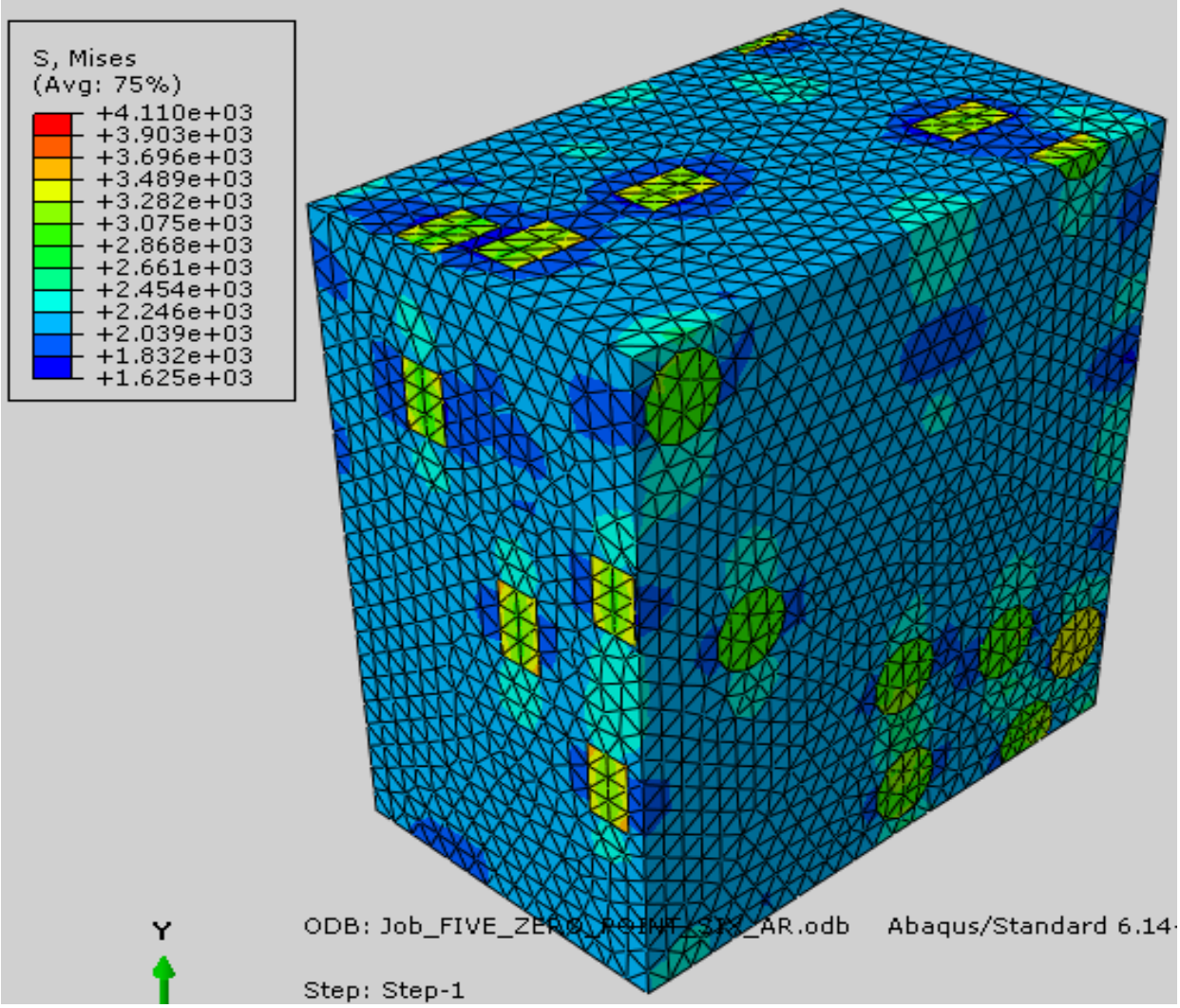

Figure 4.12 RVE values for 0.6 aspect ratio

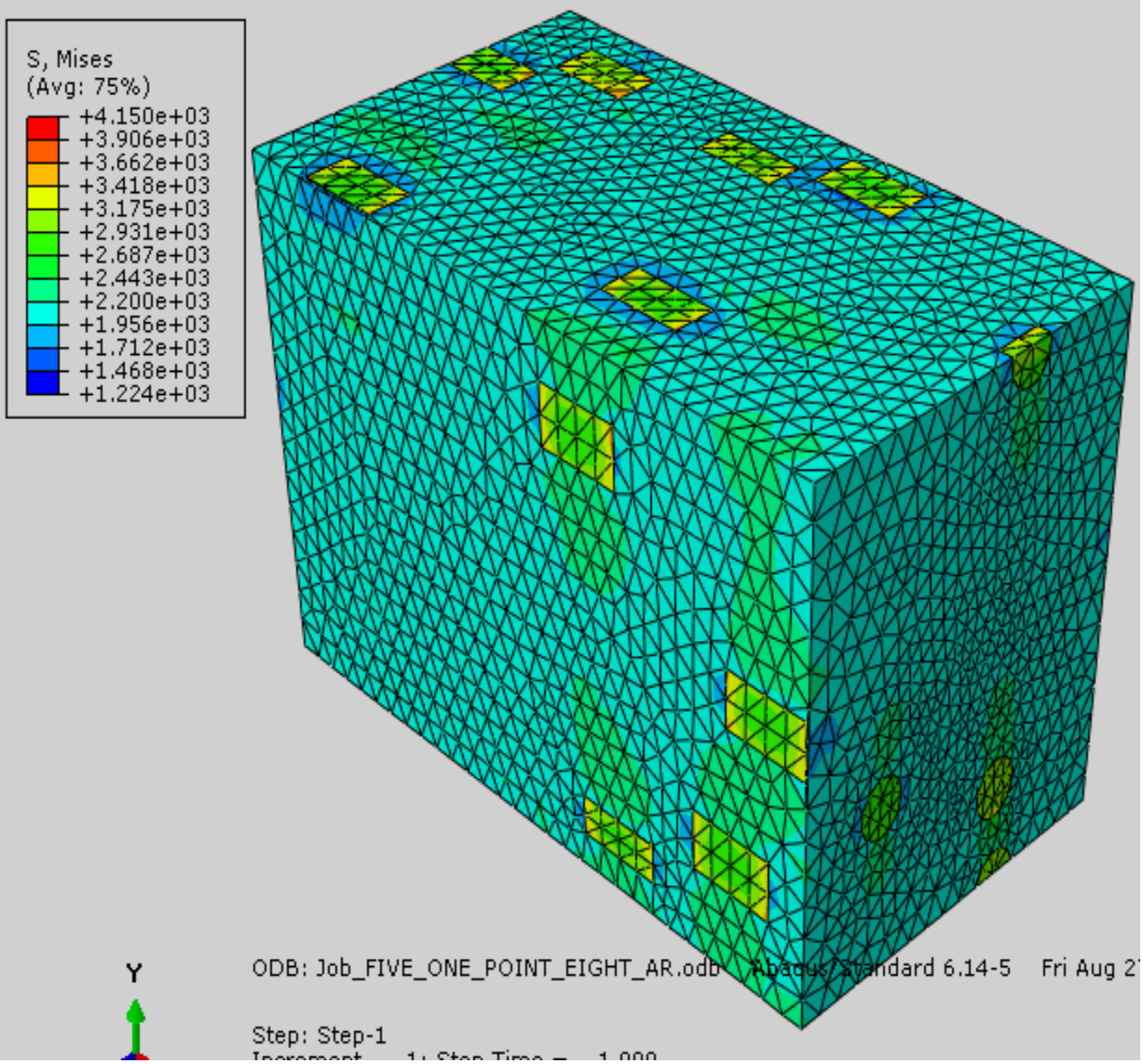

Figure 4.13 RVE values for1.8 aspect ratio

From Figure 4.12 and Figure 4.13 which is the RVE analysis of AA60661-SiC PRMMC under 0.6 and 1.8 aspect ratio.It could be observed that the range of stress is higher in the 1.8 aspect ratio than the 0.6 aspect ratio.The results in the figures including those in the appendex indicated that stress is concentrated at the matrix where particulates are found.It could be noticed that as the volume fraction of the composites increased the Von-Mises stress values showed a fluctuating increment.The highest stress values were found in the 1.8 aspect ratio than 0.6.Because, a lesser aspect ratio accomodates particulates in a lesser space that crates a clustering of the particulates which are prone to failure that propagates throughout the composite.The work of Alfonzo et al.[64] has shown that the mechanical properties like young's modulus and stress values increased as the

aspect ratio incrased.The cylinderical particle shape used in their research presented the closest values to the experimental result.

Von-Mises stress of particulate composites from the representative volume element/RVE/ from DIGIMAT incorporated into ABAQUS is given in table 4.24 and 4.25 as well as figure 4.14 and 4.15 as:-

Table 4.24 Von-Misses stress values of RVE analysis of 0.6 A.R

	Volume Fraction	Minimum Values (MPa)	Maximum Values (MPa)
	5 %	1625.3	4110.03
	10 %	769.259	4559.58
FOR 0.6 AR	15 %	876.041	4680.78
	20 %	1390.18	4605.78
	25 %	1565.68	4459.46
	30 %	1583.46	4939.35

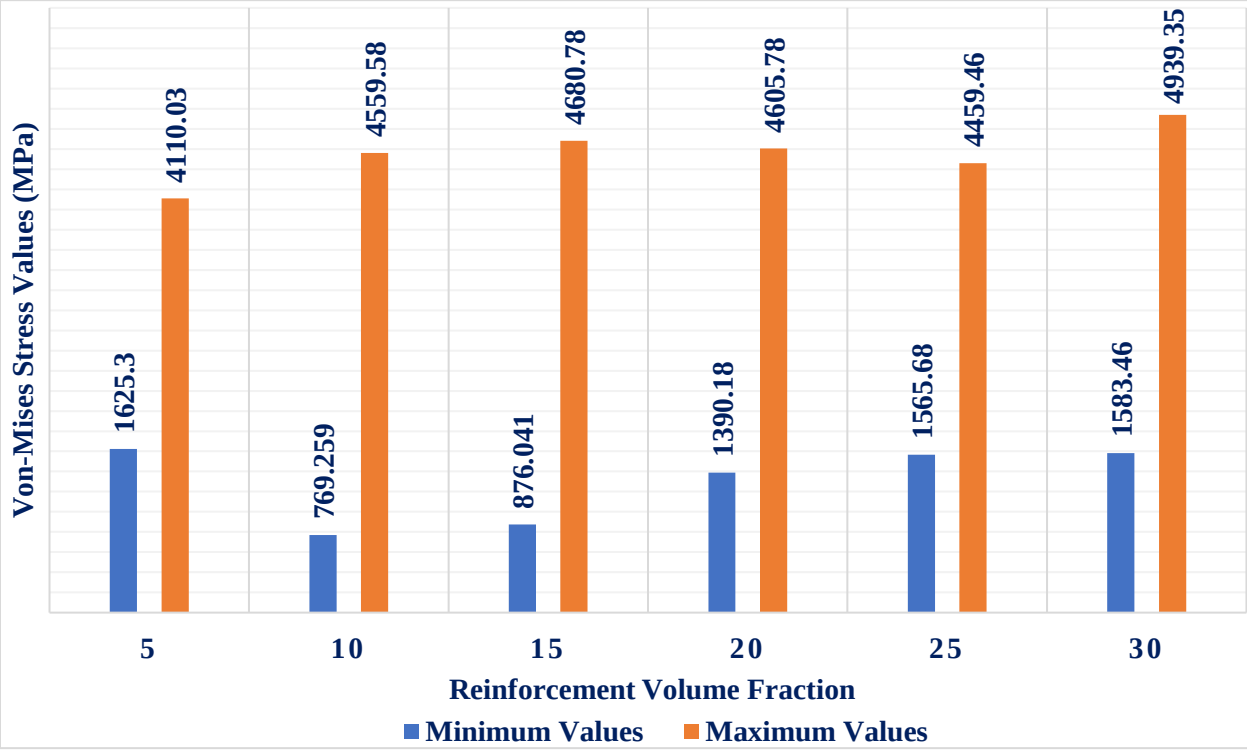

Figure 4.14 Von-Mises stress values for 0.6 A.R particulate composite /RVE/

From table 4.24 and figure 4.14 it could be observed that the minimum values range from 750 to 1700 MPa, The maximum values range from 4100 to 5000 MPA

Table 4.25 Von-Misses stress values of RVE analysis of 1.8 A.R

	Volume Fraction	Minimum Values (MPa)	Maximum Values (MPa)
	5 %	1224.35	4149.83
	10 %	967.087	4336.9
For 1.8 AR	15 %	871.677	4466.01
	20 %	859.289	4584.43
	25 %	1255.45	4667.79
	30 %	1605.6	4394.01

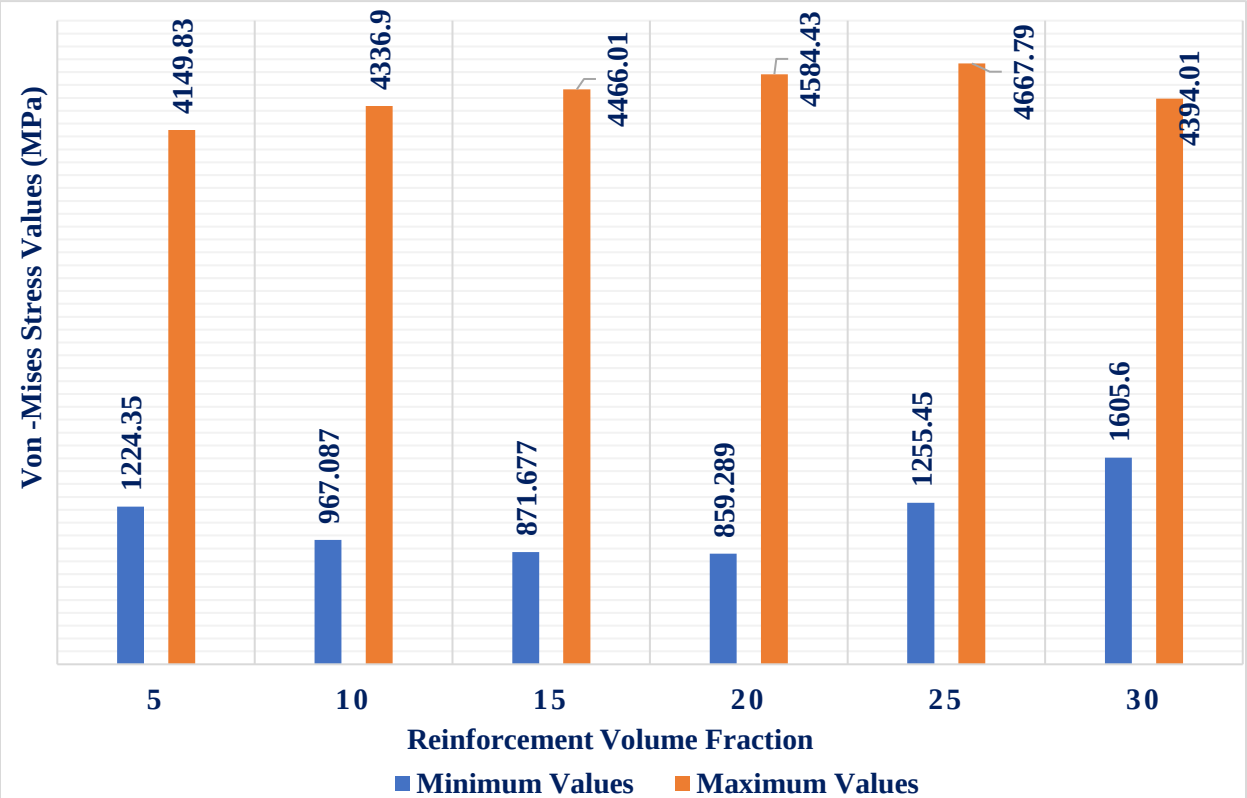

Figure 4.15 Von-Mises stress values for 1.8 A.R particulate composite /RVE/

From table 4.25 and figure 4.15 it could be observed that the minimum values range from 850 to 1610 MPa, while the maximum values range from 4100 to 4700 MPa.Additionally, the minimum values decreased steadily while the maximum values increased steadily until they reached 20% and 25% reinforcement volume fraction respectively to change their values for the rest of the reinforcement volume fraction.

Chapter Five

5. Conclusions and Recommendations

5.1. Conclusions

The effect of varying volume fractions, laminate orientations, and particulate aspect ratio of AA6061-SiC on the modeling, analysis, and failure prediction of automobile connecting rods was studied using numerical modeling coupled with FEM modeling and analysis using ABAQUS. Additionally, the representative volume element (RVE) analysis of particulates was made using DIGIMAT software.

The validity of the failure prediction models was checked by comparing numerical results with fem simulation ones using error percentage. Finally, the author preferred model for connecting rod application is selected. Thus the conclusions reached based on the approached results are:-

- ➔ The gradual increase of reinforcement volume fraction from five percent to thirty percent created an increase of mechanical properties such as elastic modulus and tensile strength of the AA6061-SiC composite.
- ➔ The increased mechanical properties of the composite caused a decrease in thickness and other geometric dimensions such as piston head and crank head of the connecting rod model.
- ➔ The Tsai-Wu criterion values obtained were higher than the Tsai-Hill criterion values due to the consideration of both tensile and compressive stress in their analysis. Thus the values from the Tsai-Wu criterion were chosen as the parameters for model selection. In addition the increment of volume fraction caused a gradual decrease of these values.
- ➔ The laminate reinforced models which are found in the medium volume fraction ranges (15, 20, and 25) were chosen because they have values in the medium ranges. The observation from the FEM simulations showed these connecting rod models deformed normally with a negligible effect on the models during load application. In addition the

connecting rod models with zero and ninety degree laminate orientation were chosen because they have the lowest Tsai-Wu criterion values.

- ➔ The connecting rod models with thirty and forty-five degree laminate orientation, as well as, volume fraction less than fifteen percent deformed at an extent which damaged the structural integrity of the connecting rod. These connecting rod models were considered as a failed connecting rod models as compared to the rest models.
- ➔ The particulate reinforced models showed fluctuating minimum values for both aspect ratios but increased gradually in their maximum values.
- ➔ The results of Von-Mises values of particulates from the RVE analysis show that even though the material properties increase as reinforcement volume fraction increase. The Von-Mises stress values do not necessarily increase but rather fluctuate, which was hard for selection.
- ➔ The RVE analysis of particulate reinforcement shows a decrease in the minimum values as well as an increase in maximum values until they reach twenty percent volume fraction, but it can be concluded that both 0.6 and 1.8 aspect ratios have somehow similar results.
- ➔ The particulate reinforced connecting rod models with a five percent volume fraction for both 0.6 and 1.8 AR were chosen from the FEM actual modelling and RVE modelling. These was because they yielded the lowest Von-Mises stress maximum values.
- ➔ The FEM results indicated that areas of load application, areas where the SiC reinforcements are found, edges and the middle cross-section of the connecting rod to be stress concentrated regions. Thus if failure is to occur on the models these would be the potential initiation and propagation sites.
- ✪ Generally the laminate reinforced connecting rod models with twenty percent volume fraction at either zero or ninety degree orientation as well as particulate reinforced models with five percent volume fraction were chosen to be suitable for application. These is due to their fem and analytical values which is in the optimum range.

5.2. Recommendation

The thesis studied the effects of varying volume fraction, laminate orientation and aspect ratio in the modeling of the dimensions of an automobile connecting rod of AA6061-SiC composites.it also predicted the instances of failure occurrence as well as microstructure analysis using representative volume element/RVE/ using software's like ABAQUS and DIGIMAT. From the research it was observed that increasing the content of reinforcement in the composite model increased the mechanical properties of the composites. But, has certain disadvantages that cause failure of the designed components like britility and particle clustering. The laminate reinforced components sustained lower load gradients than the particulate ones. Thus, the particulate reinforced composite connecting rod with five percent volume fraction is recommended as the ideal connecting rod for further processing based on the authors design. But, if there is a need for the usage of laminate reinforced connecting rod 0^o or 90^o laminate orientation is recommended with twenty percent volume fraction.

5.3. Future Works

When the analysis and numerical modelling of failure in AMMC's connecting rods is concerned, there are lots of potential study areas for researchers.

- ➔ Further investigation on the effects of varying volume fraction, laminate orientation as well as aspect ratio of composites in another automobile components. Which, are subjected to different loading and design conditions.
- ➔ Investigation on variables which could cause failure on the connecting rod in the long run such as temperature, fatigue fracture, hydrolock and overrevving.
- ➔ Investigation on the addition of other reinforcements on the composite to enhance ductility and other factor which inhibited the use of higher volume fraction of composites which had a better mechanical properties.

References

[1] J. E. King, “Failure in Composite Materials Polymer Matrix Composites,” met. Mater. Int., vol.5,no.12,pp.720–726,2000.

[2] C. Liu,“Transverse Failure mechanisms of Composite laminates with yarn-level,” Department of Mechanical, Aerospace and Civil Engineering the University of Manchester 2019.

[3] I. M. Daniel, “Failure Mechanisms in Fiber-Reinforced Composites,” Lit Research Institute Chicago, Illinois 60616,2004.

[4] F. Nturanabo, l. Masu, and j. Baptist kirabira, “Novel applications of Aluminium Metal Matrix Composites,” alum. Alloy. Compos., 2020, doi: 10.5772/intechopen.86225.

[5] H. M, G. N. M. Rao, and B. D. Prasad, “Review on Optimization of Metal Matrix Composite Connecting Rod,” int. Res. J. Adv. Sci. Hub, vol. 2, no. 7, pp. 94–99, 2020, doi: 10.47392/irjash.2020.71.

[6] G. Yadav, r. S. Rana, r. K. Dwivedi, and a. Tiwari, “Development and Analysis of Automotive Component using aluminium alloy nano silicon carbide composite,” appl. Mech.Mater., vol. 813–814, pp. 257–262, 2015, doi: 10.4028/www.scientific.net/amm.813-814.257.

[7] Surappa m.k., “Aluminium matrix composites: Challenges and Opportunities // Sadhana. Department of Metallurgy, Indian Institute of Science, bangalore 560 012, india,” vol. 28, no. 1–2, pp. 319–334, 2003.

[8] A. Schmidt, S. Siebeck, u. Götze, g. Wagner, and d. Nestler, “Particle-Reinforced Aluminum matrix composites (AMCs)-selected results of an integrated technology, user, and market analysis and forecast,” metals (basel)., vol. 8, no. 2, 2018, doi: 10.3390/met8020143.

[9] M. S. Satbhai and p. S. Talmale, “Review on design and analysis of ic engine connecting rod,” int. Res. J. Eng. Technol., vol. 04, no. Sep, pp. 1055–1059, 2017.

[10] N. Publications, i. Journal, o. F. Innovations, and i. N. Engineering, "Analysis of fatigue failure of connecting rod used in a light commercial vehicle (lcv) through fea," vol. 3, no. 3, pp. 1–14, 2016.

[11] C. Bulei, m. Todor, and i. Kiss, "Research and Development priorities in order to make," pp. 145–148, 2019.

[12] A. P. Divecha, s. G. Fishman, and s. D. Karmarkar, "Silicon Carbide reinforced aluminum—a formable composite," jom j. Miner. Met. Mater. Soc., vol. 33, no. 9, pp. 12–17, 1981, doi: 10.1007/bf03339487.

[13] S. Li, y. Su, x. Zhu, h. Jin, q. Ouyang, and d. Zhang, "Enhanced mechanical behavior and fabrication of silicon carbide particles covered by in-situ carbon nanotube reinforced 6061 aluminum matrix composites," mater. Des., vol. 107, pp. 130–138, 2016, doi: 10.1016/j.matdes.2016.06.021.

[14] M. H. Rahman and h. M. M. Al rashed, "Characterization of silicon carbide Reinforced Aluminum matrix composites," procedia eng., vol. 90, pp. 103–109, 2014, doi: 10.1016/j.proeng.2014.11.821.

[15] M. Mahendra boopathi, k. P. Arulshri, and n. Iyandurai, "Evaluation of mechanical properties of aluminium alloy 2024 reinforced with silicon carbide and fly ash hybrid metal matrix composites," am. J. Appl. Sci., vol. 10, no. 3, pp. 219–229, 2013, doi: 10.3844/ajassp.2013.219.229.

[16] J. Zhang, f. Liu, l. Zhao, j. Zhi, l. Zhou, and b. Fei, "influence of end distances on the failure of composite bolted joints," j. Reinf. Plast. Compos., vol. 34, no. 5, pp. 388–404, 2015, doi: 10.1177/0731684415572199.

[17] l. Huei-long, l. Wun-hwa, and sammy lap-ip chan, "Abrasive wear of powder metallurgy al alloy 6061-sic particle composites," wear, vol. 159, no. 2, pp. 223–231, 1992, doi: 10.1016/0043-1648(92)90305-r.

[18] R. Praveen and s. Raghuraman, "Silicon carbide reinforced aluminium metal matrix composites for aerospace applications: a literature review," int. J. Innov. Res. Sci. Eng. Technol. (an iso certif. Organ., vol. 3297, no. 11, pp. 6336–6344, 2007

[19] H. T. Hu, w. P. Lin, and f. T. Tu, "Failure analysis of fiber-reinforced composite laminates subjected to biaxial loads," compos. Part b eng., vol. 83, pp. 153–165, 2015, doi: 10.1016/j.compositesb.2015.08.045.

[20] B. G. Falzon and p. Apruzzese, "Numerical analysis of intralaminar failure mechanisms in composite structures. Part i: fe implementation," compos. Struct., vol. 93, no. 2, pp. 1039–1046, 2011, doi: 10.1016/j.compstruct.2010.06.028.

[21] P. Nali and e. Carrera, "A Numerical assessment on two-dimensional failure criteria for composite layered structures," compos. Part b eng., vol. 43, no. 2, pp. 280–289, 2012, doi: 10.1016/j.compositesb.2011.06.018.

[22] Stephen. w.Tsai and h.Thomas Hahn,"Introduction to composite materials", vol. 12, no. 1s. 2015.

[23] k. A. Beklemysheva, a. V. Vasyukov, a. S. Ermakov, and i. B. Petrov, "Numerical Simulation of the failure of composite materials by using the grid-characteristic method," math. Model. Comput. Simulations, vol. 8, no. 5, pp. 557–567, 2016, doi: 10.1134/s2070048216050033.

[24] S. Ma and x. Wang, "Mechanical Properties and Fracture of in-situ al 3 ti particulate reinforced a356 composites," mater. Sci. Eng. A, vol. 754, pp. 46–56, 2019, doi: 10.1016/j.msea.2019.03.044.

[25] B. Chu et al., "A rate-dependent Peridynamic Model for the Dynamic behavior of ceramic materials," c. - comput. Model. Eng. Sci., vol. 124, no. 1, pp. 151–178, 2020, doi: 10.32604/cmes.2020.010115.

[26] D. J. Lloyd, "Aspects of fracture in particulate reinforced metal matrix composites," acta metall. Mater., vol. 39, no. 1, pp. 59–71, 1991, doi: 10.1016/0956-7151(91)90328-x.

[27] S. I. Gad, m. A. Attia, m. A. Hassan, and a. G. El-shafei, "Predictive computational model for damage behavior of metal-matrix composites emphasizing the effect of particle size and volume fraction," materials (basel)., vol. 14, no. 9, 2021, doi: 10.3390/ma14092143.

[28] S. I. Gad, m. A. Attia, m. A. Hassan, and a. G. El-shafei, "A random microstructure-based

model to study the effect of the shape of reinforcement particles on the damage of elastoplastic particulate metal matrix composites," ceram. Int., vol. 47, no. 3, pp. 3444–3461, 2021, doi: 10.1016/j.ceramint.2020.09.189.

[29] P. R. Budarapu, x. Zhuang, t. Rabczuk, and s. P. A. Bordas, "Multiscale modeling of material failure: theory and computational methods", 1st ed., vol. 52. Elsevier inc., 2019.

[30] J. F. Zhang, h. Andrä, x. X. Zhang, q. Z. Wang, b. L. Xiao, and z. Y. Ma, "an enhanced finite element model considering multi strengthening and damage mechanisms in particle reinforced metal matrix composites," compos. Struct., vol. 226, no. August, 2019, doi: 10.1016/j.compstruct.2019.111281.

[31] I. Weng, y. Shen, t. Fan, and j. Xu, "a study of interface damage on mechanical properties of particle-reinforced composites," jom, vol. 67, no. 7, pp. 1499–1504, 2015, doi: 10.1007/s11837-015-1413-9.

[32] Q. Wu, w. Xu, and l. Zhang, "microstructure-based modelling of fracture of particulate reinforced metal matrix composites," compos. Part b eng., vol. 163, pp. 384–392, 2019, doi: 10.1016/j.compositesb.2018.12.099.

[33] J. Zahr viñuela and j. L. Pérez-castellanos, "The anisotropic criterion of von mises (1928) as a yield condition for pmmcs. A calibration procedure based on numerical cell-analysis," compos. Struct., vol. 134, pp. 613–632, 2015, doi: 10.1016/j.compstruct.2015.08.091.

[34] A. Paknia, a. Pramanik, a. R. Dixit, and s. Chattopadhyaya, "Effect of size, content and shape of reinforcements on the behavior of metal matrix composites (mmcs) under tension," j. Mater. Eng. Perform., vol. 25, no. 10, pp. 4444–4459, 2016, doi: 10.1007/s11665-016-2307-x.

[35] X. Gao, x. Zhang, a. Li, and l. Geng, "Plastic deformation and fracture behaviors in particle-reinforced aluminum composites: a numerical approach using an enhanced finite element model," j. Compos. Mater., vol. 54, no. 15, pp. 1977–1985, 2020, doi: 10.1177/0021998319889110.

[36] M. N. Yuan, y. Q. Yang, c. Li, p. Y. Heng, and l. Z. Li, "Numerical analysis of the stress-strain distributions in the particle reinforced metal matrix composite sic/6064al," mater.

Des., vol. 38, pp. 1–6, 2012, doi: 10.1016/j.matdes.2011.12.043.

[37] Y. Suo, b. Wang, p. Jia, and y. Gong, "Numerical Analysis of mechanical properties and particle cracking probability of metal matrix composites," mater. Today commun., vol. 24, no. March, p. 101082, 2020, doi: 10.1016/j.mtcomm.2020.101082.

[38] H. Debski and j. Jonak, "Failure analysis of Thin-walled composite channel section columns,"compos.Struct.,vol.132,pp.567–574,2015,doi:10.1016/j.compstruct.2015.05.067.

[39] D. Feng and f. Aymerich, "Finite element modelling of damage induced by low-velocity impact on composite laminates," compos. Struct., vol. 108, no. 1, pp. 161–171, 2014, doi: 10.1016/j.compstruct.2013.09.004.

[40] Sebastian antony, arjun a., shinos t. K, and anoop p, "Design and analysis of a connecting rod," int. J. Eng. Res., vol. V5, no. 10, pp. 906–912, 2016, doi: 10.17577/ijertv5is100142.

[41] W. Ogierman and g. Kokot, "Particle shape influence on elastic-plastic behaviour of particle-reinforced composites," arch. Mater. Sci. Eng., vol. 67, no. 2, pp. 70–76, 2014.

[42] M. Amirmaleki, j. Samei, d. E. Green, i. Van riemsdijk, and l. Stewart, "3D micromechanical modeling of dual phase steels using the representative volume element method," mech. Mater., vol. 101, pp. 27–39, 2016, doi: 10.1016/j.mechmat.2016.07.011.

[43] B. Nayak and r. K. Sahu, "Experimental and digimat-fe based representative volume element analysis of exceptional graphene flakes/aluminium alloy nanocomposite characteristics," mater. Res. Express, vol. 6, no. 11, p. 116593, 2019, doi: 10.1088/2053-1591/ab4bb7.

[44] G. V. Jagadeesh and s. Gangi setti, "A Review on Micromechanical Methods for Evaluation of mechanical behavior of particulate reinforced metal matrix composites," j. Mater. Sci., vol. 55, no. 23, pp. 9848–9882, 2020, doi: 10.1007/s10853-020-04715-2.

[45] M. Ansar, w. Xinwei, and z. Chouwei, "Modeling Strategies of 3d woven Composites: a review," compos. Struct., vol. 93, no. 8, pp. 1947–1963, 2011, doi: 10.1016/j.compstruct.2011.03.010.

[46] D. Calneryte and r. Barauskas, “Multi-scale evaluation of the linear elastic and failure parameters of the unidirectional laminated textiles with application to transverse impact simulation,” compos. Struct., vol. 142, pp. 325–334, 2016, doi: 10.1016/j.compstruct.2016.01.104.

[47] D. L. K and a. L. K, “Design and fatigue analysis on metal matrix composite connecting rod using fea,” vol. 2, no. 12, pp. 1472–1476, 2013.

[48] B. Sriharsha and p. S. Rao, “Design considerations for connecting rod,” int. J. Eng. Adv. Technol., vol. 9, no. 3, pp. 2368–2373, 2020, doi: 10.35940/ijeat.c5759.029320.

[49] S. K. Naik, s. J. Sanjay, v. B. Math, and r. S. Matti, “Connecting rod made using particulate reinforced aluminum metal matrix composite - a review,” j. Emerg. Technol. Innov. Res., vol. 2, no. 12, pp. 228–233, 2015.

[50] Andoko and n. E. Saputro, “Strength analysis of connecting rods with pistons using finite element method,” matec web conf., vol. 204, pp. 1–6, 2018, doi: 10.1051/matecconf/201820407009.

[51] S. J. Babu, a. K. Kishore, w. Godavari, a. Pradesh, w. Godavari, and a. Pradesh, “International journal of advance scientific research and engineering trends modeling and static thermal analysis of connecting rod with metal matrix composite materials using fem m . Tech student , dept . Of mechanical engineering , akrg college of engine,” vol. 5, no. 8, pp. 60–72, 2020.

[52] P. Mukhopadhyay, “alloy designation, processing, and use of AA6xxxx series aluminium alloys,” isrn metall., vol. 2012, no. Table 1, pp. 1–15, 2012, doi: 10.5402/2012/165082.

[53] Matweb, “aluminum 6061-t6; 6061-t651,” matweb, pp. 1–3, 2015, [online]. Available: http://www.matweb.com/search/datasheet.aspx?matguid=ff6d4e6d529e4b3d97c77d6538b29693.

[54] R. Gerhardt, "Properties and applications of silicon carbide" edited by rosario gerhardt. 2011.

[55] A. Martin and l. Rover, “Add data for a new car used car auction japan general information,”

pp. 11–13, 2000.

[56] A. Ababa and f. Stations,“ assessment of regular gasoline adulteration at Addis Ababa fuel stations,” 2015.

[57] S. S. Rinju and s. Sujith, “Finite element analysis of metal matrix composite connecting rod and comparison with conventional aisi 4140 alloy steel connecting rod,” no. 11, 2016.

[58] G. Yadav, r. S. Rana, r. K. Dwivedi, and a. Tiwari, “Development and analysis of automotive component using aluminium alloy nano silicon carbide composite,” appl. Mech. Mater., vol. 813–814, no. 3, pp. 257–262, 2015, doi: 10.4028/www.scientific.net/amm.813-814.257.

[59] P. Purushothama raj and v. Ramasamy, Strength of Materials, no. 9783319035628. 2014.

[60] A. M. G. P and v. B. T, “Design and Analysis of metal matrix composite connecting rod,” vol. 3, no. 2, pp. 672–684, 2015.

[61] M. S. Lande and r. D. Bhagat, “Thermal analysis of combustion chamber of two stroke si engine,” vol. 2, no. 12, pp. 3266–3278, 2013.

[62] J. G. Kaufman, “Properties and characteristic of aluminum and aluminum alloys,” fire resist. Alum. Alum. Alloy. Meas. Eff. Fire expo. Prop. Alum. Alloy., pp. 1–7, 2016.

[63] Vijay d patil and prof. D. R. Kotkar, “Static and fatigue analysis of aluminum silicon carbide connecting rod for comparative study of mechanical parameters using fea,” int. J. Eng. Res., vol. V5, no. 03, pp. 72–79, 2016, doi: 10.17577/ijertv5is030121.

[64] I. Alfonso et al., “Estimation of elastic moduli of particulate-reinforced composites using finite element and modified halpin–tsai models,” j. Brazilian soc. Mech. Sci. Eng., vol. 38, no. 4, pp. 1317–1324, 2016, doi: 10.1007/s40430-015-0429-y.

[65] Dassault systèmes, “Analysis of composite materials with abaqus,” p. 452, 2009.

[66] e-xstream engineering, “Digimat - the material modeling platform,” 2015, [online]. Available: http://www.e-xstream.com/.

[67] M. Song, “Effects of volume fraction of sic particles on mechanical properties of sic/al

composites," trans. Nonferrous met. Soc. China (english ed., vol. 19, no. 6, pp. 1400–1404, 2009, doi: 10.1016/s1003-6326(09)60040-6.

[68] l. Dong, g. Mi, c. Li, l. Xu, and j. Wei, "Effects of SiC particle volume fraction on microstructure and mechancial properties of sicp/6061al composites," integr. Ferroelectr., vol. 210, no. 1, pp. 215–226, 2020, doi: 10.1080/10584587.2020.1728678.

[69] k. Chung, n. Ma, t. Park, d. Kim, d. Yoo, and c. Kim, "A modified damage model for advanced high strength steel sheets," int. J. Plast., vol. 27, no. 10, pp. 1485–1511, 2011, doi: 10.1016/j.ijplas.2011.01.007.

Appendixes

Appendex -I

Data's from excel calculation are:-

Compliance matrix values which are calculated using equation 25 is given as:-

Table I.A Compliance matrix

	S_{11}	S_{12}	S_{66}
5% Reinforcement	1.36E-05	-4.52E-06	0.00036
10% Reinforcement	1.308E-05	-4.35E-06	0.00018
15% Reinforcement	1.24E-05	-4.19E-06	0.00012
20% Reinforcement	1.194E-05	-4.05E-06	9.64E-05
25% Reinforcement	1.154E-05	-3.919E-06	7.74E-05
30% Reinforcement	1.10E-05	-3.79E-06	6.47E-05

Transformed compliance matrix values are calculated using equation 26 is given as:-

Table I.B Transformed compliance matrix

For Zero Degree

0°	$\overline{S_{11}}$	$\overline{S_{12}}$	$\overline{S_{22}}$	$\overline{S_{16}}$	$\overline{S_{26}}$	$\overline{S_{66}}$
5%	1.36E-05	-4.52E-06	0	0	0	0.00036
10%	1.30E-05	-4.35E-06	0	0	0	0.00018
15%	1.24E-05	-4.19E-06	0	0	0	0.00012
20%	1.19E-05	-4.05E-06	0	0	0	9.64E-05
25%	1.15E-05	-3.91E-06	0	0	0	7.74E-05
30%	1.10E-05	-3.79E-06	0	0	0	6.47E-05

For Thirty Degree

30°	$\overline{S_{11}}$	$\overline{S_{12}}$	$\overline{S_{22}}$	$\overline{S_{16}}$	$\overline{S_{26}}$	$\overline{S_{66}}$
5%	7.42E-05	-6.85E-05	6.74E-05	-6.77E-05	7.95E-05	0.000108
10%	4.11E-05	-3.57E-05	3.46E-05	-3.04E-05	4.17E-05	6.36E-05
15%	2.94E-05	-2.42E-05	2.31E-05	-1.76E-05	2.84E-05	4.76E-05
20%	2.33E-05	-1.83E-05	1.73E-05	-1.12E-05	2.16E-05	3.91E-05
25%	1.95E-05	-1.48E-05	1.37E-05	-7.55E-06	1.75E-05	3.38E-05
30%	1.69E-05	-1.24E-05	1.14E-05	-5.13E-06	1.47E-05	3.02E-05

For Forty- Five Degree

45^0	$\overline{S_{11}}$	$\overline{S_{12}}$	$\overline{S_{22}}$	$\overline{S_{16}}$	$\overline{S_{26}}$	$\overline{S_{66}}$
5%	9.21E-05	-8.98E-05	9.21E-05	6.81E-06	6.81E-06	2.26E-05
10%	4.83E-05	-4.62E-05	4.83E-05	6.51E-06	6.51E-06	2.17E-05
15%	3.29E-05	-3.09E-05	3.29E-05	6.24E-06	6.24E-06	2.08E-05
20%	2.50E-05	-2.31E-05	2.50E-05	5.99E-06	5.99E-06	2.009E-05
25%	2.02E-05	-1.84E-05	2.02E-05	5.76E-06	5.76E-06	1.93E-05
30%	1.70E-05	-1.53E-05	1.70E-05	5.54E-06	5.54E-06	1.86E-05

For Ninety Degree

90^0	$\overline{S_{11}}$	$\overline{S_{12}}$	$\overline{S_{22}}$	$\overline{S_{16}}$	$\overline{S_{26}}$	$\overline{S_{66}}$
5%	0	-4.52E-06	1.36E-05	0	0	0.00036
10%	0	-4.35E-06	1.30E-05	0	0	0.00018
15%	0	-4.19E-06	1.24E-05	0	0	0.00012
20%	0	-4.052E-06	1.199E-05	0	0	9.64E-05
25%	0	-3.91E-06	1.15E-05	0	0	7.74E-05
30%	0	-3.79E-06	1.10E-05	0	0	6.47E-05

Appendix-II

Plane Geometrical model of laminate reinforced connecting rods

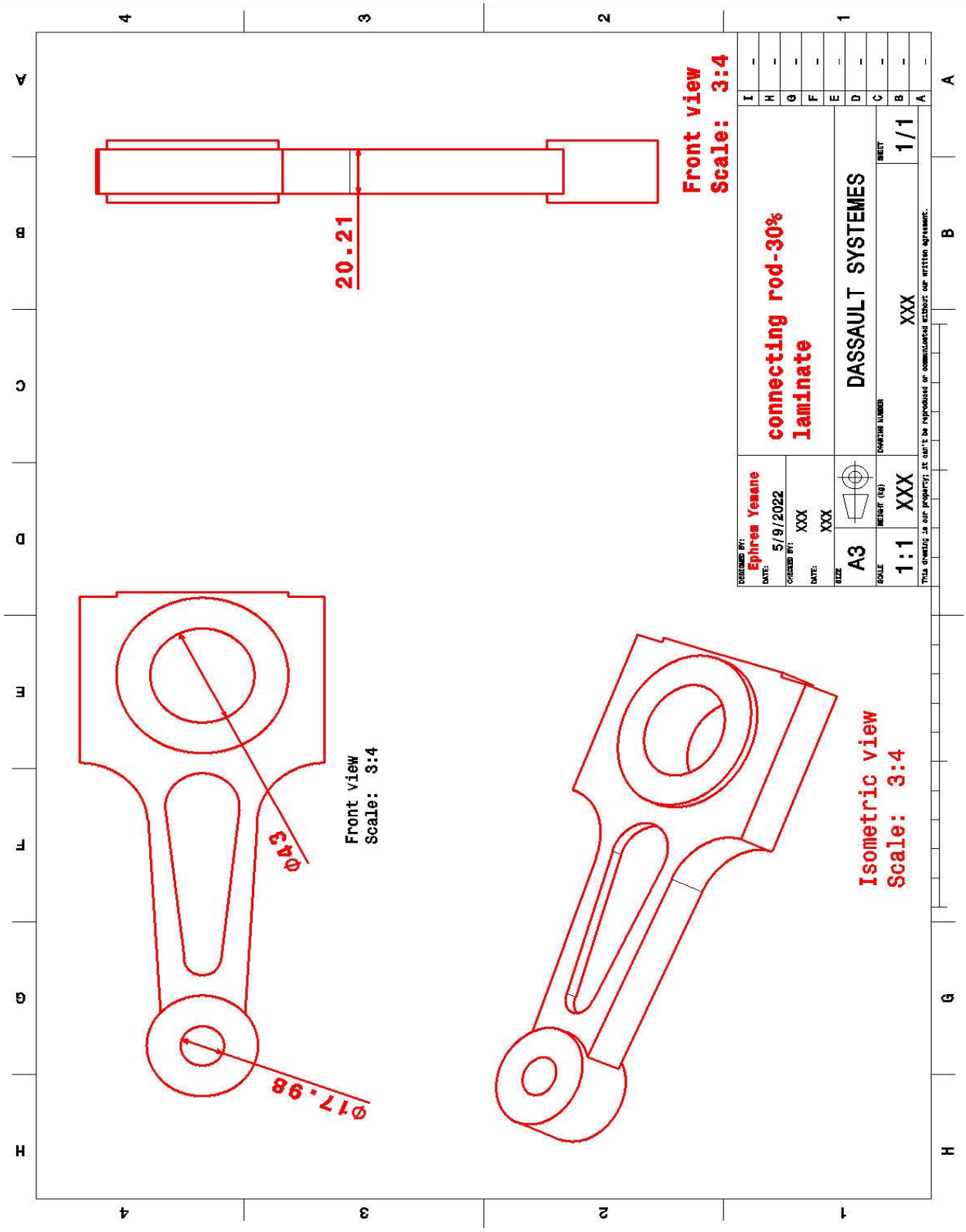

Plane geometrical model of particulate reinforced connecting rods

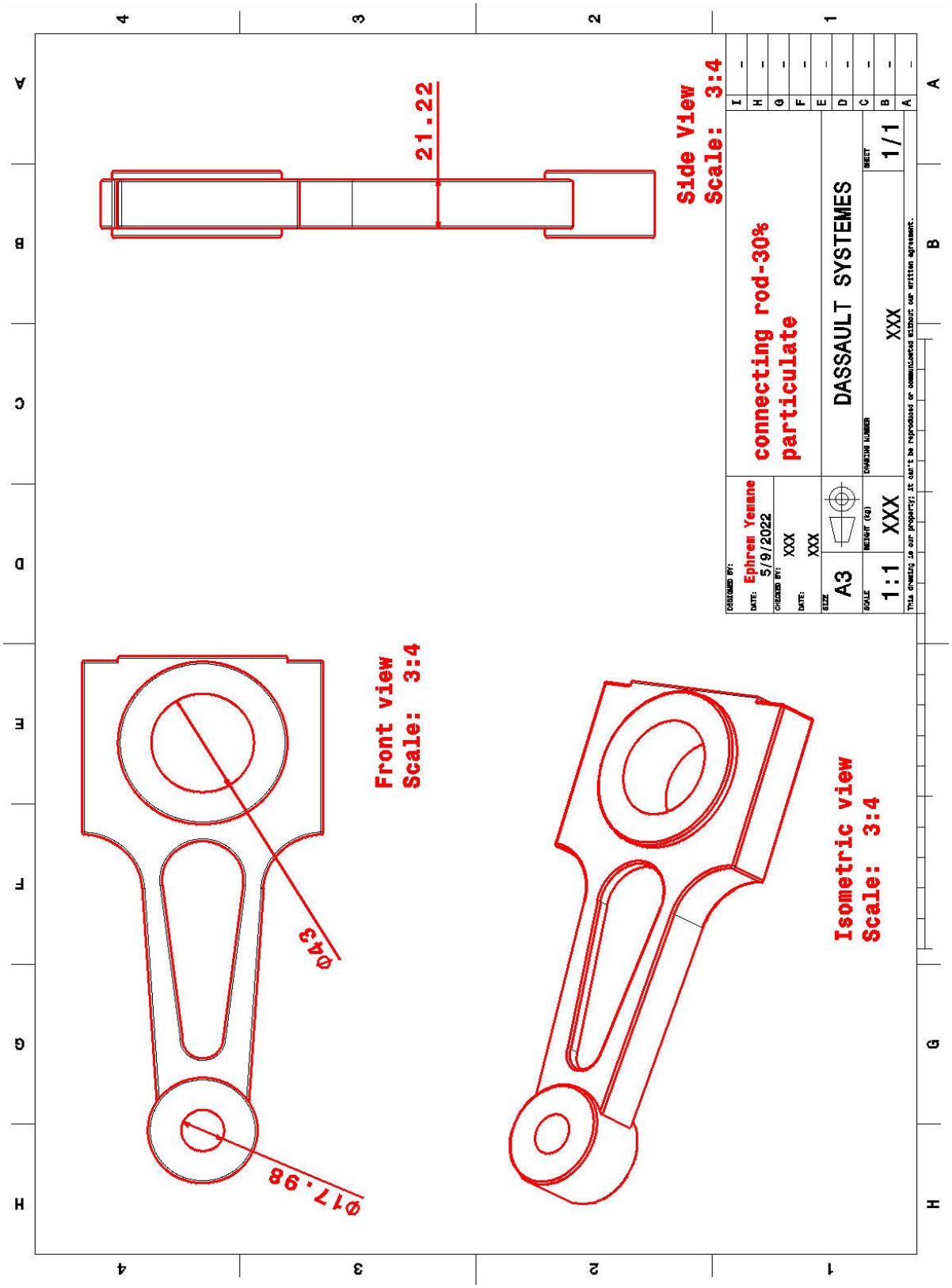

Appendex-III

Figures on ABAQUS results on laminates

Figure III.A 5 % VF 0^O Tsai-Hill Criterion Results

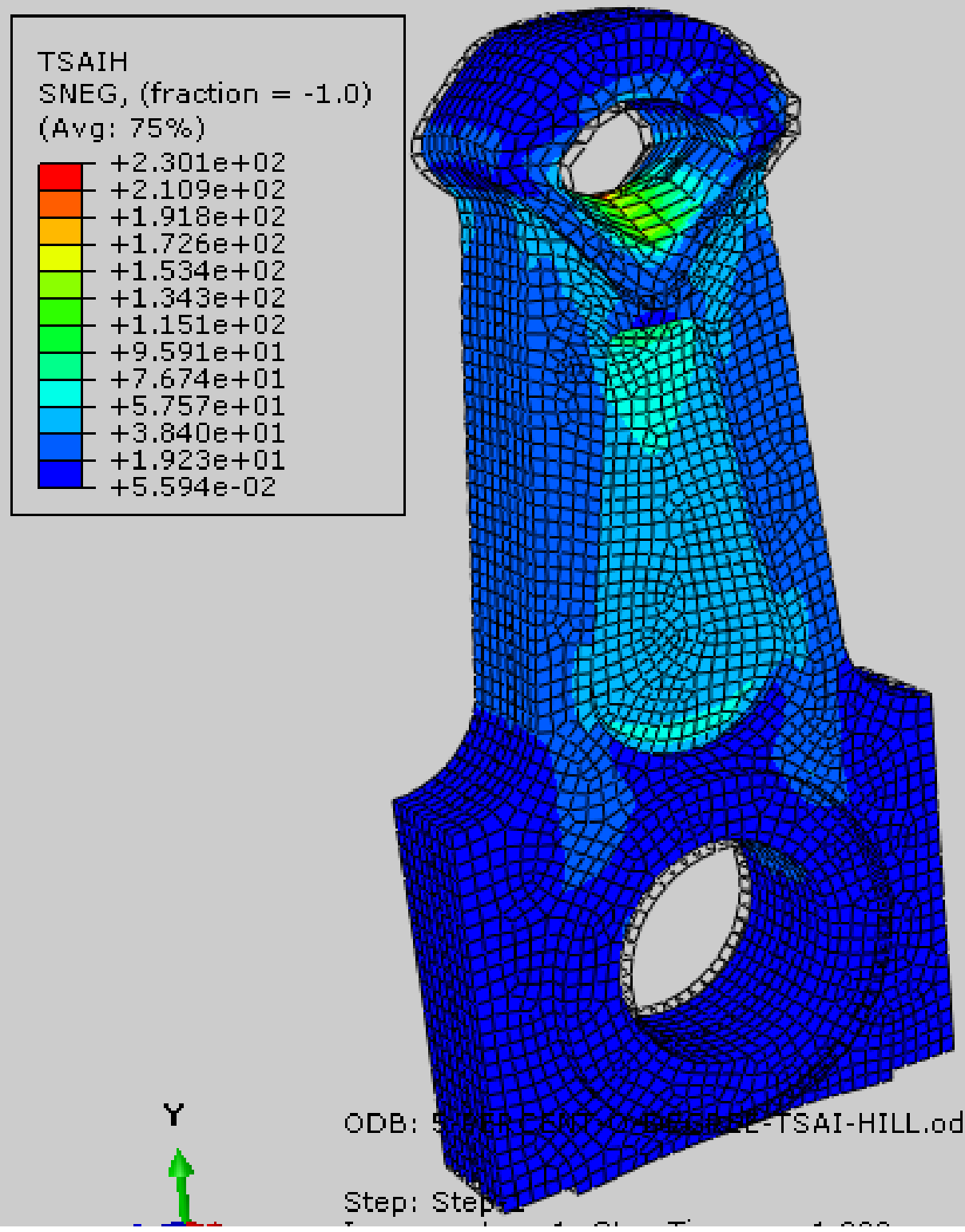

Tsai-Wu Criterion Results

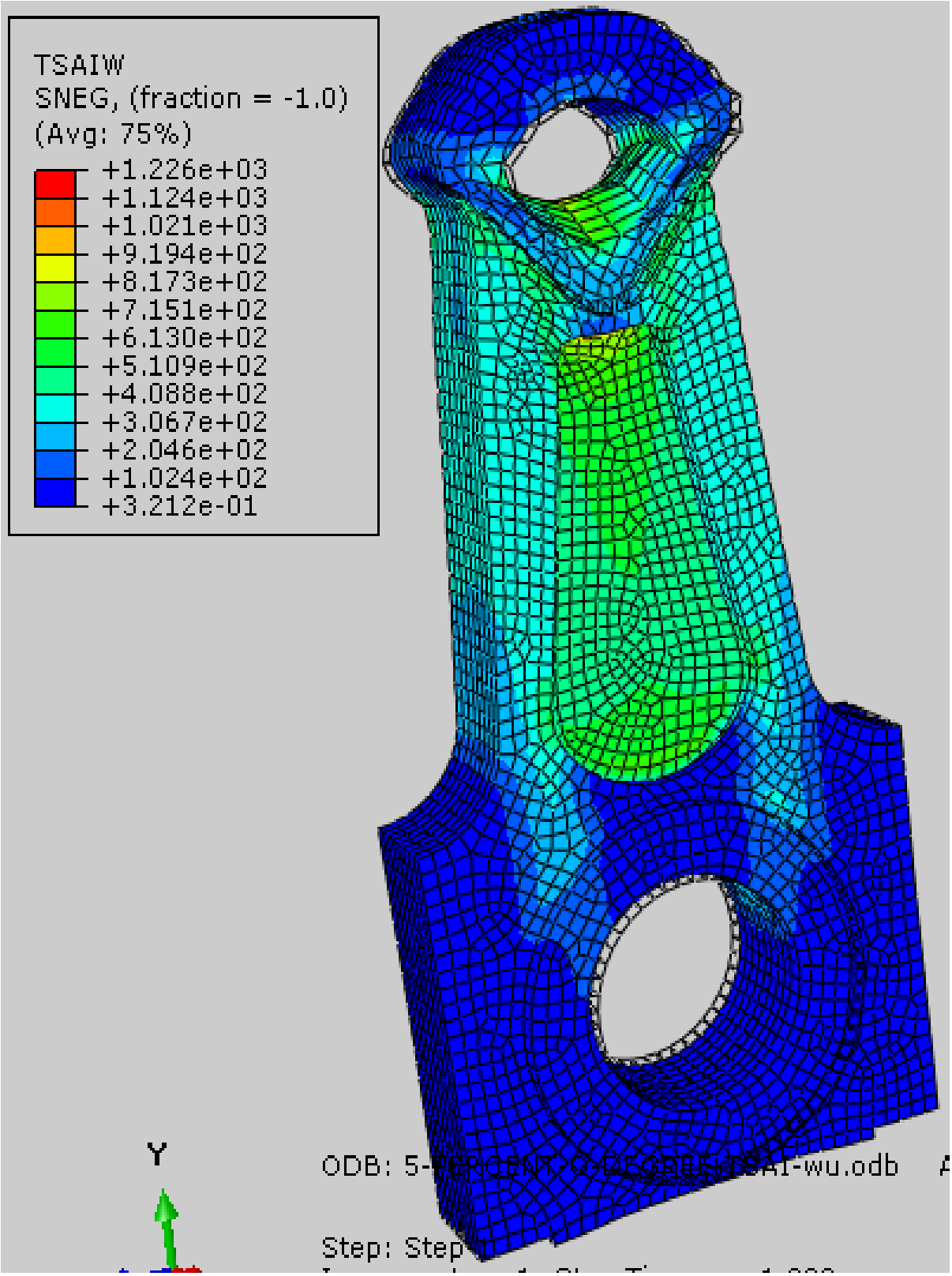

Figure III.B 30^{O} Tsai-Hill Criterion Results

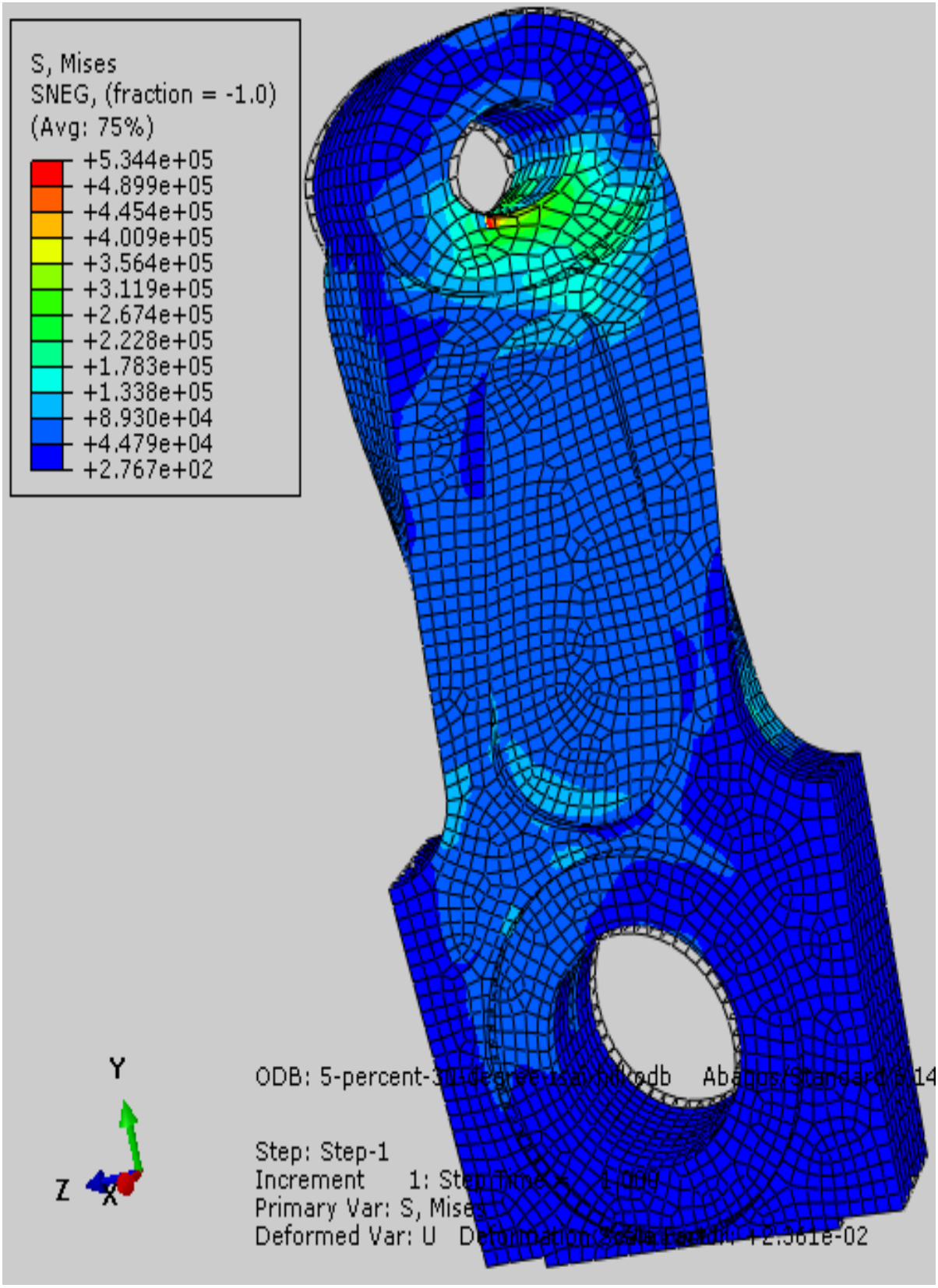

Tsai-Wu Criterion Results

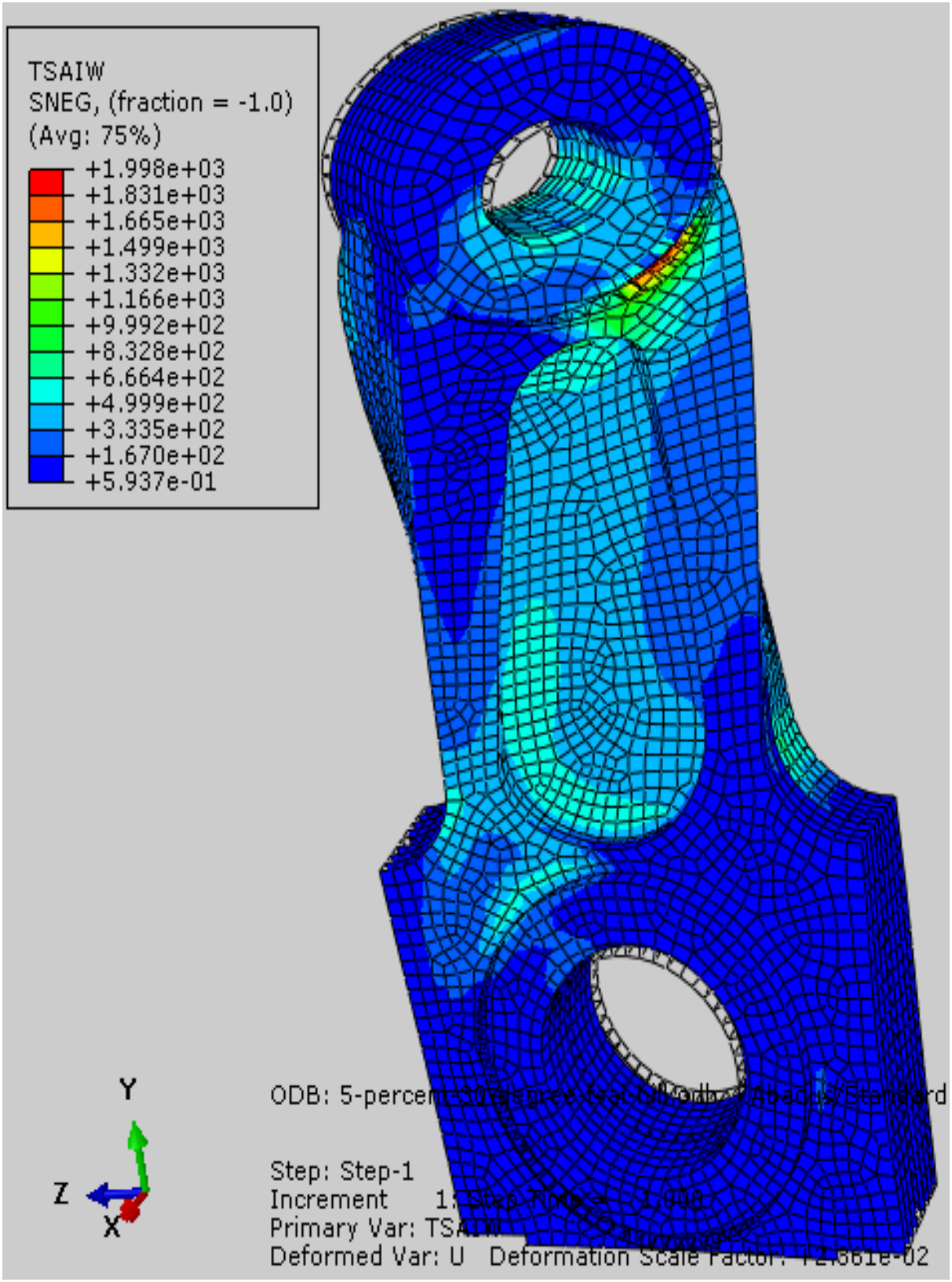

Figure III.C 45^{O} Tsai-Hill Criterion results

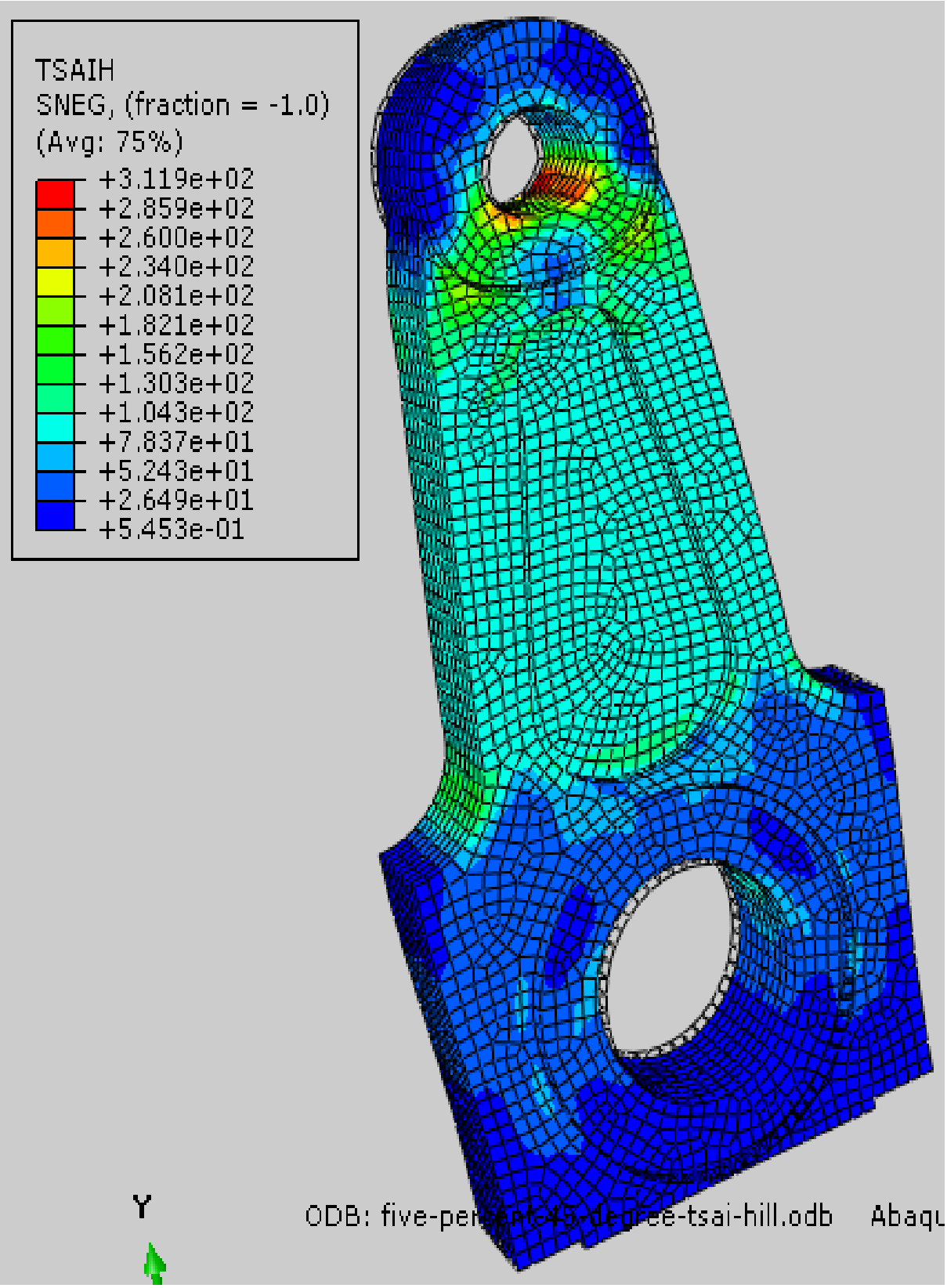

Tsai-Wu criterion results

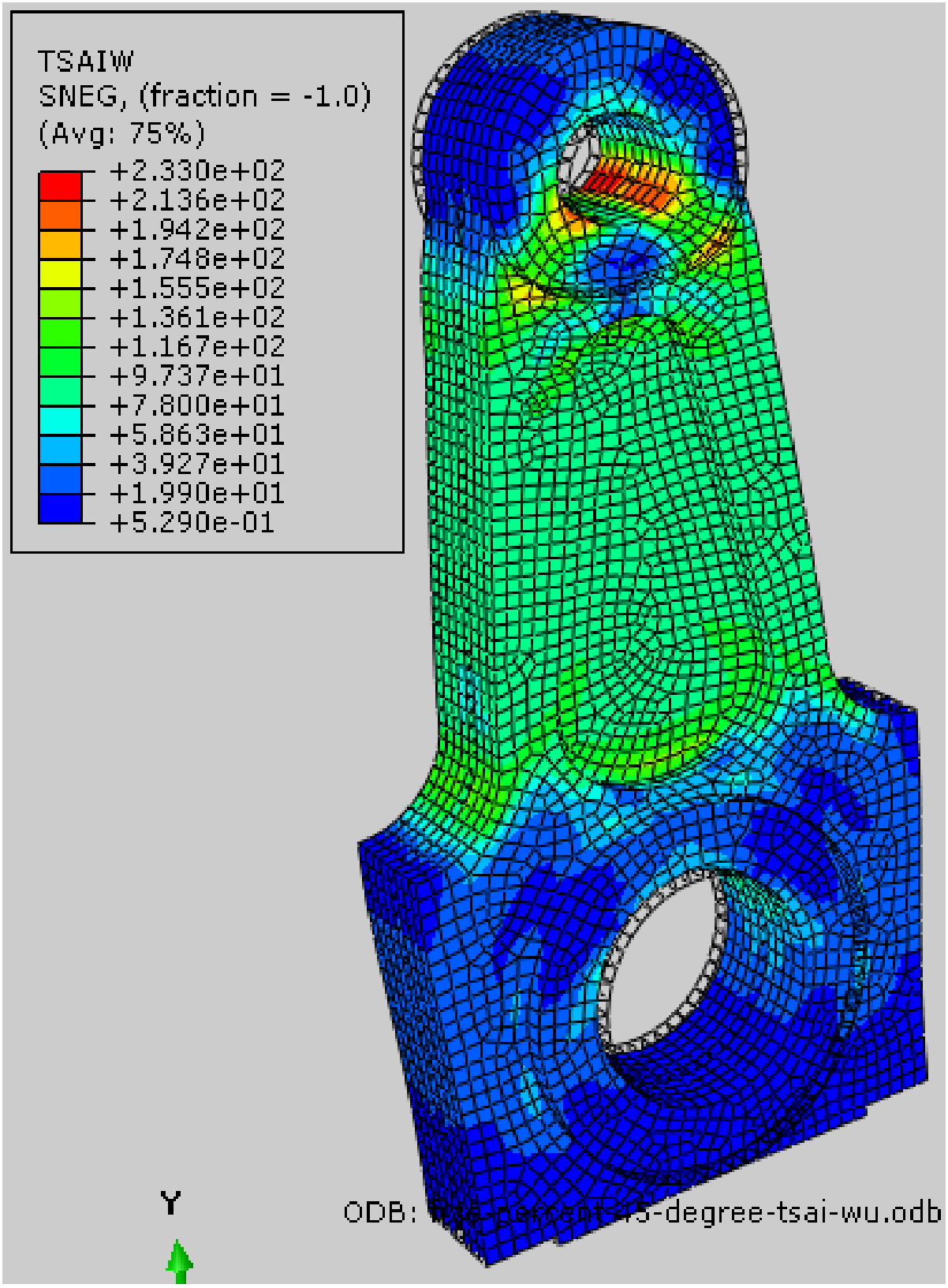

Figure III.D 90^{O} Tsai-Hill Criterion results

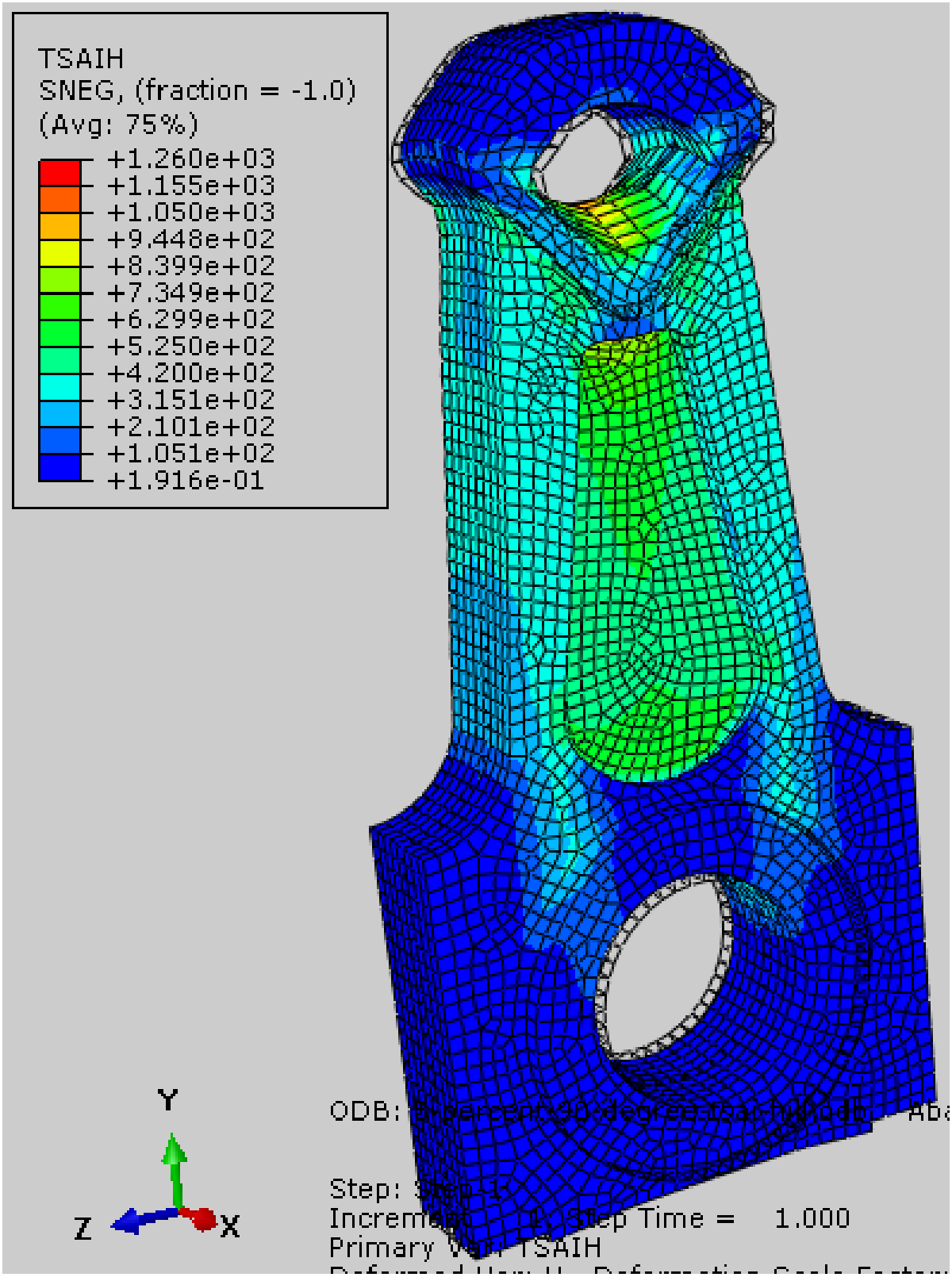

Tsai-Wu criterion results

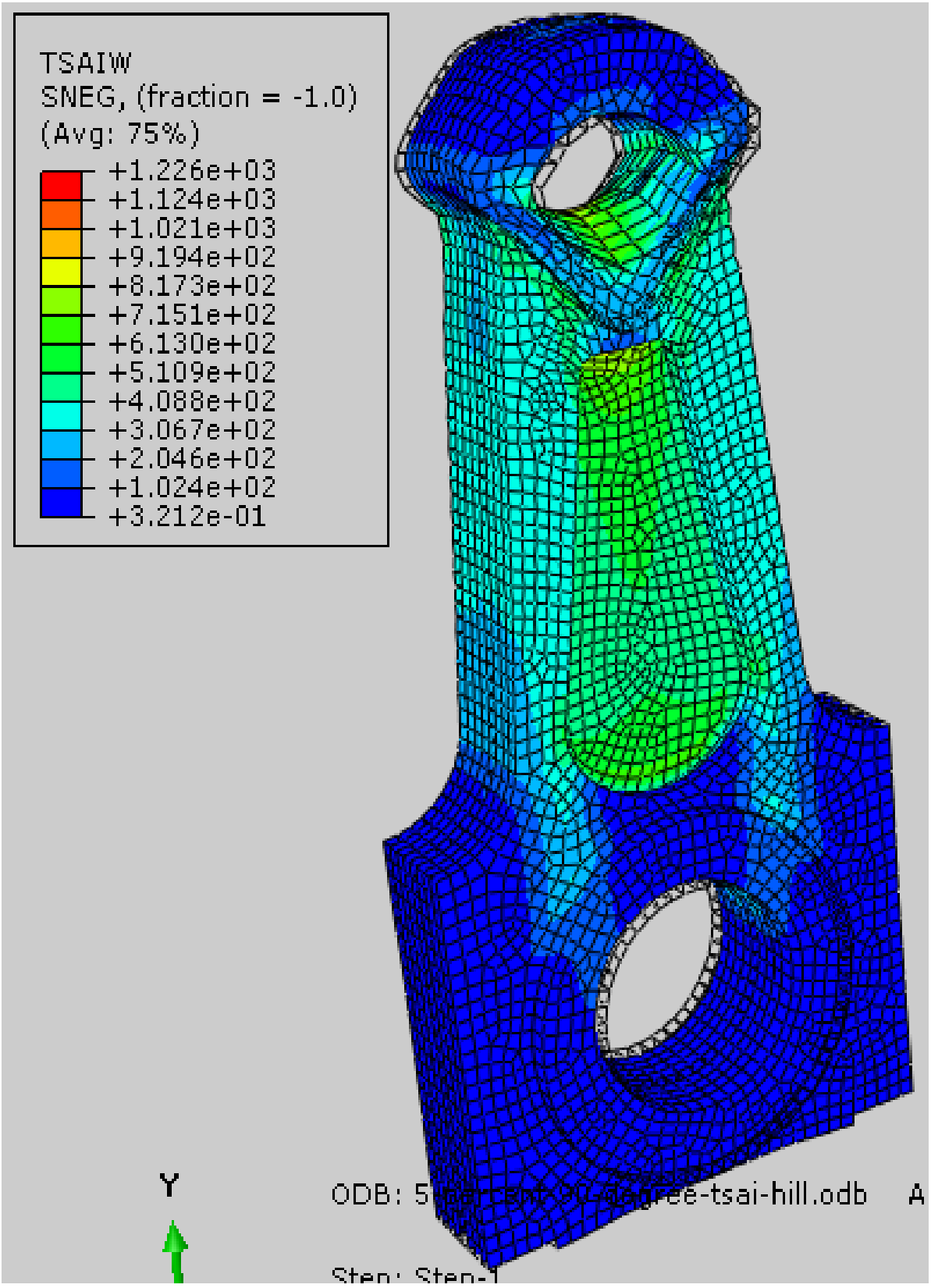

Figure III.E 20 % VF 0^{O} Tsai-Hill Criterion results

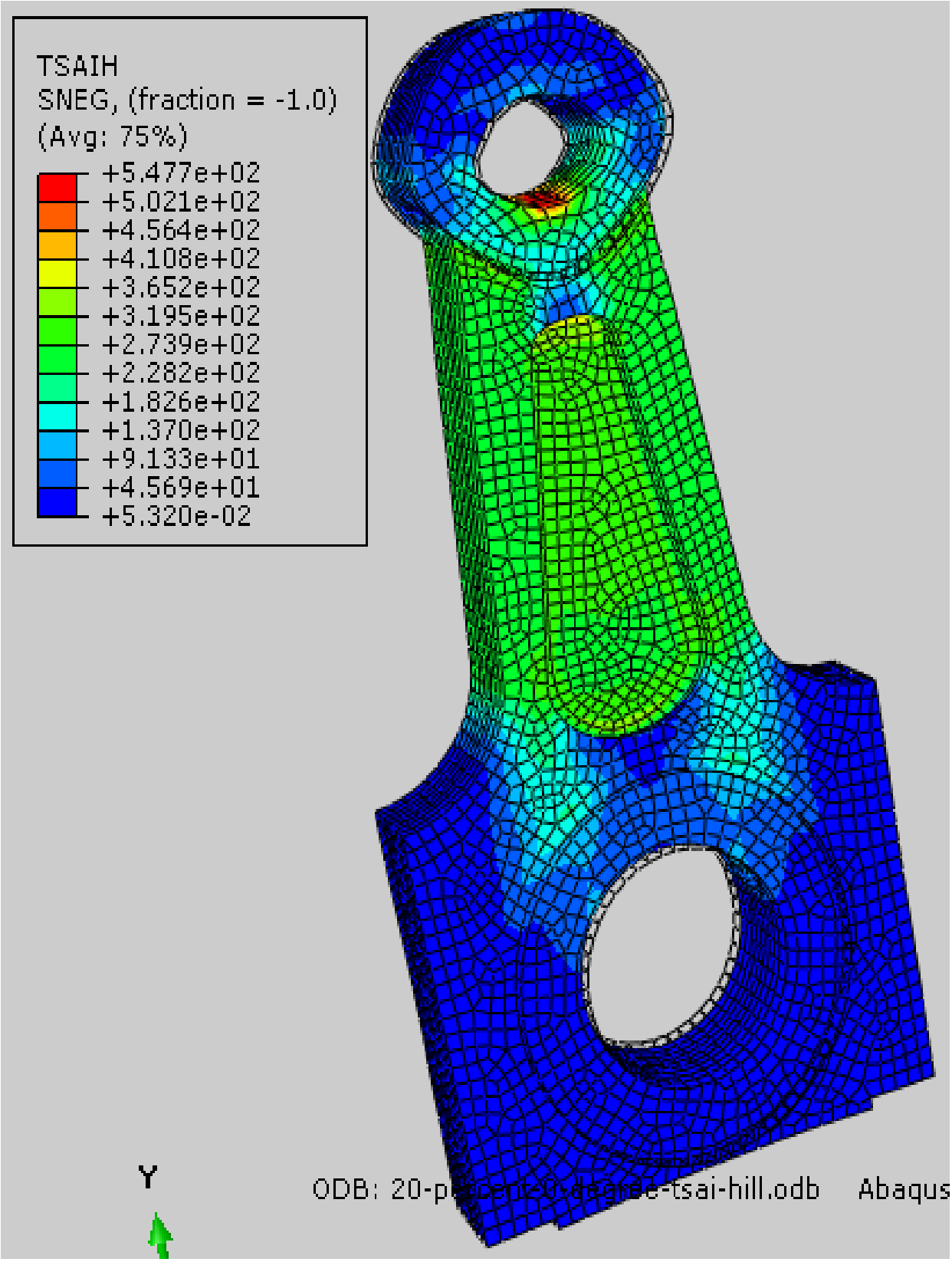

Tsai-Wu criterion results

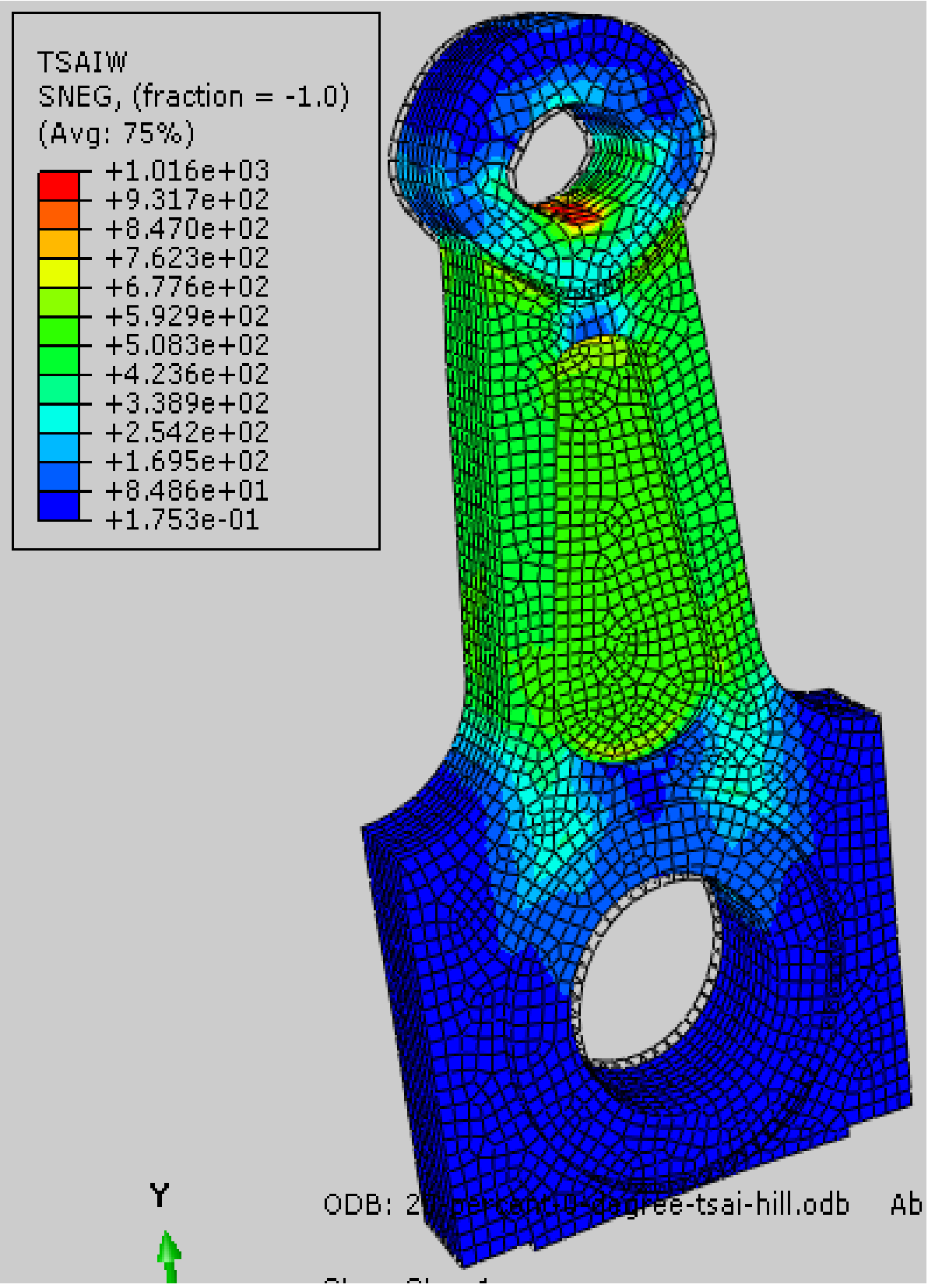

Figure III.F 30^{O} Tsai-Hill Criterion results

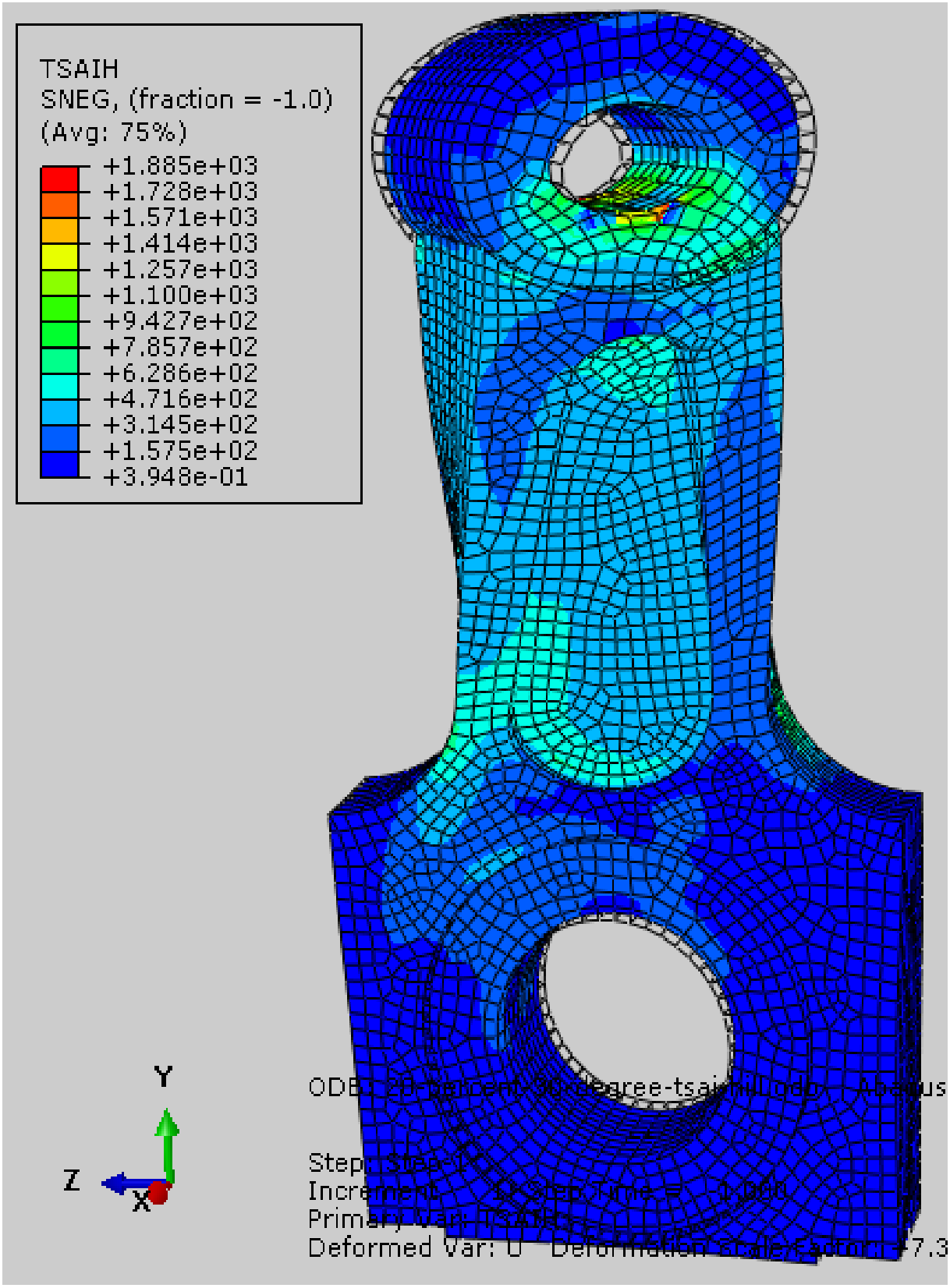

Tsai-Wu criterion results

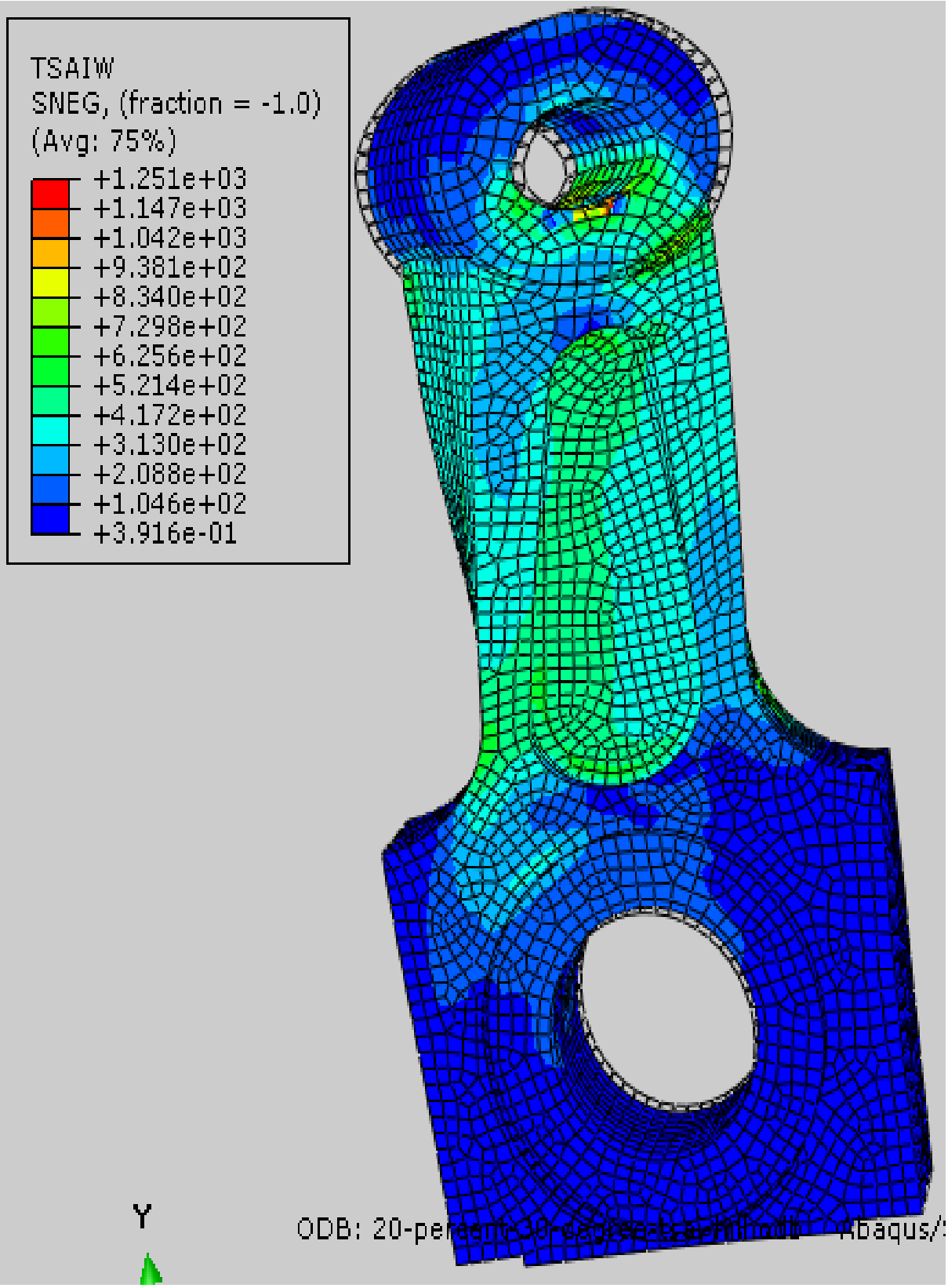

Figure III.G 45^{O} Tsai-Hill Criterion results

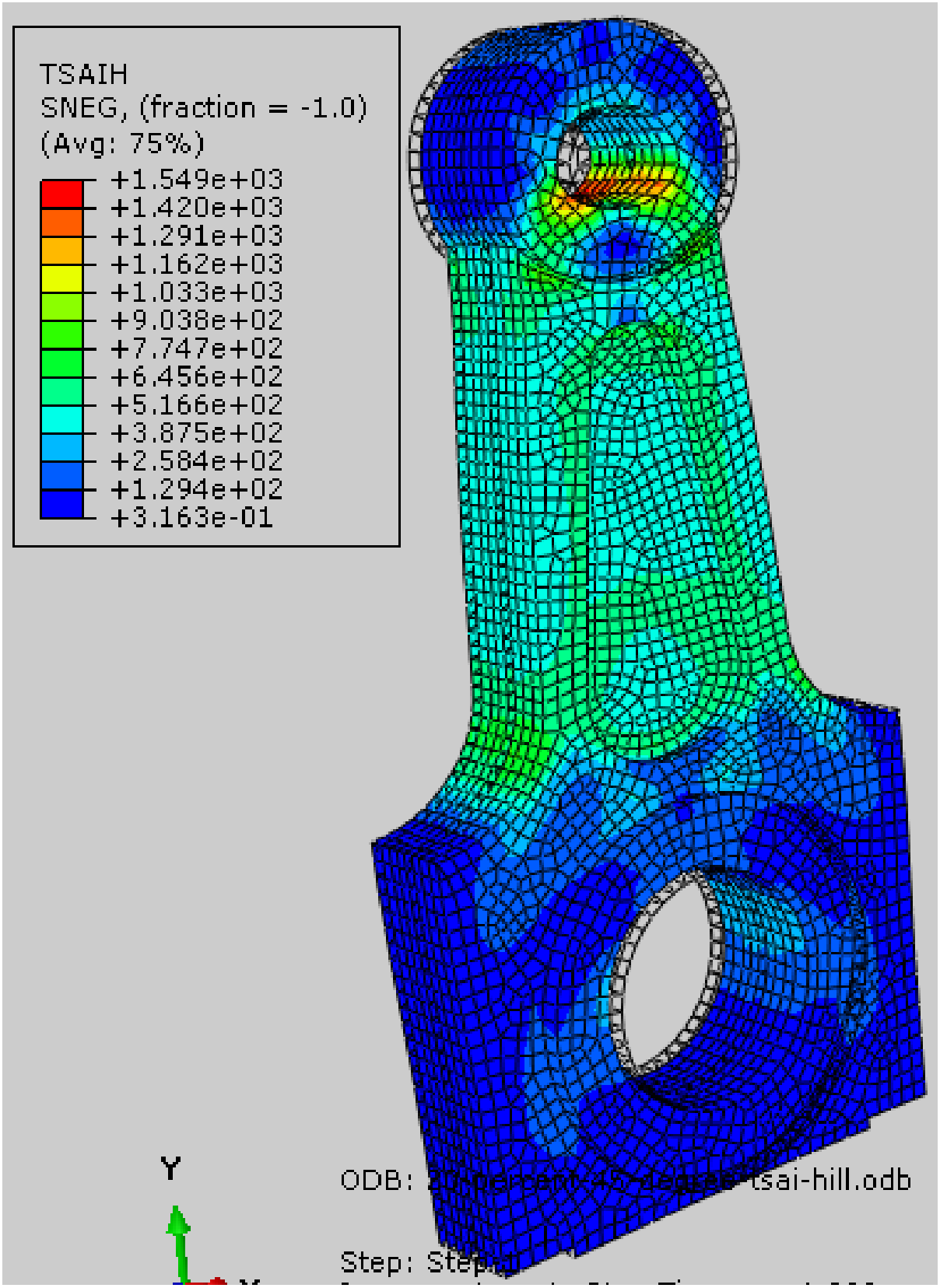

Tsai-Wu criterion results

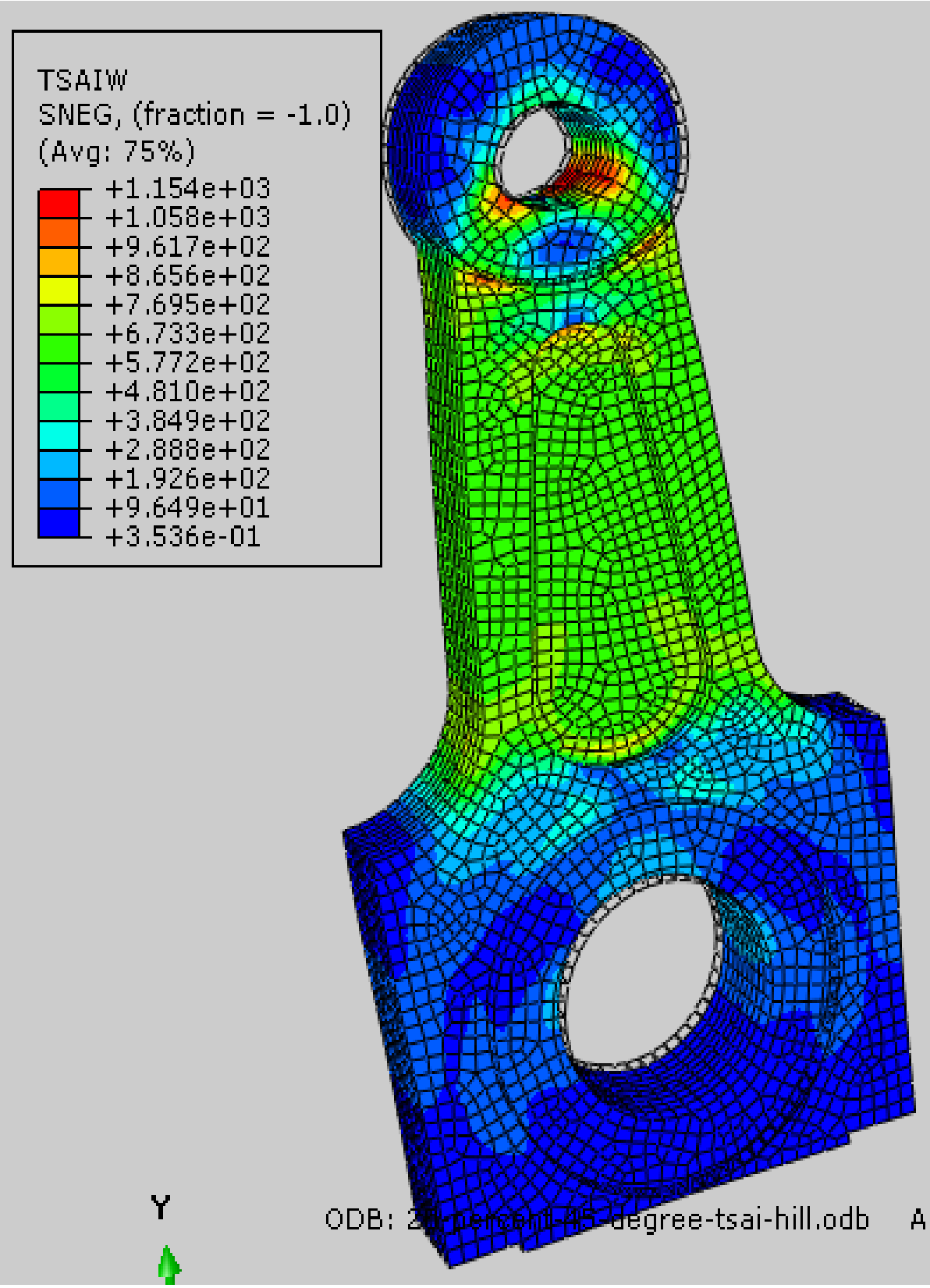

Figure III.H 90^{O} Tsai-Hill Criterion results

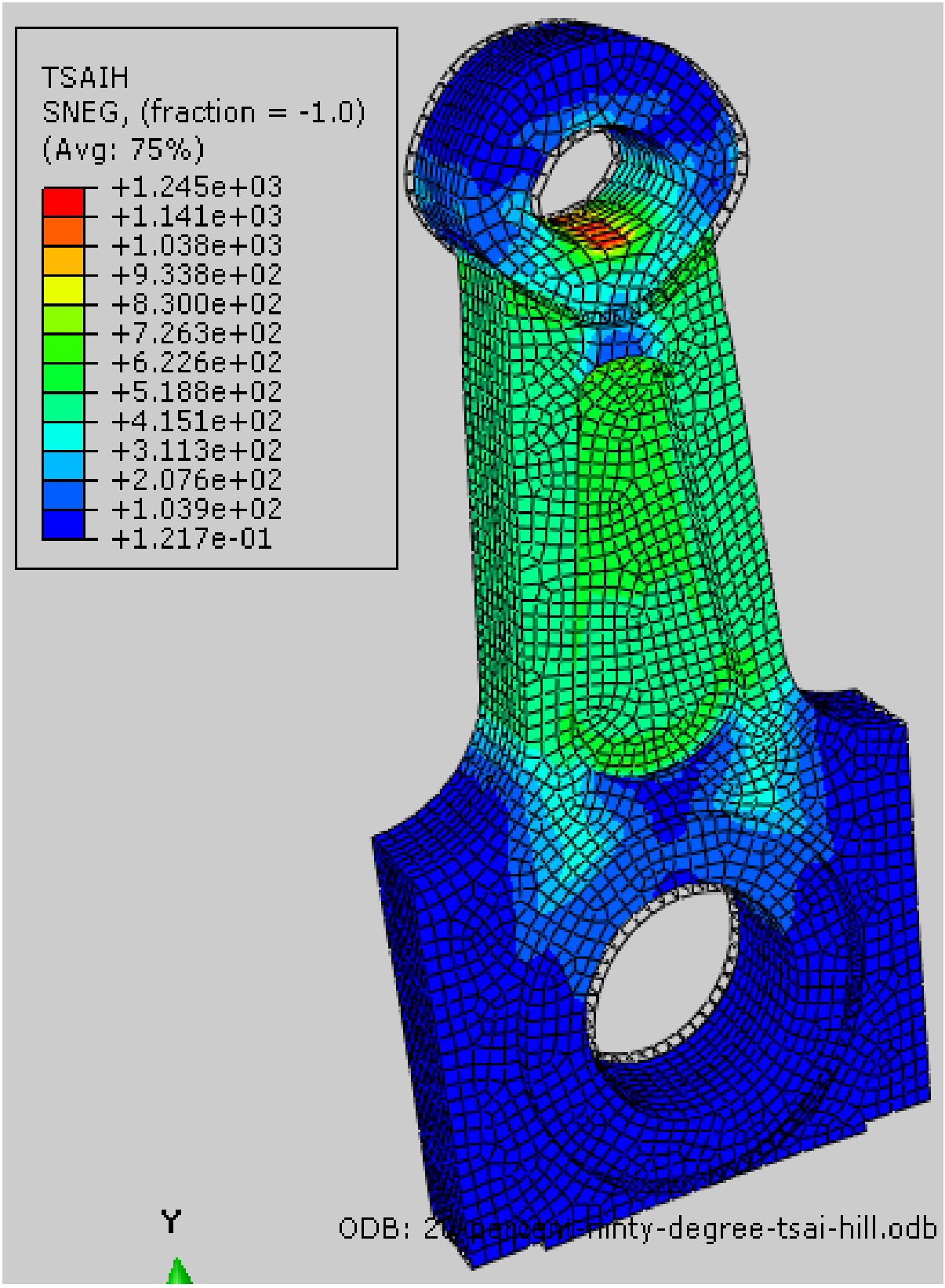

Tsai-Wu criterion results

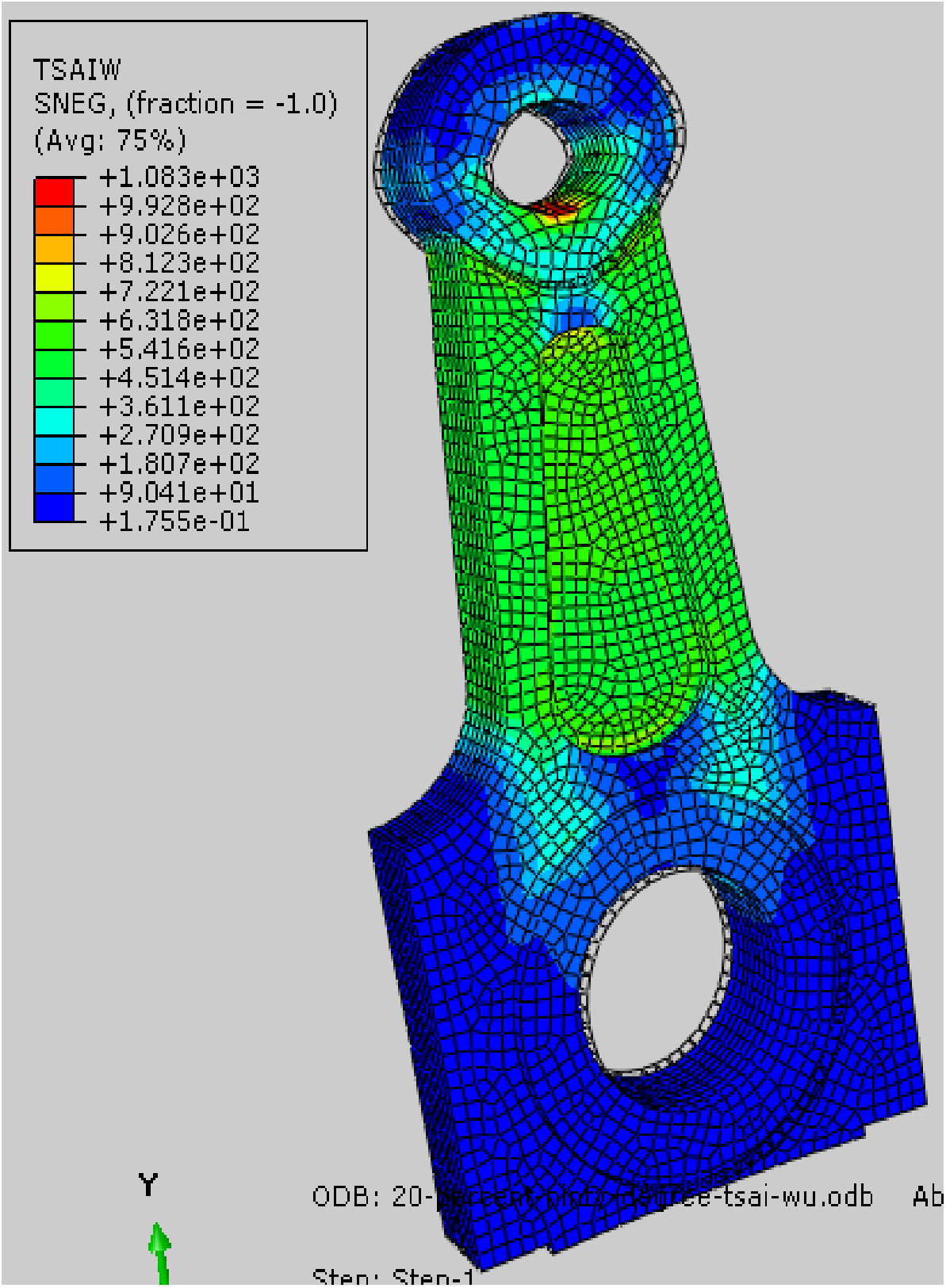

Appendex-IV

Figure IV-A. 5% volume fraction reinforcement using 0.6 and 1.8 aspect ratio respectively:-

0.6 AR

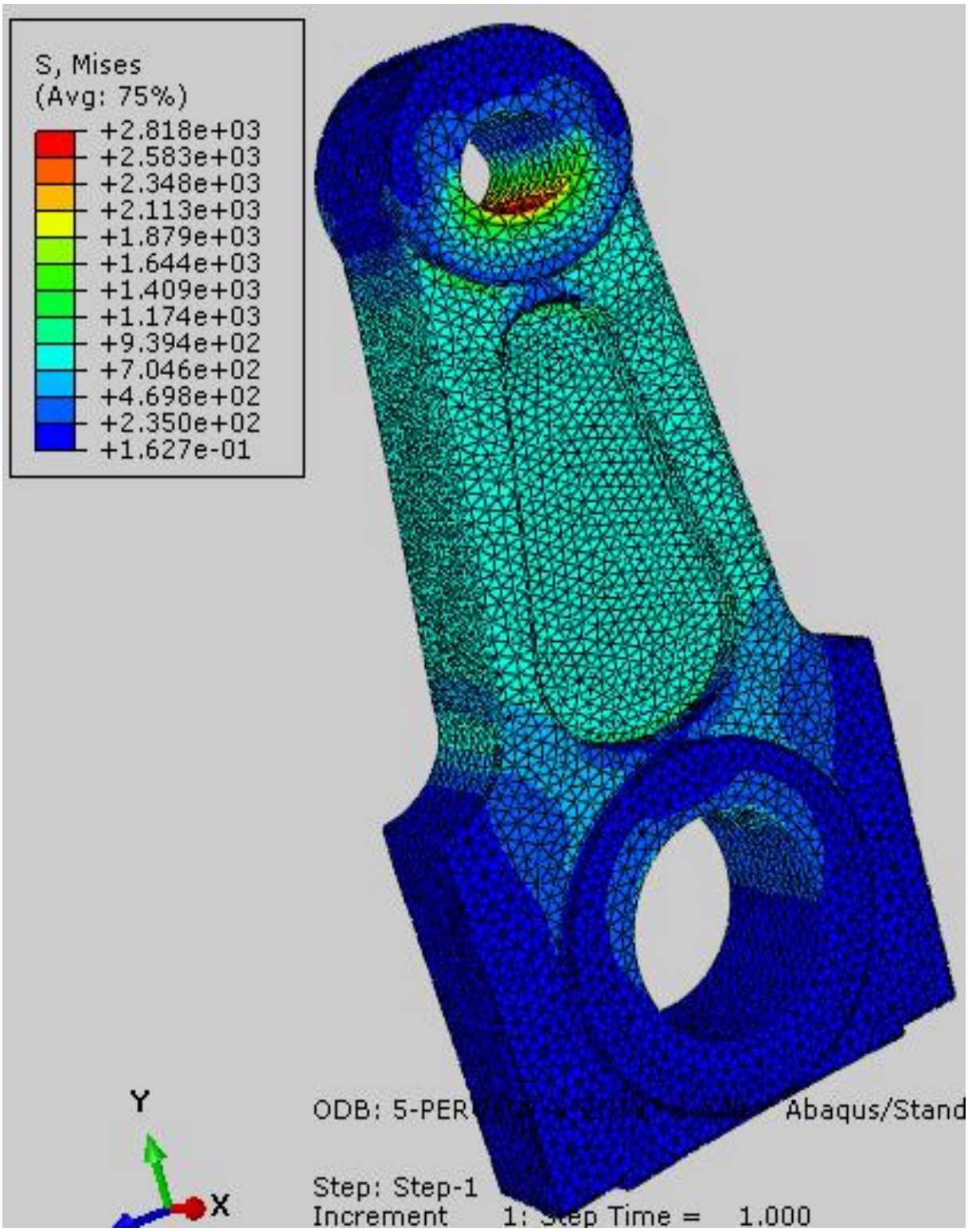

1.8 AR

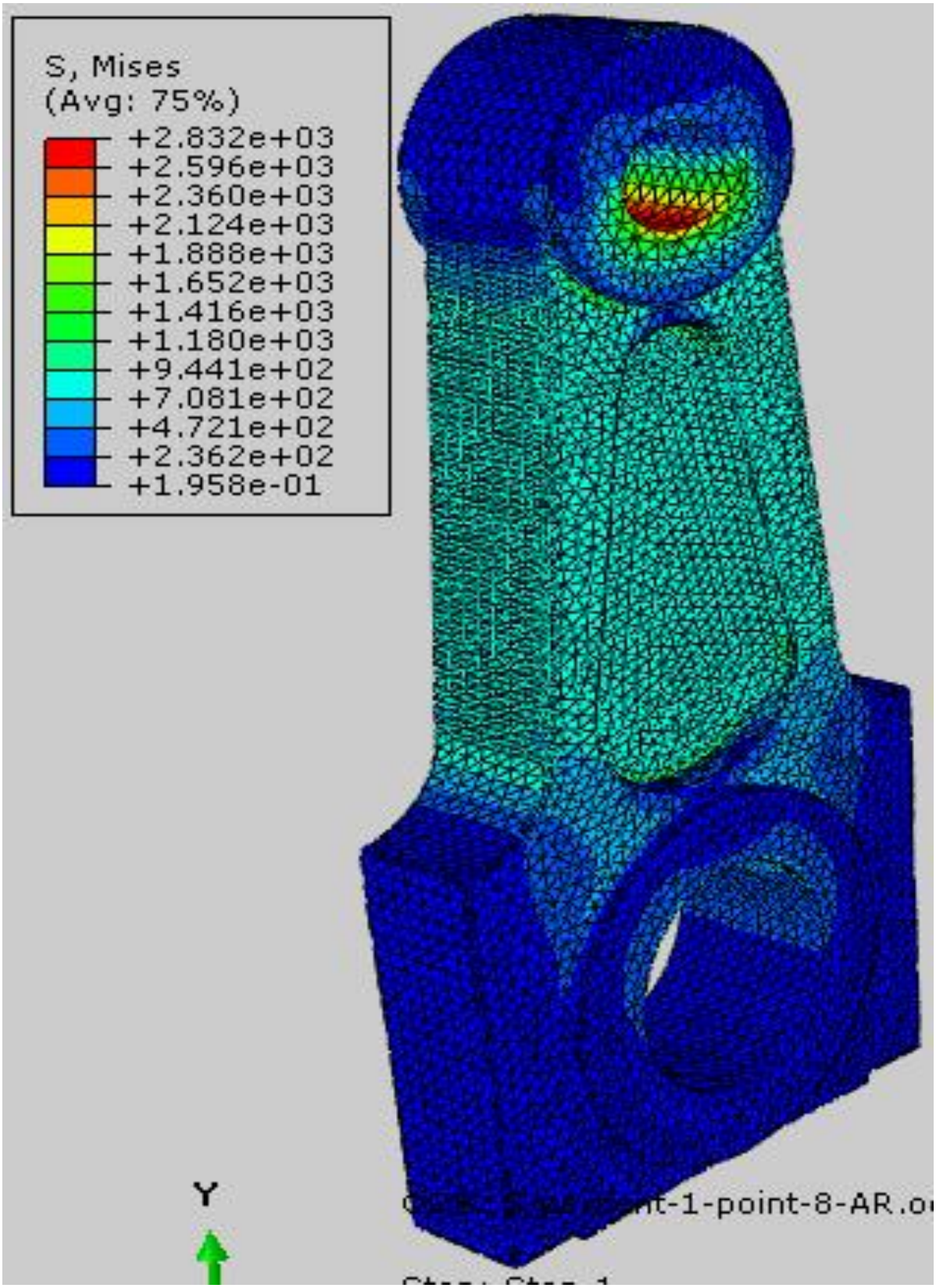
S, Mises
(Avg: 75%)
+2.832e+03
+2.596e+03
+2.360e+03
+2.124e+03
+1.888e+03
+1.652e+03
+1.416e+03
+1.180e+03
+9.441e+02
+7.081e+02
+4.721e+02
+2.362e+02
+1.958e-01
Y

Figure IV-B 20% volume fraction reinforcement using 0.6 and 1.8 aspect ratio respectively:-

0.6 AR

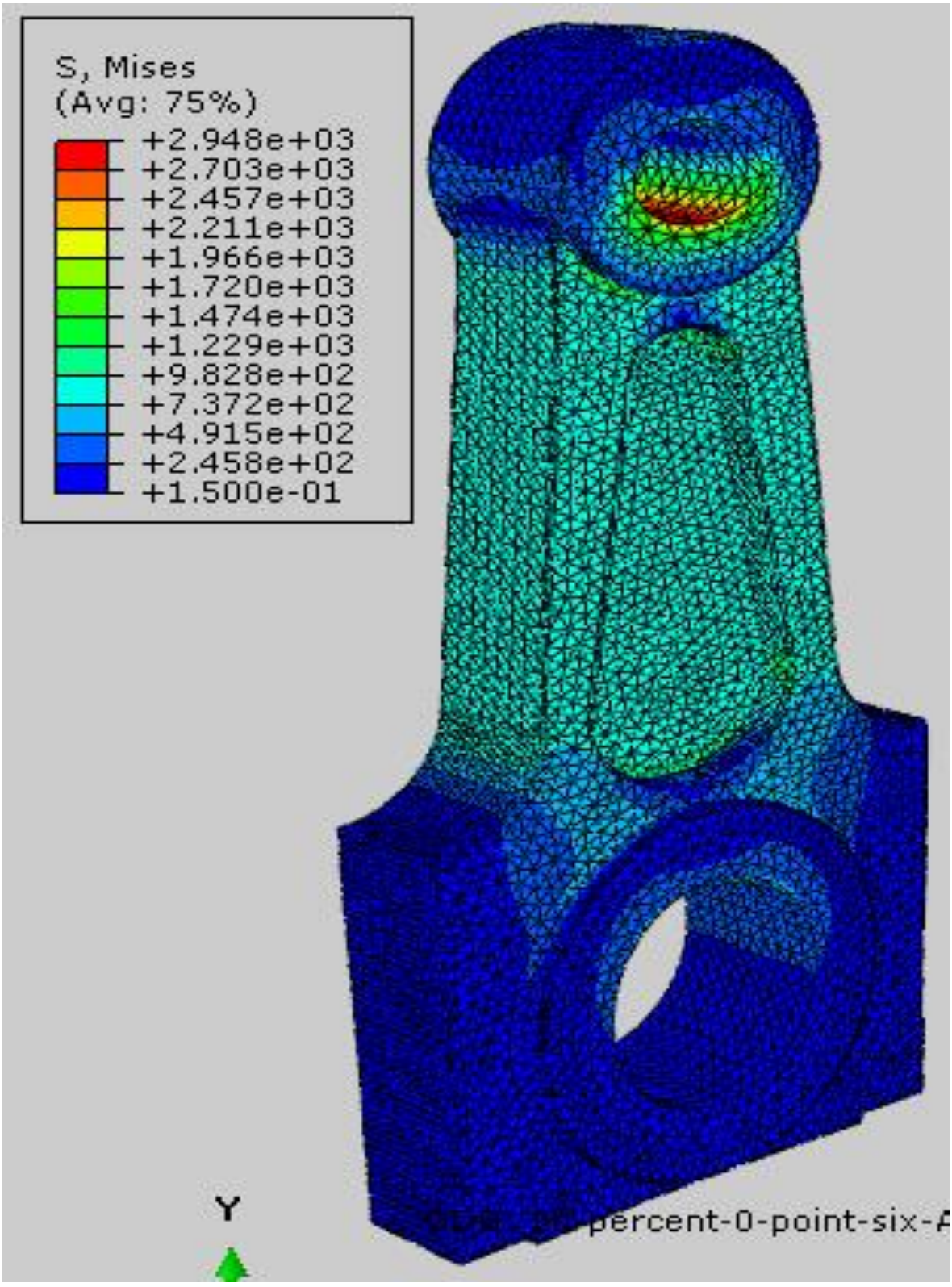

1.8 AR

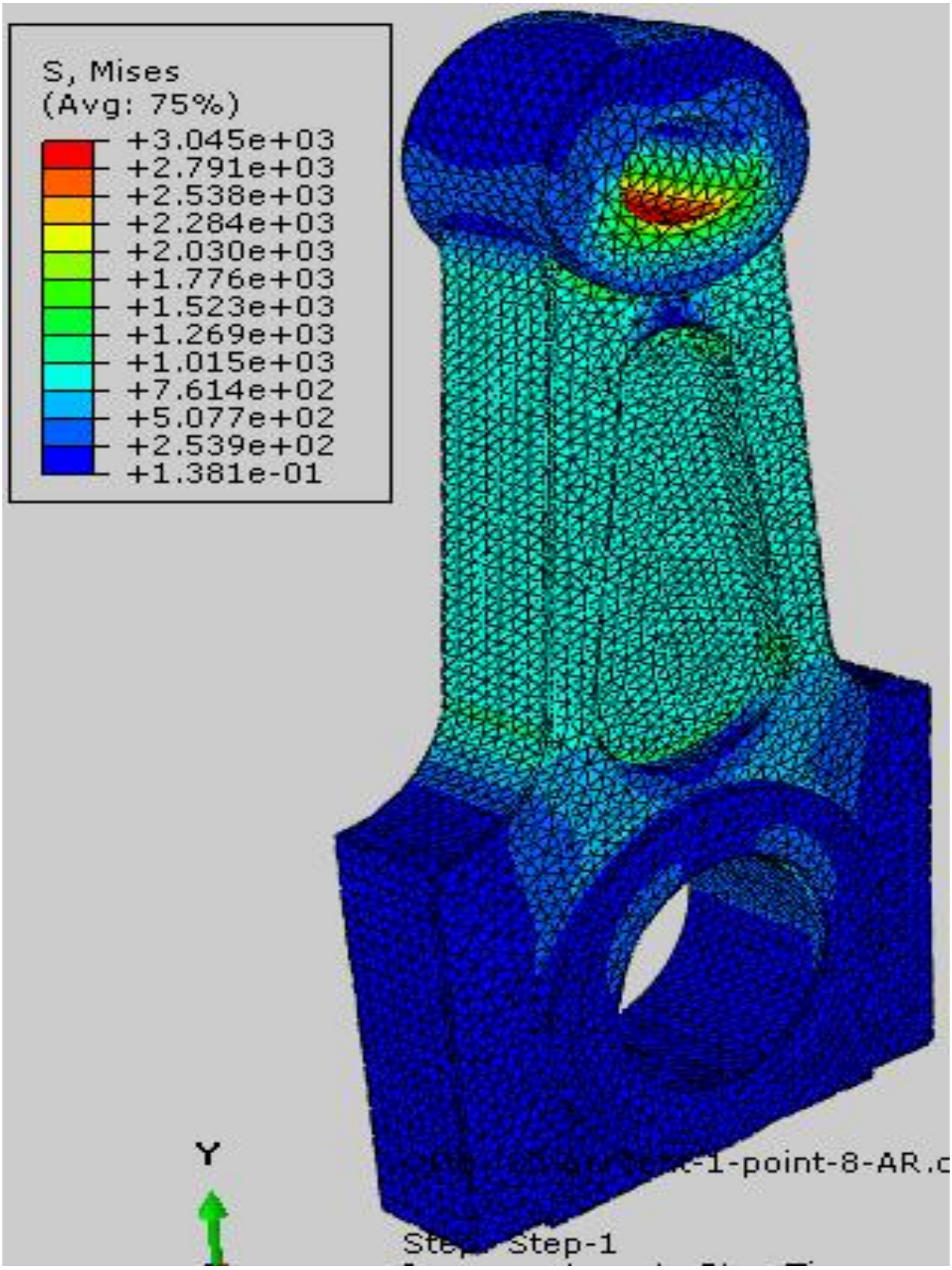
S, Mises
(Avg: 75%)
+3.045e+03
+2.791e+03
+2.538e+03
+2.284e+03
+2.030e+03
+1.776e+03
+1.523e+03
+1.269e+03
+1.015e+03
+7.614e+02
+5.077e+02
+2.539e+02
+1.381e-01
Y
Step-1

Appendex-V

Figure V.A 5% volume fraction composites with a 0.6(A) and 1.8(A) aspect ratio

0.6 AR

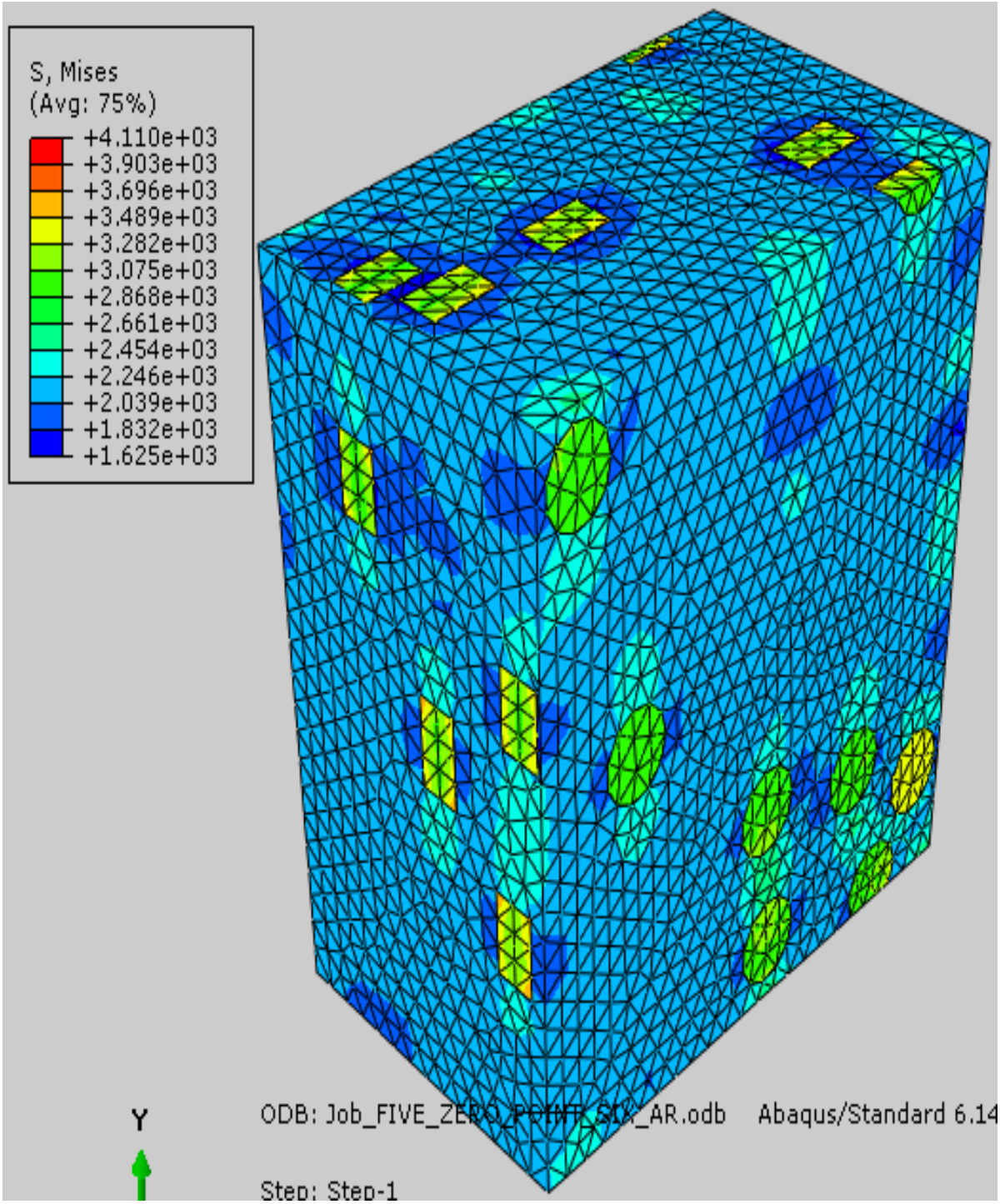

1.8 AR

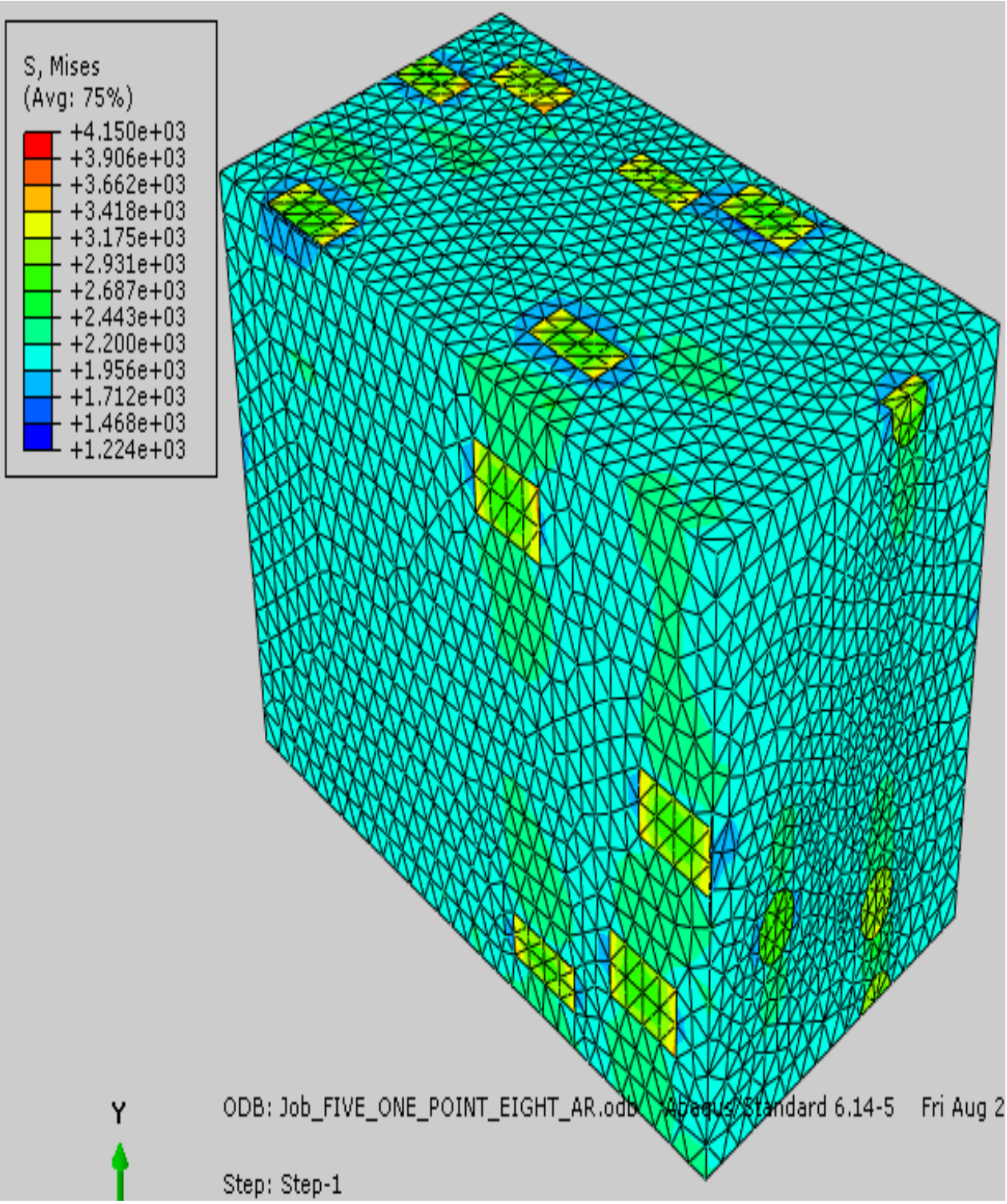
S, Mises
(Avg: 75%)
+4.150e+03
+3.906e+03
+3.662e+03
+3.418e+03
+3.175e+03
+2.931e+03
+2.687e+03
+2.443e+03
+2.200e+03
+1.956e+03
+1.712e+03
+1.468e+03
+1.224e+03
Y
ODB: Job_FIVE_ONE_POINT_EIGHT_AR.odb
Step: Step-1

Figure V.B 20% volume fraction composites with a 0.6 and 1.8 aspect ratio

0.6 AR

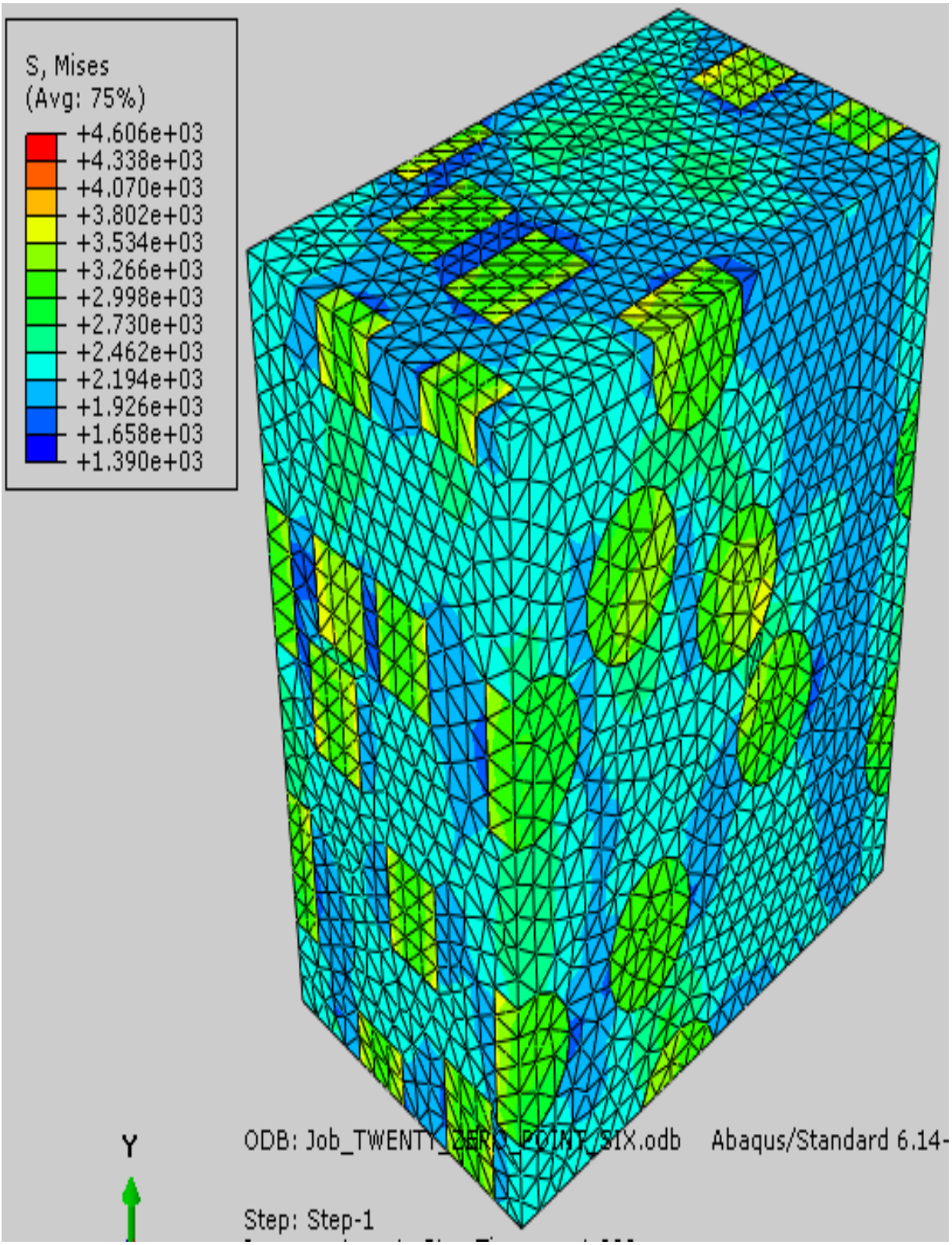

1.8 AR

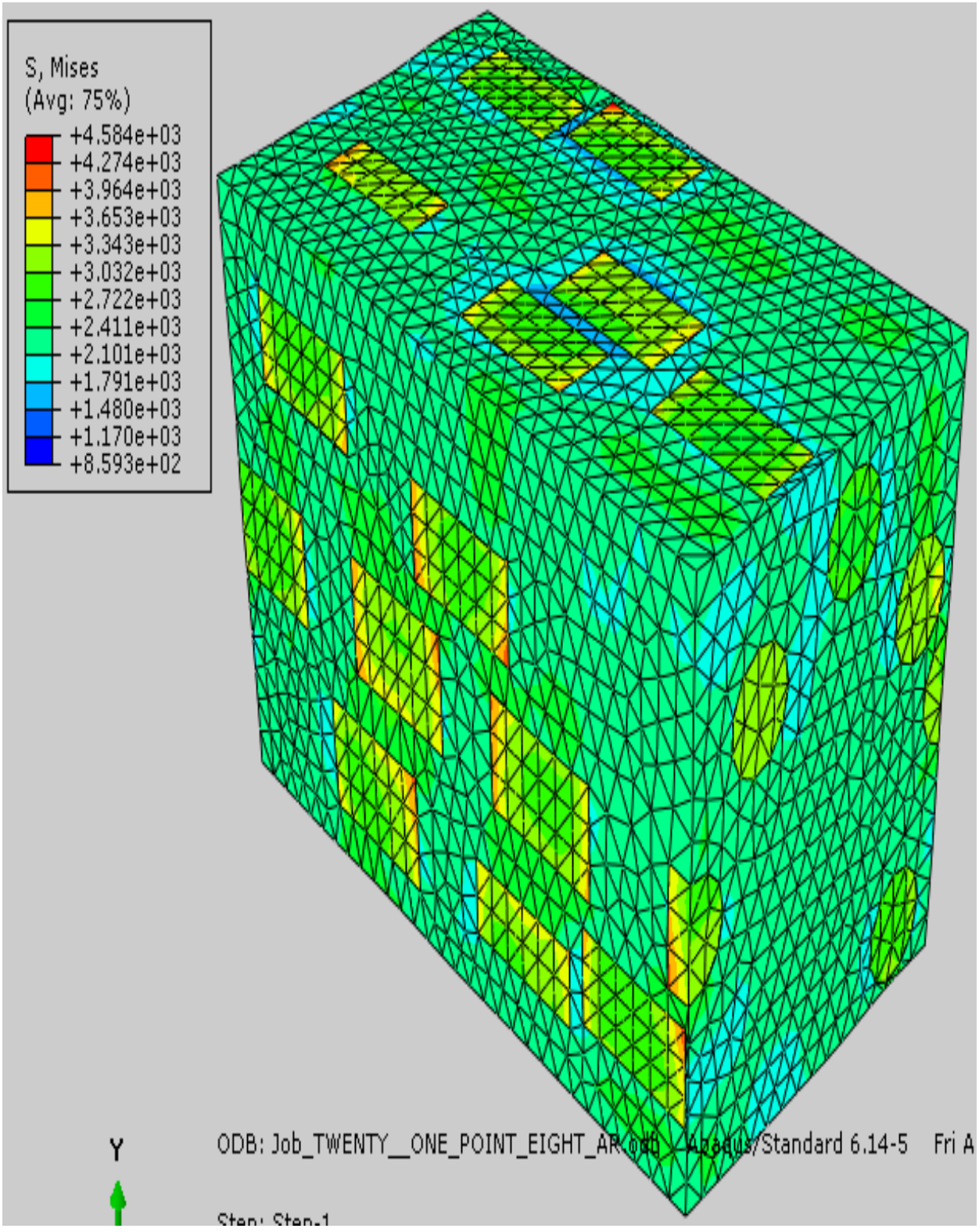
S, Mises
(Avg: 75%)
+4.584e+03
+4.274e+03
+3.964e+03
+3.653e+03
+3.343e+03
+3.032e+03
+2.722e+03
+2.411e+03
+2.101e+03
+1.791e+03
+1.480e+03
+1.170e+03
+8.593e+02
Y
ODB: Job_TWENTY__ONE_POINT_EIGHT_AR.odb Abaqus/Standard 6.14-5 Fri A
Step: Step-1